ISSN 0038-531X

Russian Original Vol. 55, No. 3, September, 1983

March, 1984

SATEAZ 55(3) 565-638 (1983)

SOVIET ATOMIC ENERGY

АТОМНАЯ ЭНЕРГИЯ
(ATOMNAYA ÉNERGIYA)

TRANSLATED FROM RUSSIAN

CONSULTANTS BUREAU, NEW YORK

SOVIET ATOMIC ENERGY

Soviet Atomic Energy is abstracted or indexed in *Chemical Abstracts, Chemical Titles, Pollution Abstracts, Science Research Abstracts, Parts A and B, Safety Science Abstracts Journal, Current Contents, Energy Research Abstracts,* and *Engineering Index.*

Mailed in the USA by Publications Expediting, Inc., 200 Meacham Avenue, Elmont, NY 11003.

POSTMASTER: Send address changes to *Soviet Atomic Energy,* Plenum Publishing Corporation, 233 Spring Street, New York, NY 10013.

Soviet Atomic Energy is a translation of *Atomnaya Énergiya,* a publication of the Academy of Sciences of the USSR.

An agreement with the Copyright Agency of the USSR (VAAP) makes available both advance copies of the Russian journal and original glossy photographs and artwork. This serves to decrease the necessary time lag between publication of the original and publication of the translation and helps to improve the quality of the latter. The translation began with the first issue of the Russian journal.

Consultants Bureau journals appear about six months after the publication of the original Russian issue. For bibliographic accuracy, the English issue published by Consultants Bureau carries the same number and date as the original Russian from which it was translated. For example, a Russian issue published in December will appear in a Consultants Bureau English translation about the following June, but the translation issue will carry the December date. When ordering any volume or particular issue of a Consultants Bureau journal, please specify the date and, where applicable, the volume and issue numbers of the original Russian. The material you will receive will be a translation of that Russian volume or issue.

Subscription (2 volumes per year)
Vols. 54 & 55: $500 (domestic); $555 (foreign)
Vols. 56 & 57: $560 (domestic); $621 (foreign)

Single Issue: $100
Single Article: $7.50

CONSULTANTS BUREAU, NEW YORK AND LONDON

c/b
233 Spring Street
New York, New York 10013

Published monthly. Second-class postage paid at Jamaica, New York 11431.

SOVIET ATOMIC ENERGY

A translation of *Atomnaya Énergiya*

March, 1984

Volume 55, Number 3 **September, 1983**

CONTENTS

Engl./Russ.

CONTENTS

(continued)

Engl./Russ.

The Russian press date (podpisano k pechati) of this issue was 8/24/1983. Publication therefore did not occur prior to this date, but must be assumed to have taken place reasonably soon thereafter.

ARTICLES

DETERMINATION OF THE BURNUP AND ISOTOPIC COMPOSITION OF VVÉR-440 SPENT FUEL

A. V. Stepanov, T. P. Makarova, B. A. Bibichev,
B. N. Belyaev, A. M. Fridkin, A. V. Lovtsyus,
L. D. Preobrazhenskaya, A. A. Lipovskii, G. A. Akopov,
G. A. Kulakov, V. D. Sidorenko, L. S. Bulyanitsa,
S. A. Nikitina, N. A. Malyshev, and M. A. Razuvaeva

UDC 621.039.524.4

In order to verify the accuracy of the calculation of the nuclide content of the actinide elements in VVÉR spent fuel and to improve the computational methods and programs, experimental data are essential about the burnup and conditions of irradiation. In [1, 2] experimental data are given about the content of U, Pu, Am, and Cm nuclides in samples of VVÉR-365 fuel elements, and the results are compared for experiment and calculation. In the present paper, similar experimental and calculated data are given for the spent fuel of the VVÉR-440 of the Novovoronezh nuclear power station.

The isotopic composition of the fuel in samples of fuel elements of length ~ 3 cm, cut-off from four fuel element assemblies of the VVÉR-440 with initial fuel enrichment of $\varepsilon = 3.3$ and 3.6%, was investigated. Table 1 shows the numbers of the fuel elements from which the samples were cut-off, and the positions of the sectioned samples over the height of the fuel elements. The location of the fuel elements in the fuel element assemblies is shown in Fig. 1.

In order to study the effect of a change of neutron spectrum over the cross section of the fuel elements on the isotopic composition of the fuel, the samples were cut-off from fuel elements of the outer series (fuel elements 58, 25), from fuel elements located near the central tube (fuel elements 63, 64), and from fuel elements of the intermediate region (region with an asymptotic neutron spectrum, fuel elements 97 and 107). Samples of fuel elements 1-7 were cut-off from fuel-element assemblies RP-3.3 No. 71A (block III), 8 and 9 from fuel element assemblies RP-3.3 No. 77A (block III), 10-20 from fuel-element assemblies R-3.6 No. 213 (block IV), and sample 25 from fuel-element assembly R-3.6 No. 216 (block IV); fuel element RP-3.3 No. 71A was irradiated during a single run; RP-3.3, No. 77A for five runs; R-3.6 No. 213 and R-3.6 No. 216 for three runs. The average fuel burnup in the fuel-element assemblies amounted to 16, 49, 31, and 33 kg/ton U, respectively.

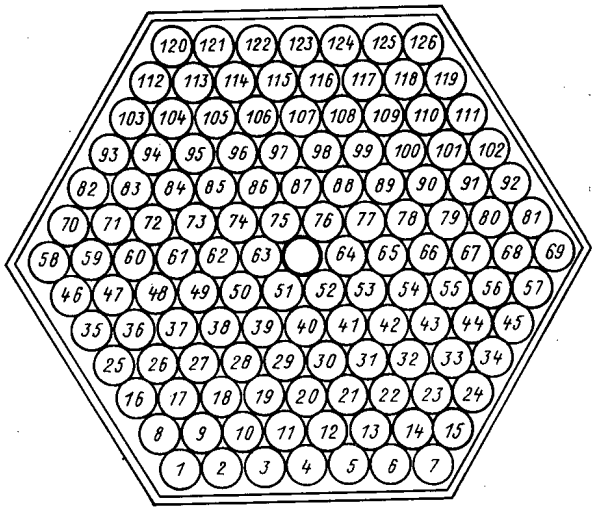

Fig. 1. Recorder chart of the location of the fuel elements in the fuel-element assemblies investigated.

Translated from Atomaya Énergiya, Vol. 55, No. 3, pp. 141-145, September, 1983. Original article submitted November 22, 1982.

0038-531X/83/5503-0565$07.50

TABLE 1. Positions of Sectioned Samples over the Height of the Fuel Elements and the Burnup Values of the Fuel in the Samples Obtained by Three Methods

Sample number	Fuel element number	Position along the height of the fuel element from the base of the core, mm	Burnup, kg/ton U			
			by the method of heavy atoms	by ^{137}Cs	by ^{148}Nd	weighted mean value
1	63	1875	16,8 (7) *	16,9 (3) *	—	16,9 (3) *
2	97	2170	13,7 (7)	14,3 (2)	—	14,3 (2)
3	97	200	9,3 (6)	8,6 (2)	—	8,7 (2)
4	58	200	13,7 (7)	13,3 (2)	—	13,3 (2)
5	63	375	13,9 (7)	13,9 (2)	—	13,9 (2)
6	97	300	12,6 (7)	11,6 (2)	—	11,7 (3)
7	—	—	14,4 (7)	14,8 (3)	14,1 (4)	14,6 (4)
8	63	850	55,8 (18)	54,2 (8)	55,5 (10)	54,8 (8)
9	63	1350	55,0 (18)	54,0 (9)	56,6 (13)	54,7 (9)
10	25	2285	21,5 (9)	21,4 (4)	20,4 (4)	21,0 (4)
11	25	125	27,3 (9)	27,7 (4)	27,8 (6)	27,7 (4)
12	25	1625	37,6 (12)	38,9 (7)	38,8 (8)	38,6 (7)
13	25	625	36,6 (12)	38,5 (6)	38,1 (8)	38,1 (6)
14	25	1125	38,0 (12)	38,4 (6)	—	38,3 (6)
15	64	2225	21,9 (9)	21,8 (3)	22,1 (3)	22,0 (3)
16	64	125	20,3 (8)	20,4 (3)	—	20,4 (3)
17	64	1625	36,0 (12)	34,3 (5)	35,3 (6)	34,9 (5)
18	63	1875	32,0 (10)	32,5 (5)	32,8 (5)	32,6 (5)
19	63	375	33,2 (11)	32,9 (5)	33,5 (7)	33,1 (5)
20	107	875	35,3 (11)	35,2 (5)	33,4 (8)	34,8 (5)
21	63	1350	35,8 (12)	35,6 (5)	34,0 (7)	35,2 (5)

*Here and in Tables 2 and 3, the figures in brackets show the confidence limits of the total error of the measurement result for a confidence coefficient of p = 0.95. The confidence limits are related to the last significant figure of the measurement result. For example, 16.8 (7) corresponds to 16.8 ± 0.7 etc.

TABLE 2. Mass Fractions of Nuclides of Uranium and Plutonium, Related to the Initial Uranium, in Samples of Fuel Elements at the End of Irradiation, 10^{-3}

No. of sample	^{234}U	^{235}U	^{236}U	^{238}U	^{238}Pu	^{239}Pu	^{240}Pu	^{241}Pu	^{242}Pu	ΣPu
1	0,19/ (6)	17,6 (1)	3,00 (2)	959 (4)	0,0248 (3)	4,26 (5)	1,06 (1)	0,531 (8)	0,093 (12)	5,90 (7)
2	0,292 (4)	19,77 (14)	2,72 (2)	954 (4)	0,0204 (3)	4,53 (6)	0,90 (1)	0,425 (6)	0,0416 (16)	5,92 (8)
3	—	23,5 (2)	2,1 (3)	962 (4)	0,0049 (1)	2,97 (3)	0,419 (4)	0,133 (2)	0,0115 (12)	3,54 (3)
4	—	20,0 (2)	2,6 (3)	959 (4)	0,0127 (2)	3,99 (4)	0,79 (1)	0,326 (5)	0,038 (3)	5,16 (5)
5	—	19,60 (14)	2,9 (3)	958 (4)	0,0187 (1)	4,42 (2)	0,89 (1)	0,426 (3)	0,053 (2)	5,80 (2)
6	—	20,9 (2)	2,4 (3)	960 (4)	0,0120 (1)	3,89 (4)	0,665 (7)	0,289 (4)	0,0283 (7)	4,89 (5)
7	0,259 (4)	19,6 (1)	2,68 (3)	956 (4)	0,0221 (5)	4,85 (11)	0,97 (2)	0,48 (1)	0,060 (3)	6,38 (15)
8	0,138 (2)	3,18 (2)	4,68 (4)	919 (4)	0,452 (3)	6,15 (6)	3,12 (3)	2,00 (2)	1,378 (13)	13,09 (12)
9	0,142 (5)	3,48 (2)	4,68 (4)	917 (4)	0,454 (3)	6,45 (6)	3,33 (3)	2,07 (2)	1,356 (13)	13,66 (13)
10	—	16,56 (7)	3,54 (2)	951 (4)	0,050 (1)	4,96 (10)	1,32 (3)	0,714 (14)	0,133 (3)	7,17 (14)
11	0,23 (1)	13,28 (6)	4,16 (3)	946 (4)	0,098 (2)	5,62 (13)	1,81 (4)	1,044 (25)	0,268 (7)	8,83 (20)
12	0,197 (7)	8,28 (5)	4,85 (3)	936 (4)	0,201 (2)	5,98 (6)	2,45 (3)	1,512 (16)	0,597 (6)	10,75 (11)
13	0,200 (4)	8,88 (5)	4,72 (4)	937 (4)	0,196 (2)	5,97 (6)	2,42 (2)	1,479 (14)	0,568 (6)	10,63 (10)
14	0,197 (6)	8,47 (5)	4,77 (4)	937 (4)	0,214 (3)	6,20 (8)	2,49 (3)	1,58 (2)	0,620 (8)	11,11 (15)
15	0,256 (2)	16,47 (7)	3,60 (2)	949 (4)	0,0560 (3)	5,29 (3)	1,405 (7)	0,781 (4)	0,149 (1)	7,68 (4)
16	0,261 (2)	17,72 (7)	3,42 (2)	950 (4)	0,0496 (5)	5,28 (5)	1,33 (1)	0,729 (7)	0,126 (1)	7,50 (8)
17	0,203 (1)	9,38 (4)	4,64 (2)	939 (4)	0,189 (1)	6,25 (4)	2,40 (2)	1,50 (1)	0,532 (4)	10,87 (7)
18	0,218 (2)	11,26 (5)	4,38 (2)	940 (4)	0,144 (1)	6,12 (6)	2,15 (2)	1,345 (14)	0,408 (4)	10,16 (10)
19	0,213 (1)	10,57 (4)	4,46 (2)	940 (4)	0,146 (1)	6,08 (6)	2,19 (2)	1,380 (14)	0,439 (5)	10,23 (11)
20	0,204 (1)	9,58 (4)	4,64 (2)	939 (4)	0,186 (2)	6,17 (6)	2,36 (2)	1,464 (15)	0,511 (5)	10,69 (11)
21	0,200 (2)	9,54 (4)	4,63 (2)	936 (4)	0,201 (1)	6,27 (4)	2,38 (2)	1,50 (1)	0,523 (3)	10,86 (7)

TABLE 3. Mass Fractions of Nuclides of TPE, Related to the Initial Uranium, in Samples of Fuel Elements at the End of Irradiation, 10^{-6}

No. of sample	^{243}Am	^{242}Cm	^{244}Cm
1	2,2 (5)	1,0 (1)	0,41 (4)
2	—	0,22 (2)	0,023 (2)
4	1,4 (4)	0,79 (8)	0,19 (2)
5	2,3 (5)	1,2 (1)	0,38 (3)
6	1,6 (4)	0,93 (8)	0,19 (2)
7	1,8 (5)	0,65 (6)	0,37 (4)
8	440 (40)	42 (1)	233 (6)
9	340 (40)	44 (1)	225 (5)
10	13 (1)	4,4 (5)	2,1 (2)
11	48 (4)	10 (1)	9,6 (9)
12	99 (5)	17 (2)	42 (5)
13	93 (5)	15 (2)	34 (4)
14	106 (5)	17 (2)	41 (5)
15	13,6 (11)	6,34 (11)	3,28 (8)
16	11,4 (10)	5,78 (20)	2,41 (11)
17	79 (8)	20,6 (6)	37,4 (10)
18	57,5 (16)	16,0 (3)	21,9 (6)
19	65 (4)	16,4 (4)	23,9 (10)
20	74 (8)	19,3 (5)	35,6 (13)
21	110 (5)	24,9 (5)	39,8 (12)

TABLE 4. Average Deviations of the Calculated Values of the U, Pu, Am, and Cm Nuclide Content from the Experimental Data, %

Nuclides	ROR	UNIRASSOS	ROR	UNIRASSOS
	$\varepsilon = 3,3$ %		$\varepsilon = 3,6$ %	
^{235}U	3,3	4,3	6,7	9,4
^{236}U	25	15	14	5,7
^{239}Pu	6,7	6,3	12	8,2
^{240}Pu	7,4	7,0	17	3,6
^{241}Pu	11	12	4,2	4,4
^{242}Pu	12	11	8,3	4,8
^{243}Am	—	47	—	22
^{244}Cm	—	41	—	19

The fuel-element samples were dissolved in a solution of 8 M HNO_3 at t = 90-95°C. The solution obtained was diluted with 2 M HNO_3 to a concentration of about 2 mg/ml with respect to uranium. Weighed aliquots were taken from the solution for measurement of the mass fractions of isotopes of U, Pu, Nd, and ^{137}Cs. The mass fraction of uranium was determined by the differential spectrophotometry method [3]. The error of the uranium determination amounted to 0.4%. The concentration of Pu was measured by the isotopic dilution method with ^{238}Pu in conjuction with α-spectrometric analysis [4]. The isotopic composition of U and Pu after their chromatographic purification was measured mass-spectrometrically, except for ^{238}Pu, for which α-spectrometry was used.

The chemical extraction of Am and Cm from the solutions was carried out after separation of U and Pu. The separation of the total rate-earth and transplutonium elements (TPE), coprecipitated previously with lanthanum fluoride, was carried out by the method of electromigration [5] and extraction [6]. The mass fraction of the nuclides Am and Cm in samples 1-7 and 10-14 was determined by the method of direct α-spectrometric analysis of the total TPE fraction. For this, the fraction which comprised the Am and Cm in the total TPE fraction was monitored by the α-line of ^{242}Cm (E = 977.6 J), easily identified in the α-spectrum of the initial fuel solution. In order to increase the sensitivity and to reduce the error, samples 8-9 and 14-21 were analyzed by using the method of isotopic dilution with ^{241}Am and ^{244}Cm in conjunction with α- and mass-spectrometric analysis [7].

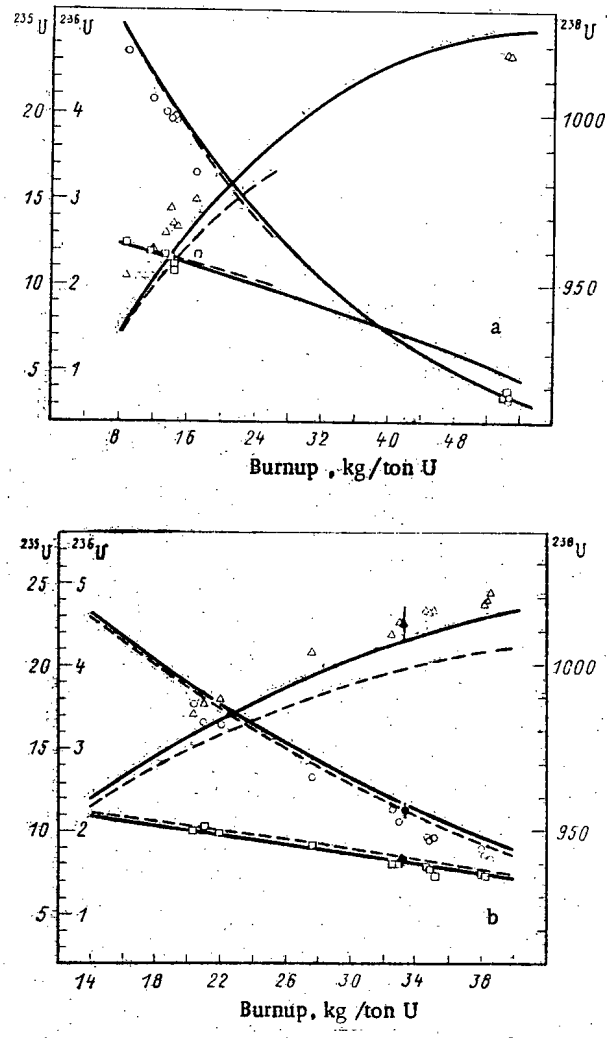

Fig. 2. Dependence of the content of isotopes of U (in kg/ton U) on the fuel burnup for $\varepsilon = 3.3$ (a) and 3.6 % (b): —— and ---) calculation programs UNIRASSOS and ROR; ○, △, □) ^{235}U, ^{236}U, ^{238}U (data of present paper); ▲, ●, ■) data of [10].

The fuel burnup was determined by three methods: by the change of isotopic composition of the actinide elements [8], by the content of ^{148}Nd, and by the content of ^{137}Cs in the fuel [2, 8]. Table 1 shows the results obtained by these methods and also the weighted mean burnup values. When calculating the weighted mean values of the burnup, a weighting inversely proportional to the error of each method was used. It can be seen from Table 1 that these values coincide with one another within the limits of the measurement error. The conclusion can be drawn, therefore, that migration of ^{137}Cs over the height of the VVÉR-440 fuel elements is absent right up to a burnup of 55 kg/ton U.

Tables 2 and 3 show the measurement results of the content of U, Pu, Am, and Cm nuclides in the fuel-element samples investigated at the end of irradiation. For comparison of these results with the calculated isotopic composition of the fuel by the program used at the nuclear power station for the computation of the content of actinide nuclide in spen fuel-element assemblies, Figs. 2 and 3 show the calculated curves of the content of U and Pu nuclides versus the fuel burnup in VVÉR-440 fuel-element assemblies with $\varepsilon = 3.3$ and 3.6%, obtained by the ROR program [9]. The calculations of the isotopic composition of the fuel by this program were performed at the Novovoronezh nuclear power station. Figures 2-4 show the similar curves of the content of U, Pu, Am, and Cm nuclides versus the fuel burnup, obtained by the UNIRASSOS program [9]. The UNIRASSOS program, by comparison with the ROR program, contains a number of methodical refinements in the description of the neutron spectrum, the calculation of the effective cross sections for the actinides and fission nuclides, etc. Figures 2-4 also show

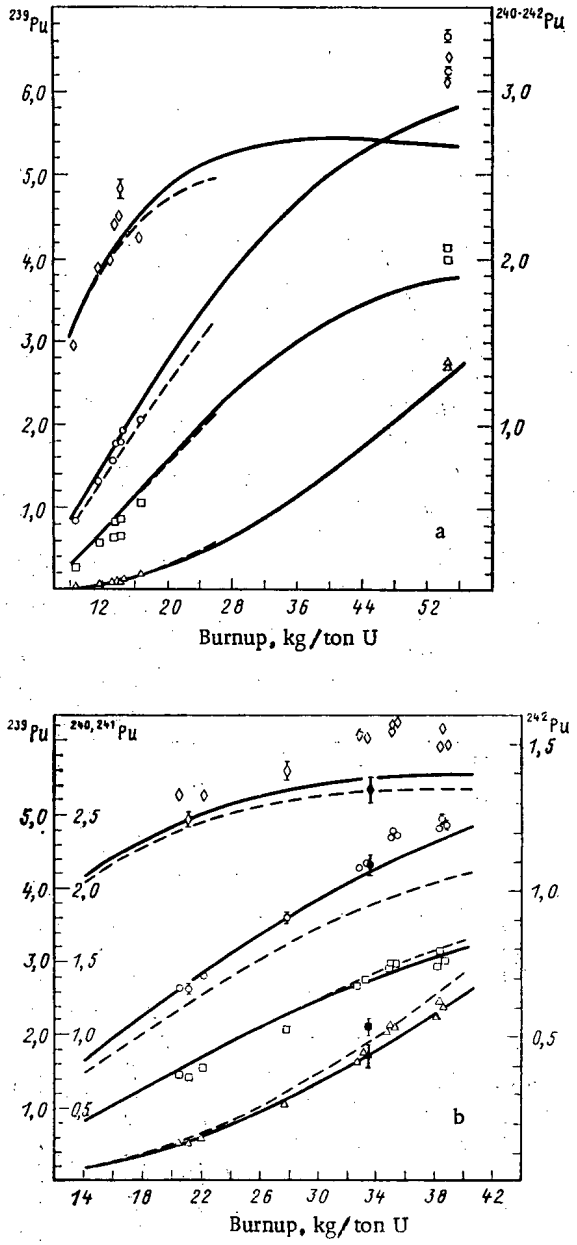

Fig. 3. Dependence of the content of Pu isotopes (in kg/ton U) on the fuel burnup for $\varepsilon = 3.3$ (a) and 3.6% (b): —— and ---) calculation by programs UNIRASSOS and ROR; ◇, ○, □, △) ^{239}Pu, ^{240}Pu, ^{241}Pu, and ^{242}Pu (data of present paper); ◆, ●, ■, ▲) data of [10].

the experimental values of the content of U, Pu, Am, and Cm nuclides in samples of fuel elements, obtained in the present project and in [10], in which a single specimen cut out from the center of fuel element assembly R-3.6 No. 216 was analyzed.

It can be seen from Fig. 2 that for $\varepsilon = 3.3$ and 3.6% the experimental points are systemmatically below the calculated curves for ^{235}U, above for ^{236}U and they coincide with the calculated data for ^{238}U. The experimental data concerning the content of U isotopes, obtained in the present project and [10], coincide within the limits of the measurement error. The systemmatic deviations of the calculated and experimental data are characteristic also for the content of plutonium isotopes (see Fig. 3). For $\varepsilon = 3.3\%$, the experimental points at higher burnup values lie systemmatically above the calculated curves for $^{240,241}Pu$, and for $\varepsilon = 3.6\%$ the same systematic deviation is observed for ^{239}Pu. The experimental and calculated data differ most significantly for ^{243}Am and ^{244}Cm (see Fig. 4). With a fuel burnup of less than 22 kg/ton U, the calculated content of these nuclides is greater than the experimental data by a factor of 1.5-2. It should be noted also that a deviation is observed also in the

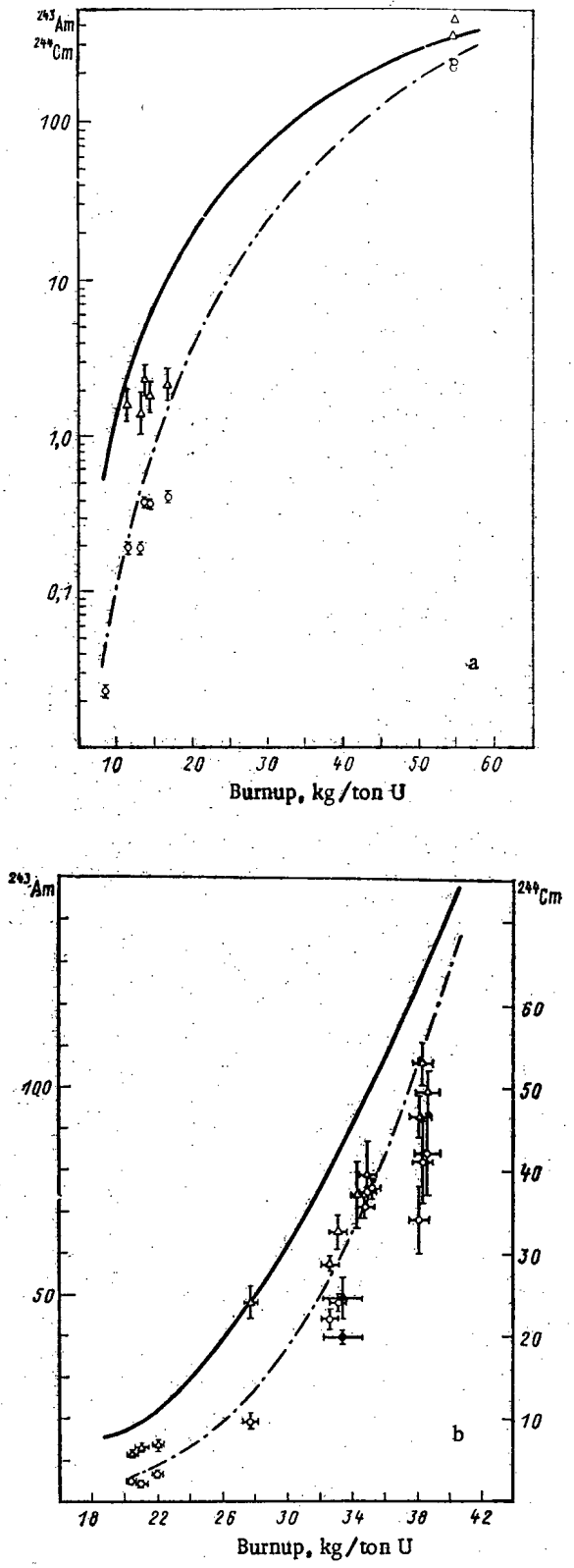

Fig. 4. Dependence of the content of ^{243}Am and ^{244}Cm (in kg/ton U) on the fuel burnup for $\varepsilon = 3.3$ (a) and 3.6% (b): —— and ---) calculated content of ^{243}Am and ^{244}Cm by the UNIRASSOS program; Δ, ○) ^{243}Am and ^{244}Cm (present paper); ▲, ●) data of [10].

experimental data on the content of ^{239,241}Pu, obtained in the present project and in [10]. It is possible that this is related with fundamental difficulties of the α-spectrometric method used by the authors of [10] for measuring the isotopic composition of plutonium.

Table 4 gives the average deviations of the calculated content of U, Pu, Am, and Cm nuclides, obtained by means of the ROR and UNIRASSOS programs, from experimental data of two groups of fuel-element samples. It can be seen from Table 4 that for different nuclides the deviation amounts to 3.3-47% and that the UNIRASSOS program gives a somewhat better agreement with the experimental data for the majority of nuclides. The systematic deviations of the calculated and experimental data, obviously, can be reduced significantly by means of a correction of the effective cross section used in these programs, by the procedure described in [11].

It can be seen also from Figs. 3 and 4 that the spread of the experimental points for similar burnup values, exceeds the experimental error for certain nuclides of plutonium and TPE. This same relationship is observed also for the VVÉR-365 fuel [1, 2]. This spread may be related with local variations of the neutron spectrum from fuel element to fuel within the fuel-element assembly and over the height of the fuel elements, and also with unevaluated systematic errors in the experimental data, associated with dissolution of the samples. The volume of experimental data obtained in this present project and in [10], on the content of nuclides of plutonium and the transplutonium elements in certain fuel elements located at the periphery and in the inner region of the fuel-element assemblies, are still insufficient for the investigation of the dependence of the isotopic composition of the fuel on the location of the fuel element in the fuel-element assembly and the position of the sample cut out along the height of the fuel element. Further experimental and computational investigations are required for this. It should be noted also that the spread of the experimental points in the case of similar burnup values of the fuel for the majority of the plutonium and TPE nuclides is significantly less than the systematic deviation of the calculated and experimental data.

LITERATURE CITED

1. Yu. B. Novikov, V. Ya. Gabeskiriya, and M. N. Maslennikova, At. Energ., 43, No. 4, 278 (1977).
2. A. V. Stepanov et al., At. Energ., 49, No. 4, 225 (1980).
3. M. V. Ryzhinskii et al., in: Chemistry of Uranium [in Russian], Nauka, Moscow (1981).
4. A. A. Lipovskii and Yu. V. Khol'nov, in: Proceedings of a Symposium on Safeguarding Nuclear Materials [in Russian], Vol. 2, IAEA-SN-201/65, Vienna (1976), p. 165.
5. T. Makarova et al., J. Radioanal. Chem., 58, 113 (1980).
6. B. F. Myasoedov, N. P. Molochnikova, and I. P. Lebedev, Zh. Anal. Khim., 26, 1984 (1971).
7. B. N. Belyaev et al., Radiokhimiya, 24, No. 2, 185 (1982).
8. V. Ya. Gabeskiriya, V. V. Gryzina, and Yu. B. Novikov, At. Energ., 43, No. 4, 240 (1977).
9. A. N. Kamyshan and A. N. Novikov, in: Proceedings of a Symposium on Reactor Burnup Physics [in Russian], Vienna (1973), p. 125.
10. A. G. Zelenkov et al, At. Energ., 51, No. 1, 53 (1981).
11. J. Luffin, Z. Szatmary, and J. Vanuxcem, J. Nucl. Energy, 26, 627 (1972).

SURFACE STATES OF CONSTRUCTIONAL MATERIALS AFTER PROLONGED OPERATION IN BASIC SYSTEMS IN POWER STATIONS CONTAINING RBMK-1000 REACTORS

V. M. Sedov, P. G. Krutikov, N. V. Nemirov, A. I. Grushanin, N. M. Papurin, V. M. Egorov, and A. P. Eperin

UDC 621.039:620.193.01

The surface state of a constructional material is determined to a considerable extent by the properties of the metal and by the action of the medium in contact with it [1, 2]. It has previously been shown [2-4] that the state and physicochemical properties of surfaces alter at various stages in the operation of nuclear power station equipment starting with the installation period.

Considerable interest therefore attaches to the surface states of a power-station system after prolonged operation (over 60,000 h). The surface state and properties of the metal after such a time are determined only by the interaction with the working medium. There should be no effect from the initial state or from the various activating or passivating treatments during startup.

Here we examine results obtained on equipment surfaces in the steam and condensate-feed sections in a nuclear power station containing RBMK-1000 reactors that have been in operation for over 60,000 h. The opened-up equipment (separator and steam superheater, and deaerator) and the pipelines were examined visually, and samples of deposits were taken at accessible points and the specimens were sectioned. The chemical and phase compositions of the surface corrosion products were determined [5], both friable and firmly attached to the metal. The electrochemical behavior of the metal surface was examined by comparative analysis of anodic potentiodynamic curves [5]. Figure 1 shows the deposit sampling points and specimen cutting ones.

On all the surfaces there were deposits consisting of a continuous friable upper layer of red-brown color and a lower one firmly adhering to the metal. The total amount of corrosion products forming the film was on average 90-95 g/m^2 on steel 20 in steam, while on

TABLE 1. Compositions and Amounts of Corrosion Products on Inner Surfaces of Equipment

Deposit sampling point	Working conditions	Constructional material steel	Phase composition, mass %			Chemical composition, mass %					Amount of products, g/m^2
			FeO	Fe_3O_4	α-Fe_2O_3	Fe	Mn	Cr	Ni	Cu	
Pressure tube, PÉN-5	Water, 165 °C	20	—	39	61	74,6	0,2	0,4	0,09	0,05	—
Deaerator* (wall of guide apparatus)	Water, 164 °C, $p \approx 7$ MPa	OKh18N10T	—	—	100	69,2	0,07	0,9	0,07	0,05	65±10
Deaerator, upper part	Steam, 164°C $p \approx 7$ MPa	3	—	27	73	70,4	0,8	0,03	0,02	0,044	90±15
Deaerator, lower part	Water, 164 °C	20	—	15	85	69,8	0,15	0,45	0,08	0,02	—
Live-steam pipe in second stage of SSH	Steam, 280°C $p \approx 65$ MPa	20	26	20	54	—	—	—	—	—	95±15
Steam pipe after HCP† in first stage of SSH	Steam, 211°C, $p \approx 19$ MPa	OKh18N10T	—	—	—	—	—	—	—	—	10±3
Pipe for separated water from SSH	Water, 136 °C	OKh18N10T	—	—	—	—	—	—	—	—	50±10

*Only friable part of deposits.
†High-pressure cylinder.

Translated from Atomnaya Énergiya, Vol. 55, No. 3, pp. 145-147, September, 1983. Original article submitted September 21, 1982.

 0038-531X/83/5503-0572$07.50

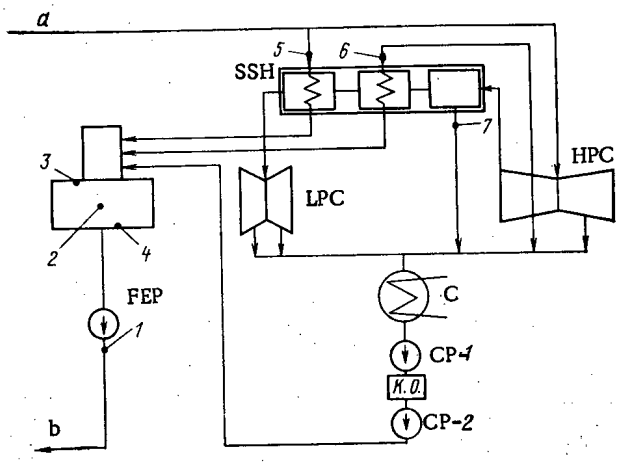

Fig. 1. Essential scheme for the condensate-feed section in a nuclear power station containing RBMK-1000 reactiors: 1) pressurized pipe for feed electric pump FEP; 2) wall of guide apparatus in deaerator ($p \approx 7$ MPa, $t = 164.2°C$); 3) upper part of deaerator (at manhole); 4) lower part of deaerator tank; 5) live-steam pipe in second stage of separator and steam superheater SSH; 6) steam pipe in first stage of SSH ($t = 210.7°C$, $p = 19$ MPa); 7) separated water pipe ($t = 135.9°C$); a) from separator drum ($p_0 \approx 65$ MPa, $t = 280.4°C$, $x_0 = 0.995$); b) in separator drum; LPC) low-pressure cylinder; C) turbine condenser; CP-1 and CP-2) condensate pumps of first and second stages.

steel OKh18N10T in water it was 50-65 g/m^2, and in steam it was 10 g/m^2. The amount of deposit on the metal was very small for such a prolonged operating period. Table 1 gives the chemical and phase analyses, which show that the composition of the surface corrosion products (as one of the characteristics of the surface state) differs from that after manufacture, during installation, and during the first years of operation [3, 4, 6].

A basic component of the friable layer was hematite, and the composition of the deposits was averaged over the contour, as previously observed [3, 6]. The formation of α-Fe_2O_3 indicates that there is an oxidizing medium in the working zone. The firmly adhering film on the pearlitic steel is more complicated in composition (Table 1): In the layer adjoining the metal in the case of the steam exposure there was up to 26% of oxide of wüstite type (FeO), followed by magnetite (Fe_3O_4), and hematite (α-Fe_2O_3) in the upper layer. This structure for the firmly adhering layer and the presence of wüstite are unusual for the normal working conditions of systems and loops in power systems, since the stability range of wüstite lies above a temperature of 570-575°C [7]. With the neutral-oxidizing conditions that are becoming more common in thermal power engineering, it has also been found that wüstite occurs in the viscous sublayer of the dense part of the deposits [8]. It seems that the formation of FeO in our case confirms that oxidizing processes occur at the inner surface of the loop.

After 13,000 h [6] and 21,000 h [3], the friable deposits in the major systems contained maghemite γ-Fe_2O_3. The firmly adhering corrosion products on the surfaces of major systems after installation [4] contain up to 20% γ-Fe_2O_3, which in these cases can be explained as due to formation during the manufacture of the pipes and equipment (thermal scale). Under working conditions, the surface layer on the metal is reformed, and the previously formed oxides are gradually removed and carried off into the loop. This reforming may last more than two years [3].

The above does not rule out the presence of a very thin film of maghemite (below the sensitivity of phase analysis) formed on top of the magnetite on further oxidation in air (not under working conditions). In particular, galvanostatic chronopotentiometry showed that there was a small amount of γ-Fe_2O_3 at the surface of the dense part of the deposits on the wall of the guide section of the deaerator (OKh18N10T steel), which closer to the metal passed into a mixed spinel, which contained chromium and nickel.

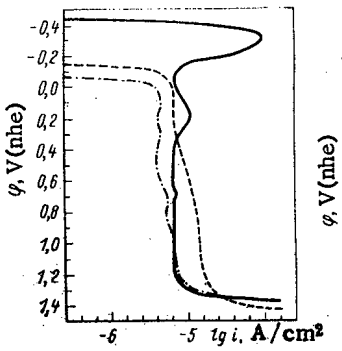

Fig. 2

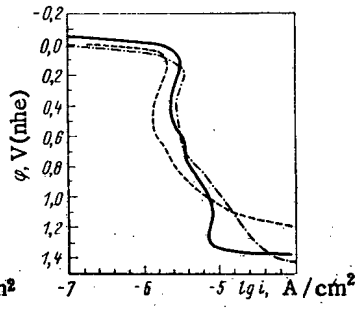

Fig. 3

Fig. 2. Anodic potentiodynamic curves for steel 20 in borate buffer (pH = 7.4; t = 20 ± 2°C): solid line, ground surface; broken line, in aerated borate buffer after 60,000 h of operation; dash–dot line, the same in deaerated borate buffer (here and in Fig. 3 nhe is the normal hydrogen electrode).

Fig. 3. Anodic potentiodynamic curves for steel OKh18N10T in borate buffer (pH = 7.4; t = 20 ± 2°C): solid line, ground surface; broken line and dash–dot line, after operation in water and steam.

The anodic potentiodynamic curves characterizing the electrochemical behavior of specimens cut from the equipment are given in Figs 2 and 3; there is no region of active dissolution on curves 2 and 3 in Fig. 2 (segments from a pipe taking steam to the separator and steam superheater), which is a characteristic feature when the surface has an adhering oxide film providing protection. The anode current in the passive region differs little from the current for the ground surface and is reduced somewhat when oxygen is eliminated from the electrolyte. The curves of Fig. 3 do not show substantial differences in behavior between the ground surface of the stainless steel and that after prolonged operation in liquid and vapor media. The deposition of corrosion products and the growth of an oxide layer have only slight effects on the protection.

Therefore, there are substantial changes in structure and properties in the surfaces of equipment made from pearlitic steel during prolonged operation. The composition and structure of the oxide layer indicate that neutral oxidizing conditions are set up in the live-steam pipelines and in the drainage pipes for the separator and steam superheater on account of the oxygen produced by radiolysis. This must be borne in mind in devising the technological conditions during startup and shutdown. The amounts of corrosion products on the carbon steel in the steam system are comparatively small after prolonged operation and are 95 ± 15 g/m^2; the initial oxide layer is reformed during operation, and the reformation lasts more than two years.

LITERATURE CITED

1. A. Adamson, Surface Physical Chemistry [Russian translation], Mir, Moscow (1979).
2. V. M. Sedov et al., At. Energ., 47, No. 5, 340 (1979).
3. V. M. Sedov et al., ibid., 46, No. 1, 23 (1979).
4. V. M. Sedov et al., ibid., 50, No. 3, 181 (1981).
5. V. M. Sedov et al., Physicochemical Methods of Examining Chemical Processes within Loops in Nuclear Power Station Systems: AINF-529 [in Russian], TsNIIatominform., Moscow (1980).
6. P. G. Krutikov et al., Teploenergetika, No. 6, 13 (1978).
7. K. Narida, The Crystal Structure of Nonmetallic Inclusions in Steel [Russian translation], Metallurgiya, Moscow (1969).
8. I. I. Chudnovskaya, Teploenergetika, No. 11, 68 (1979).

EFFECTS OF α-PARTICLE RETENTION ON THE CHARACTERISTICS OF AN AMBIPOLAR REACTOR

N. N. Vasil'ev and M. G. Kuznetsov

UDC 621.039.624

Recently, much attention has been given to the analysis of the reactor aspect of traps with ambipolar plasma containment. Concepts have been proposed [1-5] that show that such a reactor can have certain advantages over other systems with magnetic containment. One of the major advantages of an ambipolar reactor is that in principle it is possible to have a completely stationary mode of operation. At first sight, that state is realized automatically, since there is no need to maintain closed currents in the plasma by the creation of a vortex electric field, while the helium product and the impurities can be removed from the reactor in a natural fashion along the magnetic lines of force. However, the longitudinal containment time for the ions in the central trap is exponentially dependent on the charge, and therefore the helium concentration may become impermissibly high if there is a strong source of α particles and no transverse transport [1, 6]. The rate of helium accumulation in the central trap can be reduced substantially by designing the magnetic system in such a way that the adiabatic condition is not obeyed for most of the α particles produced. However, this design is not favored by energy considerations, particularly for a reactor with thermal barriers, since in that case it is not clear how one heats the ions in the central trap, which is in addition to the purely constructional problems (with a thick radiation shield, it is complicated to provide a large magnetic-field gradient).

The most suitable method of effective elimination of α particles from the central trap without losing their power would be to extract thermalized helium ions transverse to the magnetic field in the wall region. The helium emerges along the lines of force from this region in the absence of a potential barrier there (this has been demonstrated in experiments with the TMX [7]). The following are mechanisms that provide for rapid transverse helium-ion transport: classical transport due to the inverse density gradient in the main plasma and/or temperature and potential gradients, neoclassical diffusion associated with the absence of axial symmetry in the magnetic field at the ends of the central trap, and anomalous transport processes.

The scope for classical transport in an inverse gradient has been considered in the project for the TMR ambipolar reactor (without thermal barriers) [1], where it was shown that this mechanism becomes important only for $\beta \geqslant 0.95$. The following is the balance equation for the thermalized α particles, which includes the source and the longitudinal and transverse losses:

$$1/4 \langle \sigma V \rangle n_i^2 = n_\alpha/\tau_\parallel + n_\alpha/\tau_\perp$$

and from this one readily gets an expression relating the proportion of helium $C_\alpha = n_\alpha/n_i$ and β. The longitudinal time $\tau_\parallel$ can be estimated from Pastukhov's formula, while the transverse-loss time can be estimated from Rozenblyut's expression for the flux of α particles in the presence of a density gradient for the main ionic component:

$$\Gamma_{\alpha i} = \frac{6 \cdot 10^{-12}}{\sqrt{T}\, B^2 (1-\beta)} \left(Z_\alpha n_\alpha \frac{\partial n_i}{\partial r} - n_i \frac{\partial n_\alpha}{\partial r} \right).$$

As $n_\alpha/\tau_\perp = -\mathrm{div}\, \Gamma_{\alpha i}$, we substitute for all the derivatives $\partial n/\partial r \sim n/a$, $\partial^2 n/\partial r^2 \sim n/a^2$ as regards order of magnitude for estimation purposes, for the characteristic values of the temperature T, density n, magnetic field B, and plasma radius a in the TROL reactor [4], which can give $C_\alpha = 0.28$ with $\beta = 0.95$ and $C_\alpha = 0.48$ with $\beta = 0.9$. At such high β, however, it is not obvious how one stabilizes the MHD instabilities in the plasma, in particular the cylinder modes.

Translated from Atomnaya Énergiya, Vol. 55, No. 3, pp. 148-151, September, 1983. Original article submitted December 8, 1982.

0038-531X/83/5503-0575$07.50

Studies have been made [8, 9] on the use of neoclassical mechanisms for transverse α-particle transport, also for a reactor without thermal barriers. It is found that this method is effective only with a large quadrupole component in the magnetic field at the ends of the central trap, which is very complicated to produce in a system with thermal barriers. It may also be that in the axially symmetrical configurations there will be some anomalous processes leading to marked particle diffusion transverse to the magnetic field. It is therefore of interest to examine the characteristics of a reactor containing thermal barriers in relation to the transverse particle-containment time without going into the details of the particular mechanisms providing this transport.

The analysis indicates that the reactor characteristics may deteriorate not only on account of the accumulation of helium. The fast α particles during thermalization make a considerable contribution to the pressure, which is comparable with the pressure from the main plasma. This makes it necessary to increase the magnetic field in the central trap, which automatically causes an increase in the volume of the plasma in the closing traps and therefore a reduction in the power amplification coefficient Q. The constraints on β related to the MHD stability of the plasma are amongst the decisive parameters in estimating the viability, so trapping of fast α particles may be unfavorable.

Here we use a zero-dimensional model in parametric analysis of the effects of α-particle containment on the characteristics of an ambipolar reactor with thermal barriers. The parameters are the fast α-particle trapping coefficient and the transverse containment time in the central trap $\tau_{\perp}^{c}$.

Plasma-Physics Model. The model is based on the zero-dimensional energy and particle conservation equations. Also, n and T denote the plasma density and temperature (the subscripts are: i ions, e electrons, α thermalized α particles, f fast α particles, while the superscripts c, p, and b denote the parameters in the central trap, the plug traps, and the thermal barriers correspondingly).

1. The following is the energy equation for the ions in the central trap:

$$\frac{3}{2}\frac{\partial}{\partial\tau}\left[(n_i^c+n_\alpha^c)\,T_i^c\right]=K_f W_{i\alpha}^c+W_{i\perp}^c+W_{ie}^c-W_{i\parallel}^c-W_{i\perp}^c-W_{icx}^c-W_{iB}^c.$$

Here on the right with plus signs we have the energy sources from the α particles, the neutral-beam injection, and the energy exchange with the electrons correspondingly. The negative terms represent the energy sinks due to longitudinal and transverse particle loss, charge transfer, and burnup correspondingly; K_f is the proportion of trapped fast α particles $(0\leqslant K_f\leqslant 1)$. The temperature of the thermalized helium ions is taken as equal to the temperature of the fuel ions. The particles escaping along the lines of force carry off energy $Z\Delta\Phi^c+T_i^c$, where $Z\Delta\Phi^c$ is the ambipolar barrier for particles with charge Z. The intensity of the longitudinal losses is determined from the modified form of Pastukhov's formula [10].

Particles escaping radially with frequency $1/\tau_{i\perp}^c$, carry off energy equal to the temperature at the surface of the plasma $T_{ia}^c\approx 0.01T_i^c$, and the transverse times may be different in general for the fuel ions and the helium.

2. The following is the energy equation for the electrons in the central trap:

$$\frac{3}{2}\frac{\partial}{\partial\tau}\left(n_e^cT_e^c\right)=K_f W_{e\alpha}^c+2\frac{V^p}{V^c}W_e^{p\to c}-W_{ie}^c-W_{eR}^c-W_{e\parallel}^c-W_{e\perp}^c.$$

In this equation, the sources are provided by the specific power transferred from the α particles and the electrons trapped in the plug traps correspondingly, while the sinks are represented by the specific power of the energy exchange with the ions (the electrons as a rule are hotter), together with radiation and the longitudinal and transverse losses; V is plasma volume. The electrons emerging along the lines of force carry off energy $T_e^c+\Phi^c$, where Φ is the ambipolar plasma potential. The electons emerging in the transverse direction with frequency $1/\tau_{e\perp}^c$ carry off energy equal to the temperature at the plasma surface $T_{ea}^c\approx 0.01T_e^c$. The energy exchange between the electrons trapped in the plug traps and the escaping ones, whoese concentration is equal to the concentration in the thermal barriers,

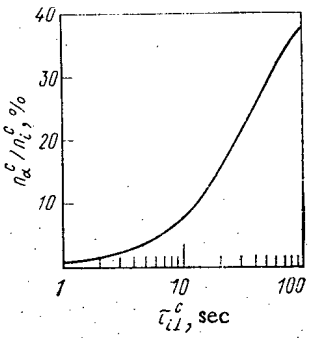

Fig. 1

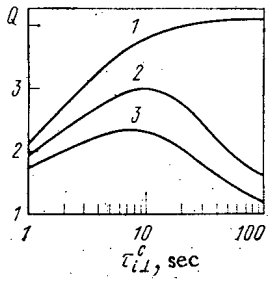

Fig. 2

Fig. 1. Dependence of the accumulation of thermalized helium n_α^c/n_i^c on transverse containment time $\tau_\perp^c$ in the central trap with complete fast α-particle trapping.

Fig. 2. Dependence of Q on $\tau_\perp^c$ with fast α-particle trapping coefficients of 0 (1), 0.5 (2) and 1 (3).

occurs in part via a potential barrier of height $\Delta\Phi^c + \Delta\Phi^b$, where $\Delta\Phi^b$ is the thermal barrier [11], and in part by radical electron diffusion in the plug traps with frequency $1/\tau_{e\perp}^p$. The latter on attaining the periphery of the plasma with its low potential barrier transfer to the group of escaping ones. The overall specific power in the exchange between the electron components is

$$W_e^{p\to c} = [(n_e^p - n_e^b)(1/\tau_e^{p\to c} + 1/\tau_{e\perp}^p)](T_e^p - T_e^c).$$

3. The following is the energy equation for the electrons in the plug traps:

$$\frac{3}{2}\frac{\partial}{\partial\tau}[(n_e^p - n_e^b)T_e^p] = W_{eI}^p + W_{eHF}^p - W_{eR}^p - W_e^{p\to c}.$$

Here the energy sources are the specific power in the energy exchange between the hot injected ions and the uhf heating correspondingly, while the sinks are the losses by radiation and by particle exchange with the escaping component.

4. The following is the conservation equation for the fuel ions in the central trap:

$$\frac{\partial}{\partial\tau}n_i^c = \frac{I^c}{V^c}\eta_i^c n_i^c - \frac{n_i^{c2}}{2}\langle\sigma V\rangle_{D-T} - \frac{n_i^c}{\tau_{i\parallel}^c} - \frac{n_i^c}{\tau_{i\perp}^c}.$$

Here I is the fast-atom injection current and η_i^c is the ion-trapping coefficient, which is determined by ionization and charge transfer.

5. The following is the ion-conservation equation for a plug trap:

$$\frac{\partial}{\partial\tau}n_i^p = \frac{I^p}{2V^p}\eta_i^p - \frac{n_i^p}{\tau_{i\parallel}^p} - \frac{n_i^p}{\tau_{i\perp}^p}.$$

Here η_i^p is the ionization coefficient for the neutral beam. The longitudinal ion-containment time $\tau_{i\parallel}^p$ may be determined from formulas that approximate the results of Föcker–Planck calculations.

6. The following is the conservation equation for the thermalized α particles:

$$(\partial/\partial\tau)n_\alpha^c = n_i^{c2}/4\langle\sigma V\rangle_{D-T}K_f - n_\alpha^c/\tau_{\alpha\parallel}^c - n_\alpha^c/\tau_{\alpha\perp}^c.$$

This system of equations is supplemented with the conditions for electrical neutrality:

$$n_e^c = n_i^c + 2\,(n_\alpha^c + n_f^c);\ n_e^p = n_i^p$$

and the balance equation for the ion and electron current, from which one determines the ambipolar potential Φ^c:

$$\frac{n_i^c}{\tau_{i\parallel}^c}+\frac{n_i^c}{\tau_{i\perp}^c}+2\left[\frac{n_\alpha^c}{\tau_{\alpha\parallel}^c}+\frac{n_\alpha^c}{\tau_{\alpha\perp}^c}+\frac{n_i^{c2}}{4}\langle\sigma V\rangle_{D\text{-}T}(1-K_f)\right]+\frac{n_i^p}{\tau_{i\parallel}^p}+\frac{n_i^p}{\tau_{i\perp}^p}-\frac{n_e^c}{\tau_{e\parallel}^c}-\frac{n_e^c}{\tau_{e\perp}^c}-\frac{n_e^p}{\tau_{e\parallel}^p}=0.$$

The potential barrier is

$$\Delta\Phi^c = \Delta\Phi'' - \Delta\Phi^b;\ \Delta\Phi'' = T_e^p \ln\left[\frac{K^p n_e^p}{n_e^c}\left(\frac{T_e^c}{T_e^p}\right)^{1/2}\right].$$

Here $K^p = n_e^p\max/n_e^p$ is the inhomogeneity coefficient for the longitudinal distribution of the particle density in the plug trap ($K^p \approx 2$ for a sinusoidal profile). The thermal barrier is taken proportional to the electron temperature $\Delta\Phi^b \sim T_e^c$.

The pressure due to the fast α particles is calculated from

$$P_f = 2/3 n_f^c E_f^0 \gamma_f,$$

where

$$n_f^c = n_i^{c2}/4\,\langle\sigma V\rangle_{D\text{-}T} K_f t_s;\ t_s \approx 3.2\cdot 10^8 \frac{A_i^c T_e^{c3/2}}{\Lambda_{fe} n_e^c};$$

$$\gamma_f\,(T_e^c) \approx 0.6 - 0.7;\ E_f^0 = 3520\ \text{keV}$$

Results and Discussion. We selected the current and injection energy for the central and plug traps together with the power of the additional uhf electron heating for Q was maximal with given geometrical dimensions, fusion power, thermal load at the first wall, and maximal magnetic field in the plugs. The calculations were performed for a reactor with a fusion power of about 800 MW and a neutron load of 1 MW/m^2 [4]. The length of the central trap and the plasma radius in it were 40 and 2.25 m correspondingly, while the maximal magnetic field in a plug was 14 T. However, certain parameters were altered relative to the project: With a vacuum spiral ratio in the plug trap $R^p = 2$, the length of the latter was 3.5 m. Also, with the addition of thermal barriers the injection energy in the plug traps was reduced to 500 keV. The limiting value of β in the central and plug traps was taken as 0.6, while the magnetic field in the central trap varied from 1.6 to 2.4 T in the various forms in accordance with the plasma pressure. Correspondingly, the radius of the plasma in the plug traps varied from 1 to 1.25 m. In the calculations, the height of the thermal barrier was taken as twice the electron temperature in the central trap [12]. The transverse component-containment times in the corresponding traps were taken as identical. The following are typical plasma parameters (these may vary slightly from case to case):

Fuel ion density in central trap, cm^{-3}	5×10^{13}
Mean deuterium ion density in plug trap, cm^{-3}	7×10^{13}
Temperature, keV:	
fuel and helium ions in central trap	30
electrons in central trap	45
electrons in plug trap	70
Plasma potential in trap, kV:	
central	130
plug	210
Thermal barrier height, kV	90

Figures 1 and 2 give the results. The equilibrium helium content may attain 40% of the fuel ion density (Fig. 1) with complete containment of the fast α particles ($K_f = 1$) and in the absence of vigorous transverse transport $\geqslant \tau_{i\perp}^c$ 100 sec. Here Q exceeds 1 only slightly (Fig.

2). On reducing $\tau_{\perp}^{c}$ to 10 sec, the proportion of helium is reduce by a factor of five, which approximately doubles Q. However, any further reduction in $\tau_{\perp}^{c}$ below 5-10 sec reduces Q on account of the marked increase in the power required to maintain the plasma density and temperature in the central trap. A similar dependence of Q on $\tau_{\perp}^{c}$ is observed for $K_f = 0.5$. An interesting point is that the optimum value of $\tau_{\perp}^{c}$ is approximately equal to $\tau_{\parallel}^{c}$. For the case $K_f = 0$ (fast α particles not contained), the dependence of Q on $\tau_{\perp}^{c}$ is monotone, and one then gets the largest value of Q, since the heating of the ions in the central trap by escaping electrons is fairly extensive with the moderate thermal-barrier height assumed here.

These results show that Q does not exceed four in spite of the use of thermal barriers, and this is substantially below the values given for example in [2]. It should be remembered however that these calculations have been performed with a more conservative assumption about $\Delta\Phi^{b}$ and lower fusion power.

The following conclusions are drawn from this study on the effects of α-particle containment on the characteristics of an ambipolar reactor with thermal barriers.

With the constraints imposed on β for the central plug traps, the trapping of fast α particles may be harmful on account of their considerable contribution to the plasma pressure.

As partial containment and subsequent thermalization of the α particles will always occur, one has the problem of providing sufficiently rapid radial plasma diffusion in the central trap with a characteristic time comparable with the longitudinal-containment time.

LITERATURE CITED

1. R. Moir et al., LLL, UCRL-52302 (1977).
2. B. Badger et al., UWFDM-400, Wisconsin (1980).
3. R. Moir et al., LLL, UCID-18808 (1980).
4. N. N. Vasil'ev et al., At. Energ., 52, No. 2, 113 (1982).
5. G. Carlson, Nucl. Fusion, 22, No. 5, 695 (1982).
6. H. Cohen, Nucl. Fusion, 19, No. 10, 1295 (1979).
7. E. Hooper et al., in: Proc. 10th European Conference on Plasma Physics and Controlled Nuclear Fusion Research, Vol. 1, Moscow (1981), p. C18.
8. T. Kammash and D. Galbraith, ibid., p. C12.
9. T. Kammash et al., in: Proc. 9th IAEA Meeting on Plasma Physics and Controlled Nuclear Fusion Research, Geteborg (1982).
10. D. Galbraith and T. Kammash, Plasma Phys., 20, 595 (1978).
11. M. Kuznetsov and A. Skovoroda, in: Proc. 10th European Conference on Plasma Physics and Controlled Nuclear Fusion Research, Vol. 2, Moscow (1981), p. J18.
12. M. Lontano, L. S. Pekker, and R. Pouuoli, Fiz. Plazmy, 6, 793 (1980).

DEFORMATION AND FAILURE IN OKh16N15M3B STAINLESS STEEL IRRADIATED TO A FLUENCE OF 1.4×10^{23} neutrons/cm^2

S. A. Averin, E. N. Loguntsev, A. N. Filonin, I. S. Golovnin, O. S. Korostin, and V. V. Romaneev

UDC 669.14.018.8:539.12.04

There are many papers on radiation embrittlement in stainless steels, particularly at high temperatures, but as a rule they present results from simulation with accelerators (V. F. Zelenskii et al., Nuclear Science and Engineering, Physics of Radiation Damage and Radiation Material Science Series [in Russian], Issue 4(18) (1981), p. 3).

Transmission electron microscopy and scanning electron microscopy TEM and SEM have been applied to the dislocation structure and the signs of slip produced by deformation as well as the surface morphology in the failure of ring specimens irradiated to a fluence of 1.4×10^{23} neutrons/cm^2 ($E \geqslant 0.1$ MeV). The ring specimens (two rings of diameter 6.1 mm, cross section 2×0.35 mm) were cut from a standard BN-350 fuel pin in which the burnup attained 5.4% of the heavy atoms. This pin was in a fuel-pin cassette that had operated for 267 effective days (160 effective days at a power $N = 0.65N_n$, 91 effective days at $N = 0.52N_n$, and 16 effective days at $N = 0.36N_n$, where N_n is the nominal reactor power). The irradiation temperature was 450-500°C.

The pin cladding was made of OKh16N15M3B steel in the form of a tube of diameter 6.1 mm in the state as supplied without additional heat treatment.

The following are the contents in mass % of the elements in the steel:

C	0,065	Ni	15,15
Mn	0,55	Mo	3,02
Si	0,40	Nb	0,62
S	0,004	N_2	0,036
P	0,015	Fe	Balance
Cr	16,4		

Table 1 gives the strength and plasticity characteristics of the specimens as determined by stretching along the longitudinal axis.

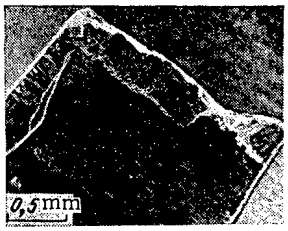

Fig. 1. Point of failure in a polished annular specimen on the inner surface (SEM).

TABLE 1. Mechanical Properties of Fuel-Pin Specimens

Temperature, °C	σ_u, MPa	δ, %	$\sigma_{0,2}$, MPa
20	623,0	47,0	—
375	524,8	33,5	245,3
650	441,6	32,5	—

Translated from Atomnaya Énergiya, Vol. 55, No. 3, pp. 151-153, September, 1983. Original article submitted January 10, 1983.

 0038-531X/83/5503-0580$07.50

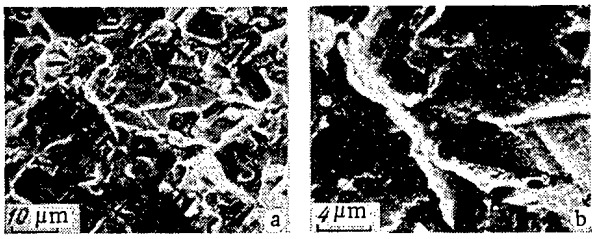

Fig. 2. Failure surface in a ring specimen made of irradiated OKh16N15M3B stainless steel (SEM) at different magnifications.

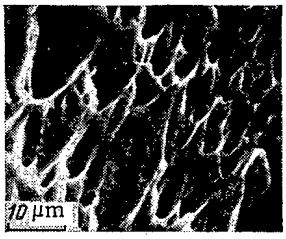

Fig. 3

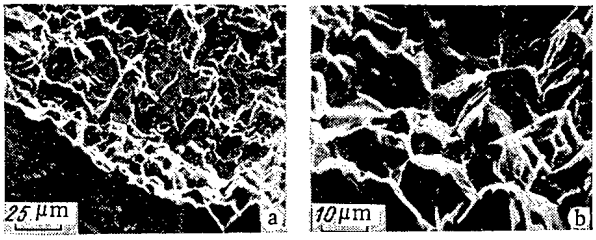

Fig. 4

Fig. 3. Failure surface in OKh16N15M3B stainless steel examined after failure at 500°C (SEM).

Fig. 4. Failure surface in a ring specimen from irradiated OKh16N15M3B stainless steel near the inner side of the ring (SEM) at different magnifications.

Fig. 5. Outer surface of a ring specimen polished before test and cut from irradiated OKh16N15M3B stainless steel near the point of failure.

The irradiated specimens were tested in stretching with a rate of 1 mm/min, test temperature 500°C. One of the specimens was polished electrochemically before testing to reveal signs of slip. The rings after failure in the mechanical tests were examined with an RÉM-200 scanning electron microscope. We examined the outer and inner surfaces of the specimens near the points of failure as well as the failure surface itself. A carbon replica was produced from the outer surface of the polished specimen near the point of failure to provide for more detailed analysis of the slip, and this was examined in an NI-200 transmission electron microscope. The replica was made by the usual method using local shielding. After the surface examination, two-sided thinning was used to prepare foils from part of the ring near the failure point and also from undeformed parts near the clamps for examination in transmission in the NI-200 at an accelerating voltage of 175 kV.

Both rings during the mechanical tests* showed small (about 1.5%) plasticity and high strength parameters ($\sigma_{0.2}$ = 430 and 620 MPa for the polished and unpolished specimens correspondingly).

The fractographic examination of the two specimens showed the following:

*The mechanical tests were performed by A. V. Kozlov.

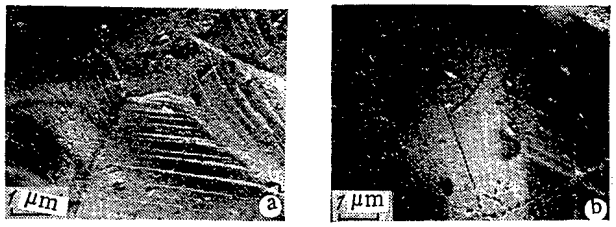

Fig. 6. Signs of slip on the outer surface of a ring specimen of irradiated OKh16N15M3B stainless steel near the point of failure (a) at a distance of 0.1 mm from the point of failure (b) (replica, TEM).

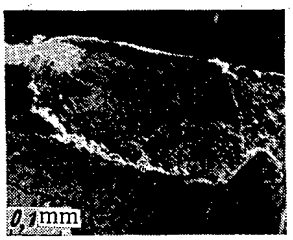

Fig. 7

Fig. 8

Fig. 7. Point of failure in an unpolished ring specimen taken on the inner surface (× 275) (SEM).

Fig. 8. Internal surface of a polished ring specimen near the point of failure (SEM).

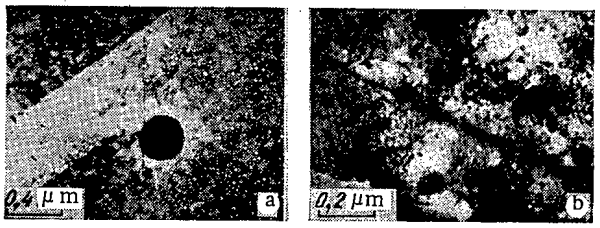

Fig. 9. Structure of the internal layers in the undeformed parts of a ring specimen of irradiated OKh16N15M3B stainless steel.

1. The failure surface in the main lay at 45° to the stretching axis, although there were parts perpendicular to it (Fig. 1).

2. The failure is mainly of transcrystallite character (Fig. 2) with a specific kink different from that usually observed. For example, Fig. 3 shows the fractogram for a specimen of unirradiated OKh16N15M3B stainless steel after failure at 500°C.

3. The fractograms showed a zone of intercrystallite failure on the inner side of the ring (Fig. 4) of thickness 2-4 grains (about 60 μm).

SEM examination of the outer surface showed signs of slip near the failure point (Fig. 5) in a zone of width not more than 50 μm. Detailed examination of the signs of slip by the replica method using the TEM confirmed the localization of the plastic deformation. Near the point of failure there were coarse tracks with effective slip transfer from grain to grain. Two slip systems could be seen in many grains (Fig. 6a). At the same time, even at a distance of only 0.1 mm from the point of failure there were signs of slip only in individual grains, and these were smaller and as a rule represented a single slip system (Fig. 6b).

SEM examination of the inner surface showed surface cracks perpendicular to the stretching axis (Fig. 7). The polished specimen showed that the cracks were of grain-boundary type

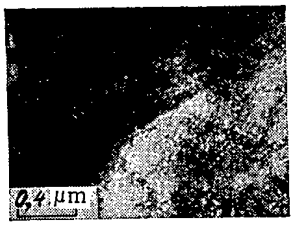

Fig. 10. Structure of the internal layers near the point of failure in a ring specimen of irradiated OKh16N15M3B stainless steel.

(Fig. 8), while signs of slip were absent. TEM examination showed that the inner layers have the usual structure of irradiated stainless steel in the undeformed state, i.e., they contained many pores, small dislocation loops, and small segregations (Fig. 9a). At some points there were phase deposits at the grain boundaries (Fig. 9b). Such a structure without any signs of plactic deformation is characteristic of the whole specimen, including the working part (the parts between the clamps during stretching). Only in narrow parts (0.1-0.2 mm) near the point of failure were there planar groups of dislocations with a very complicated structure resembling deformation microtwins (Fig. 10).

Therefore, we conclude that failure during mechanical tests after reactor irradiation for OKh16N15M3B steel irradiated to a fluence of 1.4×10^{23} neutrons/cm^2 at 450-500°C occurs mainly in a transcrystallite fashion with high strain localization.

ACTIVATION METHODS FOR DETERMINING THE CONTENT OF OXYGEN, NITROGEN, AND FLUORINE IN NUCLEAR FUEL

V. V. Ovechkin, V. I. Melent'ev, B. D. Rogozkin, V. F. Kononov, and A. E. Khokhlov

UDC 543.51/53-621.039.54

Information on the content of oxygen, nitrogen, and other elements in oxygen-free compounds of uranium and plutonium is necessary in order to standardize the chemical composition and treatment of fuel cores. In particular, a high content of oxygen in monocarbide cores can lead to liberation of free carbon, accelerated carbonization, and premature breakdown of the fuel jacket. When preparing cores made of mixed (U + Pu) mononitride, it is very important to eliminate both the formation of free metal and the appearance of excessive nitrogen, which lead to considerable degradation of the radiation properties of the fuel cores and to embrittlement of the fuel jacket after irradiation, respectively.

The currently widely used methods of chemical analysis have some significant disadvantages and limitations. For this reason, it is advantageous to use nondestructive activation methods for determining the content of oxygen and nitrogen, as well as of fluorine, in the cores and powders of nuclear fuel, which, as will be evident from what follows, do not have the disadvantages indicated. These methods, which have been developed over the last ten years, and are intended for use primarily in domestic equipment and apparatus, are being successfully used to solve different problems, related with improvement of the technology of obtaining nuclear fuel.

Equipment and Apparatus. We activated the specimens with the help of a NG-150I neutron generator with maximum neutron flux $2 \cdot 10^{11}$ sec^{-1} (E = 14 MeV). We monitored the neutron flux with the help of monitor based on a semiconductor Si(Li) detector [1], calibrated according to the activity induced in an aluminum specimen. To transport the specimens, we used a pneumatic tube conveyor with a polyethylene pneumatic tube with an inner diameter of 12 mm.

We recorded the induced activity with 150 × 150 mm (well size 33 × 70 mm) scintillation NaI(TI) detectors and two scintillation blocks based on the single crystal NaI(Tl) with dimensions 150 × 100 mm, entering into the composition of the SÉG-2-16 spectrometric setup ("Angara"). To investigate the γ spectra, we used a DGDK-50 Ge(Li) detector together with a SÉS-2-03 type setup ("Langur") and a multichannel pulse-height analyzer. We controlled all stages of the analysis according to fixed time regimes with the help of an automatic control block.

Translated from Atomnaya Énergiya, Vol. 55, No. 3, pp. 153-157, September, 1983. Original article submitted March 30, 1983.

0038-531X/83/5503-0583$07.50

Preparation of Specimens. We prepared specimens from oxygen free compounds of plutonium, uranium, and their mixture from powders obtained by carbidization and nitriding of metals and alloys in an atmosphere of propane and nitrogen, respectively, as well as carbidization of uranium and plutonium oxides with carbon [2].

We prepared control specimens with a diameter of 5-6 mm and a height of 4-13 mm with a density of 80-96% of the theoretical value by pressing. To introduce a fixed amount of oxygen, we added the computed amount of plutonium dioxide.

Determination of Oxygen Content. The neutron-activation method for determining the oxygen content is based on the nuclear reaction $^{16}O(n, p)^{16}N$, occurring under the action of fast neutrons ($E_n > 10$ MeV). The nuclide ^{16}N with a comparatively short half-life ($T_{1/2} = 7.3$ sec) that forms has a high γ-ray energy ($E_\gamma = 6.13$ MeV, yield 69%), which makes it possible to develop an efficient and selective method of analysis. The application of this method to analysis of fissioning substances (U—Pu) taking into account the interfering β^- and γ radiation of the fission products is validated in [3]. The possible noise from the competing reaction $^{19}F(n, \alpha)^{16}N$ was also pointed out [4].

To attain the minimum limit for determining the oxygen content, we chose the optimum conditions: the energy region for recording the γ radiation (5.3-7.4 MeV), time regimes ($t_{irr} = 30$ sec, $t_{cool} = 3$ sec, $t_{rec} = 30$ sec), admissible neutron flux density for a given mass of the specimen, etc. For separate specimens of nuclear fuel, based on the uranium and plutonium nuclides the specific number of pulses per 1 g of each nuclide was measured under identical conditions for performing the analysis. Relative to ^{238}U, it constitutes 1.69 ± 0.08 for ^{235}U and 1.16 ± 0.06 for ^{239}Pu, which agrees satisfactorily with the computed results (1.6 and 1.18, respectively), obtained taking into account the fission cross sections [5, 6], yield of fission products [7], and quantum yields of γ radiation [8].

During the analysis, we used two ^{238}U specimens with an oxygen content of $C_c \leqslant 0.001\%$ (oxygen-free) and $C_{cs} = 0.5$ % as the control specimens. We determined the oxygen concentration in the specimens studied (index "S") from the equation

$$C_s^O = C_{cs}^O \frac{n_s - Kn_c C_s^f}{n_{cs} - Kn_c C_{cs}^f}. \quad (1)$$

Here the symbols have the following meaning: c indicates the control oxygen-free specimens; cs indicates the control specimens with an oxygen content of 0.5%; O indicates oxygen; f indicates a fissioning substance; "5" indicates ^{235}U; "8" indicates ^{238}U; "9" indicates ^{239}Pu; $K = 1.69\ C_S^5 + C_S^8 + 1.16\ C_S^9$ is the ratio of the number of pulses from a specimen of mixed fuel to the number of pulses from a specimen of ^{239}U with the same value of the product ΦM (Φ is the indication of the neutron monitor, M is the mass of the specimen) in the chosen energy range for recording the induced activity; $n = (N - N_\Phi)/M\Phi$ is the reduced number of pulses; N_p is the number of pulses from the specimen; N_b is the background number of pulses from an empty irradiated container; C^O and C^f are the concentrations of the oxygen and fissioning element in the specimen, respectively.

We estimated the limit for determining oxygen using Eq. (2), obtained based on recommendations in [9]:

$$\eta = \frac{164\sqrt{N_p C_s^f}}{n^O M_s}\%, \quad (2)$$

where $n^O = (n_{cs} - Kn_c C_{cs}) \frac{\Phi_s}{C_{cs}}$ is the number of pulses from 1 g of oxygen.

In recording the activity of ^{16}N with two 150×100 mm NaI(TI) scintillation detectors, $\eta = 1.14 \cdot 10^{-2}$%; when using a 150×150 mm detector with a well, $\eta = 4 \cdot 10^{-2}$%. The relative mean-square deviation for determining the oxygen content is ~ 0.7% and in a specimen with mass ~ 2 g constitutes 9%. The results of the analysis of the content of oxygen impurities in the fuel using the neutron activation method agree with data obtained by other methods (for example, chemical).

We shall examine the characteristics of the high-accuray determination of the oxygen content in the oxidized (U + Pu) fuel with the composition MeO_x [10]. To decrease the error in determining the oxygen ratio $x \approx 2$, related with the fluctuation of the neutron flux while

irradiating the specimen, we surrounded the specimen by an oxygen-containing "observer." Before recording, we separated the "observer" from the specimen and then we recorded the activity of the specimen and of the "observer" using separate NaI(Tl) detectors with a well. If we denote the atomic masses of oxygen and of the fissioning substance by A_o and A_f, then for $A_f/A_o \gg x \approx 2$, we can obtain the following expression from Eq. (1):

$$n_m = ax + b, \tag{3}$$

where

$$a = (A_o/A_f)\frac{n_O}{a_m};\ b \approx n_c.$$

Therefore, with the help of the calibration dependence $n_m = f(x)$, it is possible to determine the oxygen ratio x from the results of measurements on irradiated control specimens and the specimens being analyzed.

For each specimen, we performed a series of 6-7 irradiations and measurements using the following scheme: 20 sec for irradiation, 3 sec for transportation and holding, and 20 sec for recording. For three of the specimens (mixed oxide fuel, UO_2 and uranium with an oxygen-containing substance), we determined the relative mean-square deviation according to 12-14 parallel series and, in addition, the intervals between the two successive series constituted not less than 6 min, so that over this time the activity from the preceding series decreased considerably and did not affect the results of the subsequent measurements. The values obtained $\delta = \pm (0.8\text{-}1.2)\%$ made it possible to obtain errors of $\pm 1\%$ with five parallel determinations of x for the same specimen over a time ~ 1 h. It was established that in the mixed oxide fuel, the fluorine content, which does not make an appreciable contribution to the error in determining the factor x, is less than $3 \cdot 10^{-2}$ % and is determined comparatively easily by the $(\alpha, p\gamma)$-reaction method. Satisfactory agreement was obtained between the results of the neutron-activation determination x in fuel specimens and results of independent methods of analysis.

We note that in analyzing batches of fuel cores, the real time of the analysis for a single core can be decreased 3-4-fold by alternate and repeated irradiations and measurements on 5-6 specimens. In this case, the total error in determining x for identical fuel cores, proportional to $(n)^{-1/2}$, can also be decreased.

Determination of the Nitrogen and Fluorine Content. The neutron-activation method for determining the nitrogen content in uranium is based on using the nuclear reaction $^{14}N(n,2n)^{13}N$, which occurs when specimens are irradiated with neutron energies ~ 14 MeV. We recorded the subsequent annihilation radiation ($E_\gamma = 511$ keV) with a single Ge(Li) detector or two NaI(Tl) detectors, connected in a fast-slow coincidence circuit. The choice of such a system for recording the activity of the positron emitter ^{13}N ($T_{1/2} = 9.96$ min, $E_{\beta+} = 1.19$ MeV) guarantees an effective decrease in the influence of γ radiation of the fission products forming in the specimen under the action of the neutrons. Thus, more than 20 peaks were recorded in the energy range 0.3-1.0 MeV. Analysis of the decay curves for the region of the 511-keV peak permitted separating half-lives of 17 and 4 min. The dependence of the ratio of the areas of peaks at 511 and 590 keV on the mass of the uranium specimens (0.778, 1.23, 2.58, and 4.43 g) was measured. It was established that $\sim 30\%$ of the area of the peak at 511 keV is due to the interaction of high-energy γ radiation from the fission products with the uranium matrix, leading to the formation of positrons and annihilation radiation. The remaining part of this peak is apparently formed by γ radiation from the fission products.

There are elements whose nuclides after irradiation with 14-MeV neutrons become, just as ^{13}N, positron emitters with comparable half-lives and can create interferences in determining small concentrations of nitrogen. The content of elements in fuel cores with large neutron capture cross sections is strictly limited, so that Sm, Se and the halogens (Cl, Br), whose residual content must be very small, can be neglected. Most of the other product inhibiting the reaction, aside from annihilation radiation, also emit γ radiation, the use of which it is possible to take into account correctly the corrections in determining nitrogen. It is also necessary to introduce corrections to the real content of the impurities Cu, Zn, and other elements with a large cross section for the reaction (n, 2n).

As in determining the oxygen content, to transport the specimens, we used 11 × 30 mm stainless steel transport containers, into which we placed polyethylene ampuls containing the specimens, extracted after irradiation, for the measurements. To eliminate the corrections related with the large self-absorption of the annihilation radiation in uranium, we prepared specimens for analysis and the control specimens with approximately the same dimensions and masses. As a result of the investigations performed with the semiconductor Ge(Li) detector, the following regime for the analysis turned out to be the optimum regime: 5-min irradiation, holding for 1 min, 1.5 min for recording, 20 sec for recording the data, and 10 sec for holding. The time between two successive measurements of the spectra was 2 min.

Measurements on two NaI(Tl) detectors, connected into the fast-slow coincidence circuit (resolution time $2\tau \approx 30$ nsec) with two angles of the relative position of the irradiated specimen ($\theta = 180°$ and 90°) confirmed the conclusion that γ emission of the fission products makes a significant contribution in the energy range ~ 511 keV. Optimum conditions for the analysis were chosen: specimen-detector distance $R_{opt} = 200$ mm and specimen mass 1-1.5 g including the actual neutron flux density in the specimen ($6 \cdot 10^8$ cm^{-2}·sec^{-1}). The computed dependences of the limit of determination of nitrogen for different time regimes were obtaned on a computer. Thus, for $t_{irr} = 5$ min, tcool = 1 min, and $t_m = 20$ min, these limits turned out to equal $\sim 5 \cdot 10^{-2}$ and $\sim 7 \cdot 10^{-2}$ % using a coincidence circuit with two NaI(Tl) 150 × 100 mm detectors and a single Ge(Li) detector (sensitive volume ~ 50 cm^3).

There is some reserve in decreasing the limit of determination of the elements indicated due to the increase in the neutron flux density and the irradiation time (to 20-30 min). The results of the calculations were confirmed by direct measurements on the control specimens. For a neutron flux density of $\sim 10^8$ cm^{-2}·sec^{-1} and a mass of the uranium specimen of 5 g, the limit of determination was $3.5 \cdot 10^{-2}$ %. For 11 parallel determinations, the following values of the mean-square deviation were obtained: 11% with a nitrogen content of $C_N = 2.5\%$; 6.5% with $C_N = 3.23\%$ and, 5.4% with $C_N = 4.2\%$. The improvement in accuracy (by 30-40%) is achieved by using the method of monitoring the neutron flux density according to the number of pulses from the irradiated specimen in the additional regions of the γ spectrum. Thus, for example, in the scintillation variant, the region ~ 1.2 MeV was chosen for this purpose. For the Ge(Li) detector, we used the γ energy peak at 590 keV (^{93}Sr). The results of determining nitrogen in several uranium specimens agree satisfactorily with data on the amount of nitrogen introduced. We note that with a high content of nitrogen, the use of semiconductor Ge(Li)detectors, due to the relative simplicity of the recording system, is preferable to the scintillation variant.

In the nuclear-physical method of determining light elements (nitrogen, fluorine), in mixed fuel (U + Pu) used above, the α emission of Pu, capable of inducing different nuclear reactions with emission of γ quanta, is used. Compared with the analysis of plutonium [11], the application of such a method to the analysis of a mixed fuel [12] has two peculiarities: possible presence of additional α emitters in highly enriched ^{235}U, for example, ^{232}U and its fission products, and somewhat lower yield of reactions per unit mass of mixed fuel. For this reason, for the control specimens, it is necessary to use specimens with an identical composition of α emitters in the nuclear fuel or to introduce corrections for differences in the composition.

We measured the nitrogen content with the help of a Ge(Li) detector relative to the areas of the γ peaks at energies 0.871 and 0.756-0.770 MeV (^{239}Pu); the time required to measure a single spectrum was 30 min. We compared the values obtained with the calibration curve and determined the content C_N. The relative mean-square deviation, determined for 20 parallel measurements, constituted from 10 to 7% for a nitrogen content of 3.5-7.5%. Comparison of the results of the analysis of 15 specimens of fuel with mass 0.43-3.843 g and a nitrogen content of 1.79-7.50% by mass gave good agreement with the results obtained by Kjeldahl's method. The limit of determination of nitrogen, calculated from the results of measurements on the control specimen over a time of 60 min, constituted $\eta \approx 5 \cdot 10^{-2}$%; when the mass of the specimen was increased to 5 g and the measurement time was increased to 4 h, η decreased to $\sim 1 \cdot 10^{-2}$%.

The fluorine reaction induced by the α particles from Pu is accompanied by the emission of high-energy γ radiation with energies of 1.275 and 2.082 MeV [13], which can be used to determine the fluorine content in plutonium and in the mixed fuel. In particular, in recording γ radiation with energy 2.082 MeV with the help of a NaI(Tl) detector with dimensions 150 × 150

mm with a well, in which the Pu specimen is placed, surrounded by a lead shield with a thickness of 3 mm, the limit of determination is $6 \cdot 10^{-4}$%, which scaled to the mixed fuel $3 \cdot 10^{-3}$% (specimen mass is 5 g, time for the measurements is 2 h).

Conclusions. As is evident from the material presented, activation methods of analysis of mixed (U + Pu) fuel are quite rapid and provide the possibility of determining the content of oxygen, nitrogen, and fluorine in them in quantities varying from several units $\times 10^{-2}$%, which is entirely acceptable for solving many technical problems. These methods are nondestructive. Therefore, in analyzing the fissioning materials, problems related with the possible contamination of the surrounding medium do not arise; in addition, valuable materials and parts are saved for further use.

However, the use of activation methods is complicated by some difficulties, related with the operation and technical servicing of the complex equipment, in particular, the neutron generator.

1. M. G. Borodulin et al., Applied Nuclear Spectroscopy [in Russian], Vol. 2, Atomizdat, Moscow (1971), p. 138.
2. F. G. Reshetnikov, B. D. Rogozkin, and M. G. Shishkov, At. Energ., 35, No. 6, 377 (1973).
3. V. I. Melent'ev and V. V. Ovechkin, Radiokhimiya, 18, No. 1, 161 (1976).
4. D. Taylor, Neutron Radiation and Activation Analysis [Russian translation], Atomizdat, Moscow (1965), p. 134.
5. M. Cance and G. Grenies, Nucl. Sci. Eng., 68, No. 2, 197 (1978).
6. I. D. Alkhazov et al., At. Energ., 47, No. 6, 416 (1979).
7. E. A. C. Crouch, At. Data Nucl. Data Tables, 19, No. 5, 419 (1979).
8. J. Blachot and C. Fiche, At. Data Nucl. Data Tables, 20, No. 3, 241 (1977).
9. D. Soete, R. Gijbels, and J. Hoste, in: Neutron Activation Analysis. Chemical Analysis, Wiley, New York (1972), p. 34.
10. V. F. Kononov et al., At. Energ., 46, No. 4, 259 (1979).
11. V. V. Ovechkin, V. I. Melent'ev, and V. F. Gorbunov, Radiokhimiya, 18, 152 (1976).
12. V. I. Melent'ev and V. V. Ovechkin, At. Energ., 48, No. 3, 179 (1980).
13. V. V. Ovechkin, At. Energ., 48, No. 1, 48 (1980).

RADIATION DIMENSIONAL STABILITY OF GRAPHITE WITH AN UNCALCINED COKE-FILLER

I. P. Kalyagina
and Yu. S. Virgil'ev

UDC 621.039.532.21

Graphite based on uncalcined petroleum coke is one of the strongest carbon materials, obtained by the traditional electrode technology. The use of this coke facilitates the formation of a monolithic structure without distinct boundaries between the grains of the coke-filler and the coke binder, thus affecting the dimensional stability of a product made from such graphite [1].

During radiation testing domestic coarse-grained graphite based on uncalcined petroleum coke with a pitch-binder was observed to behave in a significantly different way under irradiation than do graphites with a calcined coke-filler. At an irradiation temperature of 900-1220°K and a neutron fluence of up to $0.8 \cdot 10^{22}$ neutrons/cm^2* the specimens were not observed to shrink and the isotropic growth of size at a neutron fluence of $\sim 1.3 \cdot 10^{22}$ neutrons/cm^2 did not exceed 1% [2].

*Here and henceforth fluence is given for neutrons with $E \geqslant 0.18$ MeV.

TABLE 1. Properties of Materials Investigated

Characteristic	Reactor graphite	CGG	FGG
Density, tons/m^3			
volume	1,65—1,75	1,86—1,90	1,89—1,92
pycnometric	2,18—2,19	2,21—2,22	2,10—2,12
x-ray	2,254	2,254	2,260
Lattice parameters, 10^{-1} nm			
c	6,742	6,742	6,760
a	2,461	2,461	2,466
Axial dimensions of CSR, nm			
c	14	14	13
a	85	85	57
Degree of graphitization*	0,80	0,80	0,70
Degree of texturization†	1,60	1,10	1,20
Thermal expansion coeff., K^{-1}‡			
	2,5—4,1 / 3,4—4,6	5,9—6,1 / 6,0—6,2	7,1—7,2 / 6,0—6,2
Tensile strength, MPa			
compression	30—40	70—90	100—120
bending	7—13	28—33	47—52

*Calculated from the lattic parameters of [5].
†From the data of x-ray analysis.
‡In the range 300-400°K for directions parallel (numerator) and perpendicular (denominator) to the axis of formation.

Translated from Atomnaya Énergiya, Vol. 55, No. 3, pp. 157-159, September, 1983. Original article submitted May 4, 1982.

 0038-531X/83/5503-0588$07.50

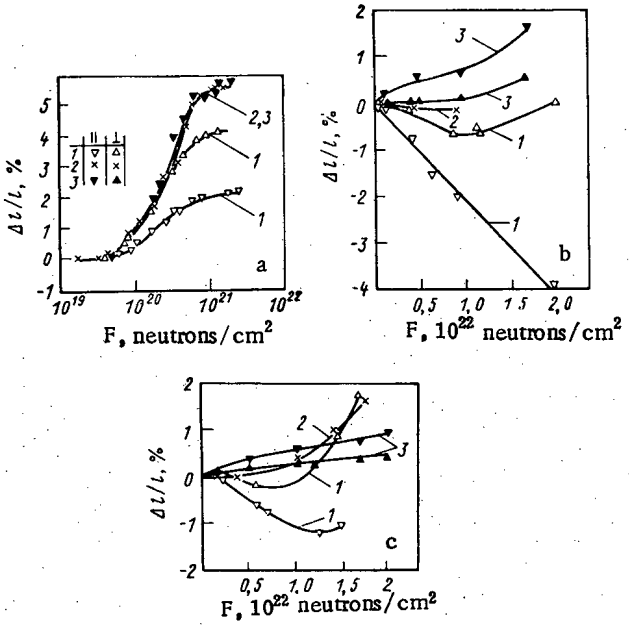

Fig. 1. Relative changes in the length of specimens of reactor graphite (1), CGG graphite (2), and FGG graphite (3), cut parallel and perpendicular to the axis of formation, as a function of the neutron fluence at an irradiation temperature of 320-340 (a), 720 (b), and 1120-1220°K (c).

TABLE 2. Influence of Irradiation at Different Temperatures and a Fluence of (0.6-0.8)•10^{22} neutrons/cm² on a Change in the Size of Graphite Specimens

Graphite	Density, tons/m³	Rel. change in volume after irradiation, %	
		720 °K	1120-1220°K
Reactor	1,65—1,72	—3,20	—0,90
CGG	1,86—1,90	—0,45	+0,30
FGG	1,90—1,92	+0,60	+1,20

Continuing this work, we investigated the radiation dimensional stability of fine-grained graphite (FGG) and coarse-grained graphite (CGG), obtained on the basis of uncalcined petroleum coke as well as reactor graphite. In preparing the CGG specimens we preserved the granulometric composition of the filler and the parameters of the technological operations for the production of reactor graphite. The difference consisted only in a slight increase in the amount of coal pitch (to 24 mass %) [3]. The final treatment temperature was 2700-2800°K. The main difference in the technology for the preparation of the fine-grained graphite is that the coke-filler is ground in a vibrating mill to a grain size of less than 150 μm, the binder being 37-40 mass % coal ptich [4]. The temperature at which the FGG specimens were treated was 2700-3100°K. Comparison of the properties of reactor graphite and CGG (Table 1) shows that when this technology is used it is possible to obtain materials with the same degree of perfection of the crystal structure, as indicated by the close values of the degree of graphitization, lattice periods, and dimensions of the coherent scattering region (CSR). The main difference between them is in the anisotropy coefficients of the properties and the density. The density of CGG is higher than that of reactor graphite, owing to the difference in porosity. The level of the total, open, and closed porosity for pycnometric liquids is observed to be much lower in CGG graphite. The degree of anisotropy of the thermal expansion is 1.1-1.4 for reactor graphite, does not exceed 1.16-1.21 for FGG, and is close to unity (1.02-1.04) for CGG. In the case of fine-grained materials the degree of graphitization is

TABLE 3. Relative Changes in Dimensions ($\Delta l/l$) and Volume ($\Delta V/V$) of the Specimens and the Anisotropy of the Deformation (Δy) after Irradiation at 720 and 1120-1220°K to a Fluence of $1.3 \cdot 10^{22}$ neutrons/cm^2, %

Graphite	Density, tons/m^3	Anisotropy of TEC	720 K			1120-1220 K		
			$\Delta l/l$*	$\Delta V/V$	Δy †	$\Delta l/l$*	$\Delta V/V$	Δy
Reactor	1,65—1,72	1,10—1,40	$\frac{-2,60}{-0,45}$	—3,50	2,15	$\frac{-1,20}{+0,40}$	—0,40	1,60
KPG	1,86—1,90	1,02—1,04	$\frac{0,60}{0,60}$	1,80	0	$\frac{1,00}{1,00}$	3,00	0
MPG	1,90—1,92	1,16—1,21	$\frac{1,00}{0,20}$	1,40	0,80	$\frac{0,70}{0,40}$	1,50	0,30

*The numerator is for the direction parallel to the axis of formaion and the denominator is for the direction perpendicular to the axis.
†The anisotropy of the deformation is the absolute value of the algebraic difference of the changes in the lengths of the specimens in the parallel and perpendicular directions.

lower than in reactor graphite (see Table 1), which is due to the long mechanochemical action during grinding and mixing as well as the high content of pitch binder. The use of only a fine filler fraction (90 mass % of the particles had a size of less than 90 μm) and an increased content of binder lead to a significant difference in the porosity of these materials. Materials of the FGG type have finer pores, no larger than 5 μm [5]. At the same time, in coarse-grained CGG graphites pores with a diameter of 5-55 μm occupy 23% of the volume. It is known that when the degree of perfection of the crystal structure is reduced the shrinkage increases with a subsequent acceleration of secondary growth at a high level of irradiation while a decrease in the volume of the pores is accompanied by an accommodation process which leads to a reduction in the radiation shrinkage and an increase in the dimensional changes in the secondary-growth region. Since the total effect depends on the relative contribution of changes in these characteristics of the structure, radiation changes in the dimensions of graphites can be determined only experimentally. For this purpose specimens of the materials mentioned above were irradiated at 320-340, 720, 1120-1220, and 1220-1270°K. At the low temperature (320-340°K) the relative changes in the dimensions of FGG and CGG graphite based on uncalcined coke are large than in the case of reactor graphite. The latter moreover has an appreciably growth anisotropy (see Fig. 1a). The graphites being compared are characterized in this case by an interrelation between the growth of dimensions and the thermal expansion coefficient (TEC) since under low-temperature irradiation no difference appears in the degree of perfection of the crystal structure [6].

Irradiation at 720°K to a fluence of $(0.6\text{-}0.8) \cdot 10^{22}$ neutrons/cm^2 led to a considerable shrinkage of the reactor graphite specimens while the shrinkage was insignificant in the case of CGG graphite and no shrinkage at all occurred in FGG (see Fig. 1b). This range of fluence values is characterized by a decrease in the volume shrinkage with the growth of the density of the materials. As the neutron fluence increases the shrinkage is reduced by "swelling" (Table 2).

Raising the irradiation temperature accelerates the transition to volume swelling of the material. After irradiation at 720°K to a fluence of $1.3 \cdot 10^{22}$ neutrons/cm^2 the specimens of reactor graphite do shrink, but at a slower rate (Table 3). The anisotropy of the deformation in this case remained proportional to the anisotropy of the thermal expansion coefficients of the graphite, measured after irradiation.

At an irradiation temperature of 1120-1220°K the anisotropy of the deformation intensified in the reactor graphite since for the perpendicular direction the shrinkage was reduced by swelling while for the parallel direction the shrinkage rate dropped to zero at a fluence above 10^{22} neutrons/cm^2. For graphites based on uncalcined petroleum pitch we observe swelling, the rate of this swelling being lower for FGG specimens (see Fig. 1c). The deformation anisotropy in this case remained proportional to the anisotropy of the properties of the material and as the density of the graphite increased the volume shrinkage was replaced by swelling. When the FGG grains were ground, however, the swelling was less than for the coarse-grained CGG (see Table 3).

It is thus clear that at a low neutron fluence a reduced degree of graphitization of FGG showed no influence at a low neutron fluence since the material did not shrink during the initial period of irradiation. After prolonged irradiation the characteristics of the crystal lattice of reactor graphite and CGG and FGG graphites are similar. Thus, for 1220°K and a fluence of $2 \cdot 10^{22}$ neutrons/cm^2 the lattice parameters are 0.6770 ± 0.03 nm and 0.245 ± 0.05 nm while the dimensions of the crystallites along the c and a axes are 7-8 and 25-30 mm, respectively. It can be assumed that defects of the type of aggregations of knock-on atoms and vacancies, which are formed after prolonged, low-temperature irradiation are commensurate in size with the crystallite size. The comparatively close values of the coherent scattering regions (CSR) of reactor graphite and FGG graphite create similar conditions for the nucleation of aggregations of defects in their structure. Thus, the difference in the behavior of the graphites compared here is due to the anisotropy and porosity of the material. In this case the main porosity, which accommodates the growth of crystals along the c axis at a low level of irradiation [$(2\text{-}4) \cdot 10^{21}$ neutron/cm^2] is the porosity inherent to the aggregations of crystallites. Materials with uncalcined coke-filler are characterized by the presence of pore-cracks which have an extension of up to several microns and a width of about 250 Å (1 Å = 10^{-10} m) and are separated by a distance of ~ 0.5 μm [7]. In graphites based on uncalcined coke the volume of such pores is smaller than in reactor graphite and the predominant type is that of round pores with a diameter of 0.1-1 μm, which compensate the radiation changes in size less effectively. The dimensional stability of the fine-grained graphite FGG at a high neutron fluence is apparently due to its high strength, which is capable of reducing secondary swelling [8].

LITERATURE CITED

1. G. Engle, Carbon, 9, 539 (1971).
2. I. P. Kalyagina et al., At. Energ., 36, No. 3, 212 (1974).
3. Yu. S. Virgil'ev et al., Khim. Tverd. Topliva, 1, 108 (1978).
4. A. N. Deev and Yu. S. Virgil'ev, Khim. Tverd. Topliva, 6, 145 (1974).
5. Properties of Carbon-Based Structural Materials (Handbook) [in Russian], Metallurgiya, Moscow (1975).
6. V. V. Goncharov et al., Effect of Radiation on Nuclear-Reactor Graphite [in Russian], Atomizdat, Moscow (1978).
7. P. A. Platonov et al., At. Energ., 46, No. 4, 248 (1979).
8. A. Pitner, Carbon, 9, 637 (1971).

METHOD OF CALCULATING THE OPTIMAL NUMBER OF MONITORING POINTS FOR THE LOCAL AND GLOBAL RADIACTIVE CONTAMINATION OF THE ENVIRONMENT

K. P. Makhno'ko

UDC 621.039

Radiational monitoring of the contamination of environmental objects in the vicinity of active atomic power plants is performed by selecting samples at points located around the plant in a radius of up to 12-15 km. In addition, the dose rate of γ radiation in the vicinity is also observed.

If in the normal operation of the plant the dispersion of the results of oberving the radioactive contamination of objects in the local environment is known in advance, then the number of points at which samples must be taken may be calculated by specifying the required accuracy of finding the mean value of the contamination, or also the points may be optimally redistributed [1, 2]. The number of points or the observation frequency may be limited using sampling by the Latin-quadrature system [3]. However, the monitoring system must take account of the possibility of accidental release of radionuclides into the environment, while the probability of observing the consequence of such a release must be sufficiently high, which these methods do not permit.

It is obvious that, as the number of monitoring points n is increased, the results obtained improve, but increase in the number of points also increases the cost of the monitoring network, and so n cannot be increased indefinitely. The optimum number of monitoring points is calculated using the function F(n)

$$F(n)=P(n)/N(n), \tag{1}$$

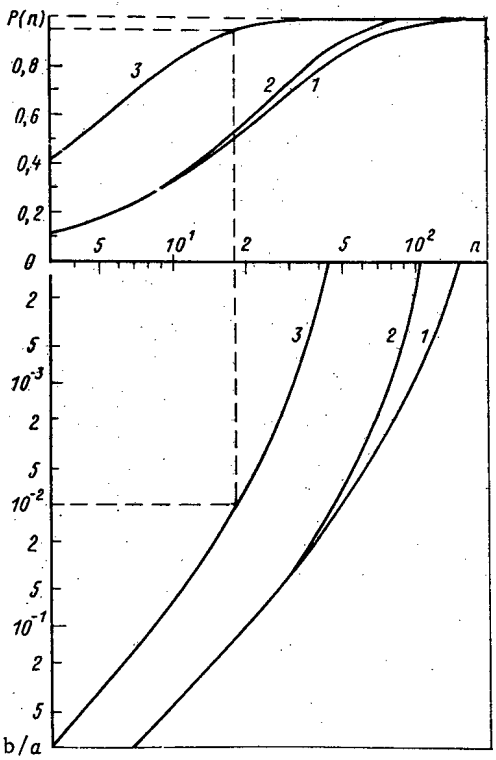

Fig. 1. Relation between the probability P(n) of observing the contaminated zone in the vicinity of an atomic power plant, the number of monitoring points n, and the cost ratio for a single monitoring point and the "control center" b/a with independent (1) and successive dependent (2) choice of points and with contribution of the search region to a single quadrant.

Translated from Atomnaya Énergiya, Vol. 55, No. 3, pp. 160-164, September, 1983. Original article submitted September 20, 1982.

 0038-531X/83/5503-0592$07.50

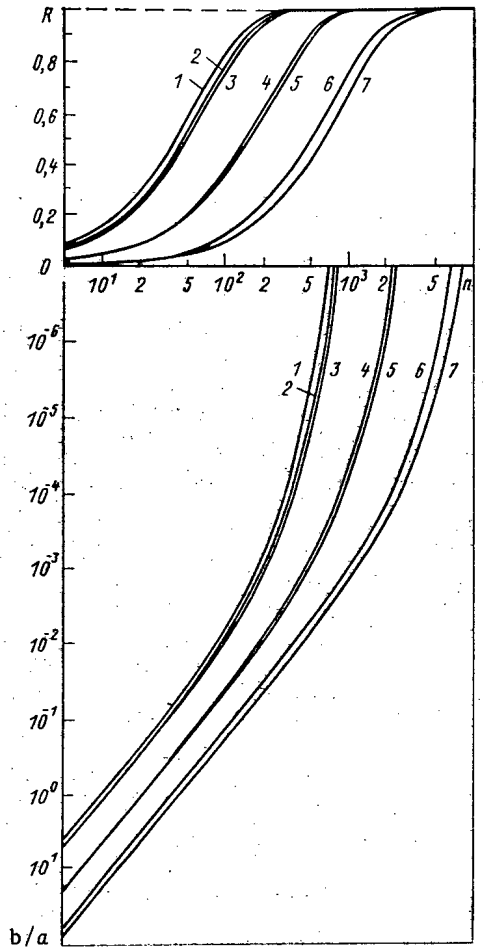

Fig. 2. Relation between the representativeness R of the observation data on the radioactivity field, the number n of observation points, and the cost ratio for one point and the observation center b/a: 1) concentration of β activity in air (USSR): 2) γ-ray dose rate in a radius of 25 km from the atomic power plant; 3, 7) ^{137}Cs concentration in the North Sea and the Pacific Ocean; 4, 6) ^{90}Sr concentration in the Baltic Sea and the Atlantic Ocean; 5) precipitation of β activity from the atmosphere (USSR).

where P(n) is the probability of recording the release; N(n) is the cost of the monitoring system.

Suppose that S_M is the region of action of a single monitoring point determined by the sensitivity of the detector in measuring the γ-ray dose or by the extent to which the given sample is representative; S_0 is the monitoring region in the vicinity of the atomic power plant, the boundaries of which are determined by the sensitivity of the monitoring methods employed. The probability of recording the radioactive release P(n) increases with and increase in the number of points n until the whole of the area S_0 is overlapped by the areas S_M, i.e., with increase in n, the numerator in Eq. (1) reaches saturation. The cost N(n) of the monitoring system increases indefinitely with increase in n, and hence it follows that F(n) has a maximum corresponding to the optimal number of monitoring points n_0, which may be found by setting $dF/dn = 0$. An additional condition is the need for sufficiently high probability of recording the radioactive release.

Equation (1) is general in character, and the form of the functions P(n) and F(n) may be different in different conditions. Some typical cases are considered. Note, as a preliminary, that if the network of monitoring points is regular in character (for example, the points are at the nodes of a grid with a constant step), the step decreases with increase in n, while the probability P(n) reaches a value P(n) = 1 at which the dimensions of the monitored region S_M or the contamination region S_C overlap the dimensions of the grid cell.

TABLE 1. Monitoring Radius r, Optimal Number of Observation Points n_0, and Ratio of the Cost Elements b/a in Observing Radioactivity Fields at R = 70-80%

Region	Radioactivity field	r, km	n_0	b/a, 10^{-3}
Within a radius of 25 km from the atomic power plant USSR	Dose rate of γ radiation	3	80—110	6—14
	Radioactivity in air	350	70—95	7—16
USSR	Radioactive precipitations	175	300—400	2—4
Baltic Sea	^{90}Sr in water	25	260—360	2—5
North Sea	^{137}Cs in water	50	90—120	6—13
Atlantic Ocean	^{90}Sr in water	200	900—1200	0,6—1,2
Pacific Ocean	^{137}Cs in water	250	1100—1500	0,5—1,0

In practice, however, the principle of grid regularity cannot be satisfied, since the position of the monitoring points depends on the presence of roads, populated centers, and other features of the specific locality. The regions S_M corresponding to the individual points may even overlap in regions of intense monitoring. Therefore, the network of monitoring points in the locality usually appears as if the points are positioned randomly. This will be taken into account in the subsequent discussions and the form of the function P(n) will be determined.

Independent Choice of Points

Assume that, as a result of the atmospheric release of radionuclides in the locality, a contaminted region of area S_C is formed. The probability of observation of this region P(n) by taking n samples of soil or vegetation in regions S_0 is found, if the samples are analyzed in the laboratory, i.e., the results of analyzing individual samples are unknown in advance and have no influence on the selection of sampling points. The probability of observation of the contaminated region in selecting a single random sample $p = S_C/S_0$. According to the Bernoulli scheme for successive independent measurements [4], the probability of observing radionuclides in at least one sample is

$$P(n) = 1 - (1 - p)^n. \quad (2)$$

If the radioactive cloud of a single release covers the monitoring points in region S_0 randomly, the probability that it covers at least one point is also expressed by Eq. (2).

Dependent Choice of Points

If the samples selected are analyzed immediately in situ (or the density of radioactive contamination of locality is measured in the field) and the results of the measurements influence the selection of the subsequent monitoring points, the probability of not observing the contaminated region with measurements at a single point is $q_1 = (1 - S_C/S_0) = (1 - p)$. Let $S_C/S_0 = p_M$, the relative dimension of the region over which measurements at its center may extend. Then the probability of not observing the contaminated region in successive dependent measurements at two points is

$$q_2 = (1 - S_C/S_0)\left(1 - \frac{S_C}{S_0 - S_M}\right) = (1 - p)\left(1 - \frac{p}{1 - p_M}\right),$$

and with measurements at i points

$$q_i = (1-p)\left(1-\frac{p}{1-p_M}\right)\cdots\left(1-\frac{p}{1-(i-1)\,p_M}\right).$$

Thus, with successive dependent tests, the probability of observing the radionuclides in a single sample may be written in the form

$$P(n) = 1-\prod_{i=1}^{n}\left(1-\frac{p}{1-(i-1)\,p_M}\right). \tag{3}$$

In deriving Eq. (3), it has been assumed that $S_M \ll S_C$. If this is not the case, then the numerator in the expression $p = S_C/S_o$ must be increased, expanding the boundary of the region S_C by the radius r of a circle of area S_M. In the particular case when the form of the region S_C may be approximated by an ellipse with a semiaxis ratio $\alpha/\beta = k$, the new value of the probability of observing the radioactive release, taking account of the area $S_M = \pi r^2$, is given by the formula

$$p' = p + p_M\left(1+\frac{\alpha+\beta}{r}\right), \tag{4}$$

and hence it follows that $p' \approx p'$ with a relative error

$$\frac{\Delta p}{p} = \frac{1}{k}\left(\frac{r}{\beta}\right)^2\left(1+\frac{1+k}{r/\beta}\right). \tag{5}$$

For example, $p' \approx p$ with an error of 10% if $r \leqslant 7.4\cdot 10^{-2}\beta$ with the typical value $k = 3$.

The form of the function N(n) in Eq. (1) is now determined. The requirements of the monitoring system are composed of the cost of the equipment and operation of the individual monitoring points and the cost of the centralized system of laboratory analysis, information processing, control of the monitoring, etc., called the "control center," for the sake of brevity. In the first approximation, it may be assumed that the cost of such a center does not depend greatly on the number of monitoring points, and is given by the constant a. The cost of the network of monitoring points, conversely, is directly proportional to the number of points n. If b is the cost of a single point, then $N = a + bn$. Substituting this expression into Eq. (1) yields

$$F(n) = \frac{1}{a}\frac{P(n)}{1+\frac{b}{a}n}, \tag{6}$$

where P(n) is determined by Eq. (2) or Eq. (3).

The optimal number of monitoring points n_o is found by equating to zero the derivative of Eq. (6) with respect to n. For independent tests, using Eq. (2), it is found that

$$\frac{a}{b} = \frac{(1-p)^{n_0}-1}{(1-p)^{n_0}\ln(1-p)} - n_0, \tag{7}$$

and hence it is evident that the optimal number of monitoring points depends on b/a. Since the probability of detecting the consequences of the radioactive release must by sufficiently high, it is necessary to make a preliminary selection of the required value of P(n) in Eq. (2) in designing the monitoring system, to determine n, and then substitute this into Eq. (7) so as to find the b/a at which $n = n_o$.

The relation between the parameters of the optimal monitoring network in the vicinity of an atomic power plant is shown in Fig. 1. In the upper part of Fig. 1, the probability of detecting the contaminated region at a radius of 12 km from the plant, as calculated from Eqs. (2) and (3), is shown as a function of the number of points at which samples are taken or control measurements are made. It is assumed here that a single release of radionuclides occurs with weakly unstable atmospheric stratification, when the scattering of the radioactive

cloud occurs, approximately in a sector of 14° [5], which corresponds to $S_C = 17.6$ km^2. The radius of the region over which measurements at the center may extend is 1 km. Curves 1 and 2 are calculated under the assumption that the search for the contaminated region is undertaken in all directions from the power plant. With a small number of monitoring points n, curves 1 and 2 are little different, but they begin to diverge with increase in n. The number of points required for a 90% probability of observing the contaminated region is $n_1 = 58$ (curve 1) or $n_2 = 48$ (curve 2); with $P(n) = 99\%$, $n_1 = 118$ or $n_2 = 90$, i.e., knowing the results of the preceding measurements allows the number of points to be reduced by $n_1/n_2 \approx 1.5$ times. The required number of monitoring points depends strongly on the presence of meteorological information, allowing the region of search for the contaminated region S_0 to be reduced. This is illustrated in curve 3, which is calculated for the case when information on the direction, other conditions being equal, allows the region of search to be confined to a 90° sector. It is evident that, when $P(n) = 99\%$, the number of points is reduced more than fivefold.

In the lower part of Fig. 1, the relation between the number of monitoring points and the cost ratio at the individual monitoring elements at which this number becomes optimal is shown. It is evident that passing from independent selection of the monitoring points to dependent selection decreases the optimal number of monitoring points only when $b/a \leq 10^{-2}$. Then additional meteorological information allowing the region of search for the contaminated area to be reduced to 90° sector reduces the optimal number of monitoring points at all values of b/a.

The dashed lines represent an example of the use of these curves. Specifying the probability of observing the radioactive release $P(n) = 95\%$ in the case when the quadrant in which it may be found is known, a line is drawn parallel to the axis On until it intersects with curve 3. Dropping a perpendicular from here to the axis On, the necessary number of monitoring points is found: $n = 18$. This straight line is extended until it intersects curve 3 in the lower part of Fig. 1. Dropping a perpendicular from here to the vertical exis, the value $b/a \approx 10^{-2}$ at which this network will be optimal is found.

In a series of releases or a sufficiently prolonged release, the case in which the radioactive cloud covers the whole region S_0 is possible. There then arises the problem of estimating how representative the data on the contamination of region S_0 obtained from measurements at n points in the locality are. If S is the area overlapped by n monitoring points, the degree to which this monitoring is representative may be characterized as $R = S/S_0$. Then the increment dS in the area covered by the monitoring points is proportional to the increment in the number of monitoring points dn, the area covered by a single monitoring point S_M, and the normalized number of vacant events $1 - R$:

$$dS = (1 - R)\, S_M\, dn. \tag{8}$$

Passing from dS to dR, and using the initial condition $R = 0$ when $n = 0$, it is found that

$$R = 1 - \exp\left(-\frac{S_M}{S_0} n\right). \tag{9}$$

Equation (9) may be used for calculations of the optimal number of measurement points in observations for any field of radioactivity. For example, with normal operation of the atomic power plant, the configuration of the area S_0 corresponds to the wind pattern, and the dimensions of the area are determined by the sensitivity of the monitoring instruments and the extent of the radioactive release. In observations of the levels of global background radioactivity of the atmosphere using surface monitoring instruments or of the global contamination of the soil–vegetation covering, S_0 is the land area which is monitored; in measuring the radioactivity of surface water or the bottom deposits of water bodies, S_0 is the area of the corresponding water body; in monitoring the quality of the harvest, S_0 is the area of the agricultural fields. The optimum number of monitoring points, as before, is determined from the condition of a maximum of the function in Eq. (6), where P(n) is replaced by R, which leads, on taking account of Eq. (9), to the expression

$$\frac{a}{b} = \frac{1}{p_M}[\exp(p_M n_0) - 1] - n_0. \tag{10}$$

The optimal number of monitoring points for the γ-ray dose rate in the vicinity of an atomic power plant may be estimated using Eqs. (9) and (10). For practical purposes, it is sufficient to have information that is representative to a degree R = 70-80%. Dosimeters are usually used for monitoring over a radius of 25 km from the plant. Assuming that the radius of the area which may be assigned to a single dosimeter reading is 3 km, it follows from Eq. (9) that $n \approx 100$. This number of monitoring points will be optimal if, in accordance with Eq. (10), the cost of a single point is 10^2 times less than the cost of a "monitoring center."

To estimate the optimal number of points of the observation network for fields of radioactivity of global origin, it is assumed that the distance between two adjacent points should not exceed the value r_0 at which the given characteristics of the radioactivity field are still mutually correlated. The correlation radius r_0 is defined as the distance at which the normalized correlation function decreases by a factor e [6]. Then the radius of region S_M in Eq. (9), $r = r_0/2$.

The results of measuring the chemical composition of the monthly atmospheric precipitations in the USSR [7] permit the determination of the correlation radius $r_0 = 350$ km, which may be converted to the results of observing the monthly radioactive precipitation in the period when there are no "fresh" radioactive products in the atmosphere. In observations of the mean monthly concentration of radionuclides in the low-level atmosphere over the USA, using filtering equipment, the correlation radius of the concentration values in a period when there were no nuclear tests was 700 km [6]. This value may also be used for the USSR, since the two countries lie in regions with similar conditions of atmospheric circulation. The mean correlation radii for measurements of the radionuclide concentration in the surface water of seas and oceans estimated from the data of [8, 9] take following values: for the Pacific and Atlantic Oceans, 500 and 400 km; for the North (fall) and Baltic Seas, 100 and 50 km.

The change in the representativeness of data on the radioactivity field with increase in the number of observation points is shown in the upper part of Fig. 2, and the relation between the cost elements of the observation system at which this number of points becomes optimal is shown in the lower part.

In observations of the radioactivity fields of global origin, it is usually sufficient if they are representative to a level R = 70-80%. For this value of R, Table 1 gives estimates of the optimal number of observation points n_0 and the ratio b/a between the cost of a single point and cost of a centralized system for analyzing the selected samples, processing and generalization of the information, control of the observation system, and communications with external structures (called the "observation center," for the sake of brevity). It follows from Table 1 that increasing the number of observation points must be associated with decrease in the cost of each point in comparison with the observation center. For observations of the mean monthly concentration of global radioactivity in the low-level atmosphere over the USSR, there must be around 100 points; the cost of each point must be two orders of magnitude less than the cost of the observation center. For observations of the monthly radioactive precipitation in the territories of the USSR, several hundred points must be used, and the cost of each must be approximately a quarter of that used in observing the concentration.

Although the area of the North Sea is 34% larger than that of the Baltic Sea, the great variability of the radionuclide concentration field in the surface water of the Baltic sea means that three times as many points are needed there as in the North Sea, for the same representativeness of the observations. The variability of the concentration field in the oceans is even smaller and therefore, for example, a hundred times fewer observation points are needed in a unit area of the Pacific Ocean than for the Baltic Sea.

LITERATURE CITED

1. E. A. Dmitriev, Mathematical Statistics in Soil Science [in Russian], Moscow State Univ. (1972).
2. K. P. Makhon'ko, in: Proceedings of the Institute of Experimental Meteorology [in Russian] (1977), No. 6(64), p. 42.
3. L. I. Piskunov, V. M. Gushchin, and S. I. Treiger, At. Energ., 44, No. 1. 83 (1978).
4. A. A. Borovkov, Probability Theory [in Russian], Nauka, Moscow (1976).
5. Meteorology and Atomic Energy [in Russian], Gidrometeoizdat, Leningrad (1971).
6. L. T. Myach, in: Proceedings of the Institute of Experimental Meteorology [in Russian] (1970), No. 5, p. 97.

7. I. L. Karol' and L. T. Myach, in: Proceedings of the Institute of Experimental Meteorology [in Russian] (1972), No. 1(32), p. 98.
8. O. S. Zudin and B. A. Nelepo, Statistical Analysis of Information on Radioactive Contamination of the Oceans [in Russian], Gidrometeoizdat, Leningrad (1975).
9. D. B. Styro and I. V. Kleiza, in: Problems of Investigating Atmospheric Pollution [in Russian], Mokslas, Vilnius (1981), p. 119.

SENSITIVITY OF THE DETERMINATION OF SOME ELEMENTS WITH $Z \leqslant 42$ BY A DEUTERON ACTIVATIONAL METHOD IN A CYCLOTRON

G. Vakilova, A. Vasidov, S. Mukhammedov, É. Pardaev, A. Rakhmanov, and Zh. Saidmuradov

UDC 543.53

The wide use of light-ion accelerators in applied investigations, especially in the development of high-sensitivity nuclear-physics analytical methods, has led in recent years to an urgent need to study the analytical parameters of activational methods of analysis developed using various types of accelerated particles. Considerable work has been done, for example, on estimating the sensitivity of one of the successfully developed methods — proton activational energy [1-6], especially in connection with its use for determining the content of intermediate and heavy elements in technological products [7-11] and objects in the environment [12, 13].

A very low concentration of light elements may be determined using light-ion accelerators [14-18], which is explained, in particular, by the sufficiently high activational cross sections of analytical reactions of type (d, n), (d, p), (d, α) even at small deuteron energies. In [14, 15], the sensitivity of determining elements with $Z \leqslant 30$ was estimated for deuteron energies < 14 MeV, in [19] for ∿6 MeV, and in [17, 18] for 3 MeV. The method is used to determine the concentrations of B, C, N [18, 20, 21] and several intermediate elements [22, 23] from short-lived radionuclides. The limited use of the method is explained by the poor study of its physical problems and the lack of many of the nuclear-physics data necessary for the development of specific analytical methods. A 5-6-MeV deuteron accelerator is usually recommended for analysis [24]. At higher energies, there occur reactions of type (d, 2n), in which are formed nuclides, also suitable for analysis.

In the present work, the possibility of using a cyclotron to determine the concentration of 24 elements with $Z \leq 42$ from nuclear reactions at deuterons accelerated in the cyclotron is considered in the case of radionuclides with a half-life $T_{1/2} > 30$ min. The experimental method was outlined in [1]. The only differences are the long duration of target irradiation (1-10 min) and the use solely of thick targets. The initial deuteron energy is ∿12 MeV.

Table 1 gives the main nuclear-physics characteristics of the reactions and radionuclides and the values of the yields at a deuteron energy of 4-12 MeV. The nuclide yield is

$$Y = \frac{A}{It_{\text{rad}}\left(\frac{1-e^{-\lambda t_{\text{rad}}}}{\lambda t_{\text{rad}}}\right)}, \quad \text{Bk}(\mu\text{A}\cdot\text{h}), \tag{1}$$

where A is the activity, Bk; I, is the deuteron current, μA; t_{rad} is the duration of irradiation h; λ is the decay constant, h^{-1}. The yield given in Table 1 for oxygen are obtained from [25], and those for Mg, Na, Fe, Ni, Ge, As, Y, Zr, Mo are obtained by the method of numerical integration of the excitation functions of the reaction given in [26-32], by the formula

$$Y = 3.76 \cdot 10^6 \frac{\Theta}{M} \lambda \int_{R_n}^{R_0} \sigma(x)\, dx, \tag{2}$$

Translated from Atomnaya Énergiya, Vol. 55, No. 3, pp. 164-167, September, 1983. Original article submitted September 21, 1982.

 0038-531X/83/5503-0598$07.50

TABLE 1. Yields of Radioactive Nuclides ($\times 10^n$ Bk/μA•h)

Element	Radionuclide	$T_{1/2}$, h	E_γ, keV	Deuteron energy, MeV									n	Interfering reaction	Reaction energy, MeV
				4	5	6	7	8	9	10	11	12			
O	^{18}F	1,83	511	0,2	0,3	0,4	0,5	0,7	1,0	1,5	1,7	2,4	6	—	—
Na	^{24}Na	15	1368	—	0,2	0,7	0,9	1,3	1,5	1,7	2,2	2,5	8	^{24}Mg (d, $2p$);	—7,5
														^{26}Mg (d, α)	2,9
Mg	^{24}Na	15	1368	0,1	0,6	1,4	2,0	3,0	4,0	5,0	6,0	8,0	6	—	
	^{22}Na	22 713	1274	0,6	1,0	2,0	3,0	4,0	5,0	6,0	8,0	9,0	4	—	
Cl	^{38}Cl	0,62	1642	0,3	0,5	0,9	1,3	2,0	2,5	3,1	3,7	4,7	8	^{38}Ar (d, $2p$)	—6,7
K	^{42}K	12,36	1524	0,5	0,6	0,7	0,8	0,9	1,0	1,1	1,3	1,6	6	—	
Ca	^{43}Sc	3,9	372	0,03	0,09	0,3	0,6	0,9	1,3	1,5	1,8	2,4	6	^{46}Ti (d, αn)	—5,5
	^{44}Sc	3,9	1156	0,2	0,3	0,4	0,6	0,9	2,0	5,0	6,0	9,0	5	^{46}Ti (d, α)	4,4
	^{44m}Sc	58,56	1001	—	0,04	0,24	0,8	0,9	1,0	1,2	1,5	1,8	4	^{46}Ti (d, α)	4,4
Ti	^{48}V	384	983	0,02	0,04	0,06	0,13	0,20	0,30	0,60	1,00	1,50	6	^{50}Cr (d, n)	4,9
V	^{51}Cr	672	320	—	—	0,05	0,1	0,2	0,3	0,5	0,6	0,9	6	^{60}V (d, n)	7,3
Cr	^{51}Mn	0,75	511	0,1	0,9	1,2	2,6	3,1	4,4	5,2	5,9	6,7	8	^{54}Fe (d, αn)	—5,6
	^{51}Cr	672	320	0,03	0,05	0,07	0,1	0,3	0,6	1,0	5,0	9,0	5	^{51}V (d, $2n$);	—3,9
														^{50}V (d, n)	7,3
Mn	^{52}Mn	139,2	935	—	—	—	—	—	0,15	0,33	0,80	1,30	6		
	^{56}Mn	2,8	846,6	1,7	2,1	2,7	3,0	3,5	3,8	4,7	5,7	6,7	7	^{56}Fe (d, $2p$);	—5,3
														^{58}Fe (d, α)	5,5
Fe	^{55}Co	18	931	—	0,04	0,2	0,5	0,9	1,4	1,7	2,2	2,7	6	^{58}Ni (d, αn)	—3,7
	^{56}Co	1848	846	—	—	—	—	—	0,2	0,4	0,9	1,6	5	^{58}Ni (d, α)	6,5
Co	^{60}Co	1934	1173	—	0,07	0,1	0,3	0,6	0,8	1,0	1,5	3,6	4	^{60}Ni (d, $2p$)	—4,4
Ni	^{61}Cu	3,3	656	—	0,1	0,9	1,9	3,4	4,9	6,3	7,6	8,6	7	^{64}Zn (d, αn)	—1,4
Cu	^{63}Zn	0,63	669	—	—	—	0,01	0,1	0,6	1,6	2,2	3,0	8	—	
	^{65}Zn	5880	1115	—	—	—	0,1	0,4	1,0	2,0	2,5	3,6	4	—	
	^{64}Cu	13	511	0,05	0,1	0,5	1,5	2,9	4,1	5,0	6,3	8,0	7	^{66}Zn (d, α);	—2,1
														^{67}Zn (d, αn)	0,2
Zn	^{67}Ga	79	300	—	—	—	0,04	0,3	1,7	4,1	9,4	17,0	6	^{70}Ge (d, αn)	—1,1
	^{66}Ga	9,5	1039	—	—	—	—	—	0,1	0,6	6,0	17,0	6	—	
	^{69}Zn	0,96	318	0,37	1,3	3,5	6,1	9,6	13,3	17,5	21,3	26,0	7	^{71}Ga (d, α)	9,0
Ga	^{69}Ga	39	1106	—	—	—	0,04	0,3	1,7	4,1	9,4	17,0	6	—	
	^{72}Ge	46	833	—	0,1	0,4	0,71	1,1	1,5	2,0	2,7	3,5	7	^{72}Ge (d, $2p$)	—5,6
Ge	^{71}As	65	500	—	—	—	0,3	0,6	1,0	1,7	2,1	3,0	6	—	
As	^{76}As	27	559	0,1	0,3	0,8	1,1	1,8	2,5	3,2	3,9	4,7	7	^{76}Se (d, $2p$);	—4,5
														^{78}Se (d, α)	6,0
Se	^{80m}Br	4,42	37	—	—	—	0,1	1,4	6,3	13,1	17,7	24,3	7	^{80}Kr (p, $2p$)	—3,5
	^{82}Br	35	—	—	—	—	0,1	0,7	1,8	3,6	5,4	8,0	6	—	
Br	^{82}Br	35	554	—	0,1	0,7	1,5	3,3	5,0	6,8	8,0	11,0	6	^{82}Kr (d, $2p$)	—4,6
														^{84}Kr (d, α)	5,8
Sr	^{87}Y	80,3	485	0,2	0,3	0,4	0,4	0,5	9,0	10,0	11,0	15,0	4	^{90}Zr (d, αn)	—3,2
	^{87m}Y	13,2	380	0,2	0,4	0,8	1,5	2,0	4,0	5,0	6,0	7,0	6	^{90}Zr (d, αn)	—3,2
Y	^{90m}Y	3,19	482	—	—	0,3	2,0	4,0	6,0	9,0	12,5	17,0	6	^{92}Zr (d, α)	8,7
	^{89}Y	78	909	—	0,3	0,6	1,6	3,0	6,0	9,0	15,0	19,0	6	—	
Zr	^{95}Nb	768	765	—	—	—	0,2	0,3	0,4	0,6	0,7	0,9	5	^{95}Mo (d, $2p$)	—2,4
	^{97}Nb	1,2	657	—	0,1	0,3	0,6	1,4	2,4	3,1	3,7	4,3	6	^{97}Mo (d, $2p$)	—3,4
	^{97}Zr	17	743	—	—	0,03	0,1	0,3	0,5	0,8	0,9	1,2	6	—	
	^{95}Zr	1560	756	—	—	0,4	1,0	3,0	5,0	7,0	9,0	10,0	4	—	
	^{96}Nb	23	778	—	—	0,1	0,3	0,7	1,0	2,0	3,0	3,6	6	^{96}Mo (d, $2p$)	—4,7
Mo	^{93}Tc	2	1262	0,05	0,2	0,5	0,7	1,2	1,9	2,4	2,9	3,6	7	^{96}Ru (d, αn)	0,2
	^{93m}Tc	0,72	391		0,02	0,1	0,3	1,0	1,4	1,7	2,1	2,6	7	—	
	^{94}Tc	4,83	850	—	—	—	0,01	0,1	0,5	1,0	3,4	7,0	6	^{96}Ru (d, α)	8,8
	^{95}Tc	20	765	—	—	—	0,1	0,8	1,0	1,7	2,3	3,0	6	^{98}Ru (d, αn)	0,4
	^{95}Tc	20	765	0,007	0,06	0,1	0,7	1,4	2,8	4,7	7,4	11	6	^{98}Ru (d, αn)	0,4
	^{96}Tc	103,2	849	—	—	0,05	0,1	0,2	0,5	0,8	1,0	2,0	5	^{99}Ru (d, αn)	0,9
	^{99m}Tc	6,03	618	0,03	0,2	0,7	1,5	3,0	4,0	5,0	6,0	7,5	6	^{99}Ru (d, αn)	0,9

TABLE 2. Sensitivity of Deuteron Activational Analysis and Limits of Observation of Elements with $Z \leqslant 42$

Element	Radionuclide	S, Bk/μg·g^{-1}		η, μg/g	
		6 MeV	10 MeV	6 MeV	10 MeV
O	^{18}F	2,0	7,5	0,56	0,15
Na	^{24}Na	$4,2 \cdot 10^2$	$8,8 \cdot 10^2$	$8 \cdot 10^{-2}$	$3 \cdot 10^{-2}$
Mg	^{24}Na	7,0	26,5	4,4	1,2
	^{22}Na	0,1	0,3	$2,4 \cdot 10^2$	80,0
Cl	^{38}Cl	$4,7 \cdot 10^2$	$1,5 \cdot 10^3$	0,3	0,1
K	^{42}K	3,9	5,5	65	46
Ca	^{44}Sc	0,2	6,7	47,0	3,8
	^{44m}Sc	$1,2 \cdot 10^{-2}$	$6 \cdot 10^{-2}$	$2,6 \cdot 10^1$	$5,3 \cdot 10^3$
Ti	^{48}V	0,3	3,3	12,0	1,1
V	^{51}Cr	0,3	3,4	73,0	8,0
Cr	^{51}Mn	$6,2 \cdot 10^2$	$2,6 \cdot 10^3$	$2,5 \cdot 10^{-3}$	$6 \cdot 10^{-4}$
Ga	^{69}Ge	—	25	—	1,5
	^{72}Ga	24	133	0,16	0,03
Ge	^{71}As	—	8,5	—	7,0
As	^{76}As	40	160	0,12	0,03
Se	^{82}Br	—	18	—	0,1
Br	^{82}Br	4,0	34	1,0	0,1
Sr	^{87}Y	$3 \cdot 10^{-2}$	0,9	$1,1 \cdot 10^2$	4,0
	^{87m}Y	7	50	0,5	0,1
Y	^{90m}Y	1,5	42,5	1,4	$5 \cdot 10^{-2}$
	^{89}Zr	2,7	45	1,1	0,07
	^{95}Nb		0,3	—	8,0
	^{52}Mn	—	1,65	—	2,0
Mn	^{56}Mn	$4,5 \cdot 10^2$	$7,6 \cdot 10^2$	$2 \cdot 10^{-2}$	$1,4 \cdot 10^{-2}$
Fe	^{55}Co	0,9	8,5	3,7	0,4
	^{56}Co	—	0,2	—	15,0
Co	^{60}Co	$5 \cdot 10^{-3}$	$5 \cdot 10^{-2}$	$2,2 \cdot 10^3$	$2,2 \cdot 10^2$
Ni	^{61}Cu	45	315	0,5	$7,6 \cdot 10^{-2}$
Cu	^{63}Zn	—	$7,9 \cdot 10^2$	—	$5,6 \cdot 10^{-2}$
	^{65}Zn	—	$8,5 \cdot 10^{-2}$	—	$2,1 \cdot 10^2$
	^{64}Cu	12,5	250	0,2	$2 \cdot 10^{-2}$
Zn	^{67}Ga	—	20	—	0,4
	^{66}Ga	—	3,4	—	1,6
	^{69}Zn	$1,7 \cdot 10^2$	$8,7 \cdot 10^2$	—	—
	^{97}Nb	1,5	15,0	2,0	0,2
	^{97}Zr	0,2	3,7	14,0	0,66
	^{95}Zr	$2 \cdot 10^{-2}$	0,36	—	12
	^{96}Nb	$3,5 \cdot 10^{-1}$	10	—	0,3
Mo	^{93}Tc	24	$1,2 \cdot 10^2$	0,6	0,1
	^{93m}Tc	6,5	85,0	0,6	$5 \cdot 10^{-2}$
	^{94}Tc	—	6	—	0,4
	^{95}Tc	—	8,5	—	0,3
	^{95}Tc	0,7	23,5	3,3	0,1
	^{96}Tc	—	0,4		6,4
	^{99m}Tc	3,5	25,0	5,0	0,7

where Θ, M are the abundance and mass number of the isotope, g; R_o, R_n are the deuteron paths at the initial energy and at the threshold energy of the reaction, mg/cm^2. For radionuclides with $t_{1/2} < 2$ h, the saturation factor $(1 - e^{-\lambda t_{rad}})$ is also taken into account; for all the other radionuclides, Y is measured in the present work. As is evident from Table 1, the radionuclide yields depend strongly on the deuteron energy. Therefore, it is important to determine the energy accurately before the onset of analsyis, since a deviation of ±1 MeV may lead to an error of 50-100% in the absolute method. The radionuclide yields are in the range $1 \cdot 10^4$-$5 \cdot 10^8$ Bk/μA·h.

The errors in measuring the radioactive-nuclide yield are due to the errors in measuring the current (< 1%), the detector efficiency (∼ 9%), and the statistical error (∼ 10%). The mean square error of the data is no more than 15% in the worst case. The error of the calculational data is due to the measurements of the activation cross section and the numerical integration; it is also no more than 15%. The sensitivity of the method, according to the expression

$$S = f^{-1} Y I t_{rad}, \text{ Bk/μg/g}, \quad (3)$$

where f is the proportion of the element being determined in the matrix, represents the activity at the end of irradiation induced when a matrix including 1 μg/g of the element being determined is activated with a deuteron current of 5 μA for 1 h. Table 2 gives values for the

TABLE 3. Yield Ratio of Some Radioactive Nuclides

Interfering reaction / Nuclear reaction	Deuteron energy, MeV							
	5	6	7	8	9	10	11	12
$\frac{^{26}Mg \rightarrow {}^{24}Na}{^{23}Na \rightarrow {}^{24}Na}$	0,020	0,020	0,022	0,022	0,025	0,030	0,030	0,030
$\frac{^{66}Zn \rightarrow {}^{64}Cu}{^{63}Cu \rightarrow {}^{64}Cu}$	0,12	0,05	0,03	0,03	0,04	0,04	0,05	0,06
$\frac{^{54}Fe \rightarrow {}^{52}Mn}{^{51}Cr \rightarrow {}^{52}Mn}$	—	—	—	0,16	0,09	0,07	0,05	0,04
$\frac{^{58}Ni \rightarrow {}^{60}Co}{^{56}Fe \rightarrow {}^{56}Co}$	—	—	—	—	1,2	1,4	0,8	0,6

elements investigated here. As is evident, the greatest sensitivity is attained for Na, Cl, Cr, Mn, Ni, Cu, Zn, Se, Mo, and is 10^2-10^3 Bk/μg/g. Thus, radiation detectors of sufficiently high efficiency allow these elements to be determined with very low concentration values.

The limits of observation of the elements are found for the case when the radioactivity of the nuclide is measured using a NaI(Tl) scintillation detector of dimensions 80 × 80 mm, establishing the radiochemically liberated fraction of the sample directly at the detector surface 3 h after irradiation (if $T_{1/2} < 3$ h for the radionuclide) or 10 h thereafter (if $T_{1/2} > 3$ h). As a preliminary, the natural background is measured using the same detector, placed in a lead "booth" (wall thickness 100 mm), together with the energy resolution and effficiency of radiation recording. The values of the observation limits are found from the formula

$$\eta = \frac{A_{min}}{t_{mea}\omega\varepsilon_\gamma i_\gamma S}, \quad (4)$$

where $A_{min} = 3\sqrt{A_b}$ is the minimum number of pulses recorded by the detector; A_b is the number of background pulses; $\omega\varepsilon_\gamma$ is a factor taking account of the measurement geometry and the detector efficiency; i_γ is the quantum yield in 100 decays. Table 2 gives the limits of observation of the elements at deuteron energies of 6 and 10 MeV.

As is evident, under the given conditions, the limits of observation are less than 1 μg/g for practically all the elements investigated. The limits of observation may be divided into various ranges

Element	Limits of observation
Na, Cl, Cr, Mn Cu, Ga, As, Y, Mo	10^{-4}—10^{-2}
O, Fe, Zn, Se, Br, Sr, Zr	10^{-2}—10^{-1}
Mg, Ca, Ti, V, Ge	10^{-1}—10^{0}
K, Co	10^{1} —10^{2}

The concentration of ten elements is below 10^{-2} μg/g.

As a result of the reaction (d, p), the same radioactive nuclide is formed as in the reaction (n, γ), the cross section of which is very high. Note, however, that the deuteron activational method allows a matrix with large Z to be analyzed without decomposition, which is practically impossible in neutron activational analysis. Thanks to the Coulomb barrier of the nuclei, light elements in matrices with $Z \geq 45$-50 may be determined. Another important point is that, using the deuteron activational method, low concentrations of a considerable number of light elements may be determined without disturbance; in the case of the proton activational method, for example, this is impossible.

As is evident from Table 1, interfering reactions of type (d, 2p), (d, α), (d, αn) are encountered in analysis using deuteron activation.

Table 3 gives the yield ratios of certain radioactive nuclides forming in the activation of adjacent elements. Note that this ratio increases with increase in deuteron energy and in some cases reaches 10^{-2} and higher. Therefore, before analysis, it is very important to consider all the possible analytical and interfering reaction channels. The noise may be suppressed by selecting a deuteron energy below the threshold of the interfering reactions.

Thus, deuteron activational analysis allows most of the elements from groups with $Z \leqslant 42$ to be determined at concentrations below 1 μg/g, while Na, Cl, Cu, Ni, Mn, Cr, and other elements may even be determined at 10^{-2}-10^{-4} μg/g. To suppress the noise on account of the reactions (d, 2p), (d, αn), and others, the initial deuteron energy may be 5-6 MeV, and light elements are then determined without decomposition of the heavy-element matrix.

LITERATURE CITED

1. A. Vasidov, V. A. Muminov, and S. Mukhammedov, At. Energ., 49, No. 2, 101 (1980).
2. G. Vakilova et al., in: Radioactivational Methods of Analyzing Objects of Natural Origin [in Russian], Fan, Tashkent (1980), p. 108.
3. B. V. Zatolokin, I. O. Konstantinov, and N. N. Krasnov, At. Energ., 42, No. 4, 311 (1977).
4. K. Krivan and V. Krivan, Fresen. Z. Anal. Chem., 295, No. 4, 348 (1979).
5. J. Debrun et al., Anal. Chem., 47, No. 4, 637 (1975).
6. J. Barrandon, P. Benaben, and J. Debrun, Anal Chim. Acta, 83, No. 1, 157 (1976).
7. A. Vasidov, V. A. Muminov, and S. Mukhammedov, Dokl. Akad. Nauk Uzb. SSR, No. 2, 30 (1980).
8. N. N. Krasnov et al., in: Activational Analysis in the Economy [in Russian], Fan, Tashkent (1974), p. 133.
9. I. O. Konstantinov et al., Zh. Anal. Khim., 31, 1941 (1976).
10. V. Krivan, Anal. Chem., 47, 469 (1975).
11. J. Barrandon, J. Debrun, and A. Kohn, J. Radioanal. Chem., 16, No. 2, 617 (1973).
12. C. Vondecasteele et al., Talanta, 98, 19 (1980).
13. V. A. Muminov, S. Mukhammedov, and Zh. Saidmurodov, Izv. Akad. Nauk Uzb. SSR, Ser. Fiz-Mat. Nauk, No. 1, 70 (1980).
14. V. A. Muminov et al., Izot. SSSR, No. 50, 40 (1977).
15. V. A. Muminov, S. Mukhammedov, and R. A. Khaidarov, Izot. SSSR, No. 49, 11 (1977).
16. Yu. I. Bondarenko and V. V. Ovechkin, in: Using Accelerators in Elementary Analysis [in Russian], Fan, Tashkent (1980), p. 85.
17. Yu. I. Bondarenko and V. S. Rudenko, At. Energ., 53, No. 3, 189 (1982).
18. G. Vakilova, Radiokhimiya, No. 1, 50 (1979).
19. S. Mukhameddov and A. Shodiev, Prepint R-3-12 of the Institute of Nuclear Physics, Academy of Sciences of the Uzbek SSR [in Russian], Tashkent (1980).
20. E. Schuster and K. Wohleben, Int. J. Appl. Rad. Isot., 19, No. 5, 471 (1968).
21. Yu. I. Bondarenko and V. S. Rudenko, in: Using Accelerators in Elementary Analysis [in Russian], Fan, Tashkent (1980), p. 89.
22. V. A. Muminov, S. Mukhameddov, and R. A. Khaidarov, Zavod, Lab., No. 1, 40 (1977).
23. J. McGeingly and E. Schweikert, Anal. Chem., 47, No. 14, 2403 (1975).
24. B. V. Zatolokin, I. O. Konstantinov, and N. N. Krasnov, in: Using Accelerators in Elementary Analysis [in Russian], Fan, Tashkent (1980), p. 40.
25. N. N. Krasnov et al., At. Energy., 27, No. 2, 125 (1969).
26. L. Bowen and J. Irvine, Phys. Rev., 127, No. 5, 1698 (1962).
27. K. Otozai et al., Nucl. Phys., A107, 427 (1968).
28. J. Klark, C. Fulmer, and J. Williams, Phys. Rev., 179, No. 4, 1104 (1969).
29. M. Cogneau, L. Gilly, and J. Cara, Nucl. Phys., A99, 686 (1967).
30. Z. Randa and K. Svoboda, J. Inorg. Nucl. Chem., 38, No. 12, 2289 (1976).
31. C. Riley and B. Linder, Phys. Rev., 134, No. 38, 559 (1964).
32. H. Rohm et al., J. Inorg. Nucl. Chem., 31, No. 12, 3345 (1969).

LETTERS TO THE EDITOR

COLD-NEUTRON SCATTERING CROSS SECTION AND HYDROGEN MOBILITY IN ZIRCONIUM HYDRIDE

B. E. Zhitarev, S. B. Stepanov, and Yu. B. Zasadych

UDC 539.125.516.22

The comprehensive study of metal hydrides has long been stimulated by diverse prospects for their practical application and by interest in the problems of the physics of the condensed state of matter [1]. It suffices to mention the needs of nuclear, fusion, and hydrogen power and technology and the problems of the behavior of hydrogen in metals. Conclusions reached on the basis of different methods of investigating the structure and dynamics of hydrides often differ substantially, quantitatively and even qualitatively. In this situation any additional research methods which are sufficiently accurate and sensitive are useful One such method is that of studying the dependence of the scattering cross section for very slow neutrons (with an energy $E \leqslant 10^{-5}$ eV) on their energy and on the parameters of the state of the scattering system—hydrides in this case. Rigorous theoretical calculation of the scattering cross section for such neutrons, as is known, is very difficult to carry out, including the case of hydrides. However, experimentally and on the basis of calculations according to simplified structurally dynamic models the scattering cross section for cold neutrons has been shown to be highly sensitive to the characteristics of the low-frequency thermal motion of hydrogen atoms in different substances [2, 3].

Data on the cold-neutron scattering cross section in zirconium hydride are very limited: The hydride $ZrH_{1.98}$ was investigated experimentally at 20-270°C and reported in [2], which presented the only calculations to date on the temperature dependence of the cross section. In view of this, the main goal of this paper is to demonstrate more fully the substantial dependence of the scattering cross section on the state of the hydride and the possibility of such data being used in a qualitative and quantitative description of the dynamics of hydrogen in such systems.

We studied the hydrides $ZrH_{1.01}$, $ZrH_{1.55}$, $ZrH_{1.81}$ and $ZrH_{1.81}$ at a temperature of 20, 100, 200, and 270°C. The specimens were in the form of powder with a particle size $\delta \leqslant 0.3$ mm for all hydrides while for $ZrH_{1.81}$ the particle size was $0.4 \leqslant \delta \leqslant 1$ mm. The impurity content was less than 0.3 at.%. The bulk density of the specimens in all the experiments was about 3 g/cm^3 to within 1%.

TABLE 1. Total Interaction Cross Section of ZrH_x, b*

T, °K	x	λ, nm						
		1,3	1,4	1,5	1,6	1,7	1,8	1,9
293	1,01	78±3	83±3	84±3	87±3	97±3	94±3	97±3
	1,55	131±4	132±2	135±2	134±4	138±4	140±3	146±2
	1,805	152±3	154±3	156±3	156±3	158±3	158±3	160±3
373	1,01	90±4	93±3	96±2	95±3	97±4	103±3	106±3
	1,55	141±3	138±5	139±3	147±4	146±3	154±3	155±4
	1,805	162±3	164±3	168±4	169±3	173±4	170±5	172±3
473	1,01	99±6	101±3	111±3	112±3	109±3	116±3	123±3
	1,55	161±4	157±3	169±3	168±4	173±3	174±6	182±3
	1,805	188±4	192±5	192±4	193±3	197±4	197±3	204±2
543	1,01	113±4	117±3	120±3	122±3	130±3	136±4	138±3
	1,55	175±4	178±5	185±4	183±6	192±4	196±4	202±4
	1,805	205±4	213±5	211±3	219±4	223±4	220±3	228±7

*1 b = 10^{-28} m^2.

Translated from Atomnaya Énergiya, Vol. 55, No. 3, pp. 169-170, September, 1983. Original article submitted February 5, 1982.

0038-531X/83/5503-0603$07.50

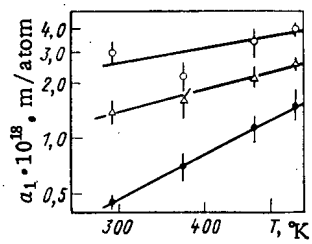

Fig. 1. Slope of the linear dependence $\sigma_s^H(\lambda)$ of the cross section for scattering on a hydrogen atom in zirconium hydride ZrH_x for x = 1.01 (○), 1.55 (△), and 1.8 (●).

The cross section for the interaction of hydrides with neutrons at a wavelength of 1.3-1.9 nm was determined on a crystal spectrometer of the "neutron guide + crystal" type [4] at a resolution of $\Delta\lambda/\lambda \leqslant 0.03$. In special experiments on this instrument on small-angle scattering in hydrides and on the transmission of reference specimens we determined the optimum distance of the hydride specimens from the detector at which the effect of refraction on powder particles and of isotropic scattering in the detector did not exceed 0.5% of the cross section. In the experiments the particle size and prolonged heating of the specimens did not display any effect on the results. Table 1 presents the total interaction cross section, calculated for the complex ZrH_x. We given the mean-square errors with allowance for the indeterminacy of the density of the specimens.

As was to be expected [2, 3], we find that the cross section depends almost linearly on the neutron wavelength: $\sigma_s^H(\lambda) = a_0 + a_1\lambda$ for $\lambda \geqslant 1.3$ nm. The scattering cross section, calculated per hydrogen atom, which in ZrH_x is almost entirely due to scattering by hydrogen, differs up to 10% for $x \approx 1$ an $x \approx 2$. The hydrogen concentration, however, was observed to have a substantial effect on the value and temperature dependence of the coefficnets a_0 and a_1. Thus, for $ZrH_{1.8}$ the contribution of the inelastic component ($a_1\lambda$) does not exceed 20% of the cross section but it does depend strongly on the temperature ($a_1 \sim T^{1.9}$). As the hydrogen concentration decreases within the limits mentioned above, the slope a_1 of the straight line $\sigma_s^H(\lambda)$ grows more than fivefold at room temperature but its temperature dependence weakens markedly ($a_1 \sim T^{0.7}$ for $ZrH_{1.01}$). These changes are illustrated by Fig. 1. The component a_0, which is determined by the probability of elastic scattering, changes in the opposite direction but does so much weakly.

The overall character of the dependence of the coefficients a_1 and a_0 on the temperature and the composition of the zirconium hydride permits a number of qualitative conclusions. The observed effects in the scattering cross section reflect mainly the influence of the state parameters (T, x) of the hydride on the low-frequency motion of the hydrogen — acoustic vibrations and diffusion transitions. This is indicated by the following data: the influence of the temperature and composition on the spectra of inelastic scattering of neutrons (in particular, the data of [5]); the absence of a concentration effect in the scattering cross section for neutrons with an energy in the region of the optical levels of ZrH_x [6]; and calculations of the cold-neutron scattering cross section from a simplified model of the frequency spectrum of zirconium hydride [2]. Analysis of the results of the last paper showed that only varying the parameters ("weight" and characteristic temperature) of the acoustic (Debye) branch of the spectrum over wide limits makes it possible to obtain qualitative agreement with the cross sections measured in our work. The dependence of the "weight" of the acoustic branch on the hydrogen concentration ($\sim 1/x$, [7]) is also in qualitative agreement with the concentration dependence of the scattering which we determined in the light of the calculated data of [2]. Consideration of all the published calculated results [2, 3, 7] shows, however, that they do not permit a quantitative description of the experimental data of this paper since they do not take account of all the characteristics of the low-frequency modes, including hydrogen diffusion. In the first place, this applies to hydride with $x \leqslant 1.5$, in which case the contribution of these modes apparently becomes particularly noticeable. The concentration effect decreases as the temperature rises; this characterizes the temperature variations in the frequency spectrum of zirconium hydrides and the thermal excitation of different modes. In accordance with the laws obtained for the variation of the scattering cross section and on the basis of the results of [3] we can establish unambiguously that the total mobility of hydrogen in ZrH_x increases with decreasing hydrogen concen-

tration in the zirconium lattice (growth of the slope a_1 with weakening of the temperature dependence, decrease in the component a_0 with intensification of the temperature dependence). This conclusion is consistent with the results of the investigation of inlastic scattering of neutrons in the region of the optical peak in ZrH_x [5] as well as the result of investigation of hydrogen diffusion by nuclear magnetic resonance [8]. The conclusion of [8] about the diffusion activation energy decreasing with decreasing hydrogen concentration is in qualitative agreement with our results.

Thus, the data on the temperature and concentration dependences of the cross section for scattering of cold neutrons in hydride systems can be used for phenomenological investigation of the hydrogen mobility and with adequate dynamic models to confirm and refine the parameters which characterize the dynamics of hydrogen in the respective systems.

The authors are grateful to V. A. Semenov and D. A. Pankratenko for supplying the hydride specimens.

LITERATURE CITED

1. Second International Congress on Hydrogen in Metals, Paris (1977).
2. J. Saastamoinen and A. Palmgren, Nucl. Eng., 25, No. 5, 189 (1971).
3. V. E. Zhitarev, Candidate's Dissertation, Moscow Engineering Physics Institute, Moscow (1980).
4. S. B. Stepanov et al., in: Neutron Physics [in Russian], Part 4, Izd. Fiz.-Energ. Inst., Obninsk (1974), p. 257.
5. J. Couch et al., Phys. Rev., B4, No. 8, 2675 (1971).
6. E. Ya. Doil'nitsyn et al., Third Genera Conf., USSR Paper No. 366.
7. W. Reichardt, in: Slow-Neutron Spectra [Russian translation], Atomizdat, Moscow (1971), p. 255.
8. E. F. Khodosov, Fiz. Met. Metallowed., 29, No. 2, 415 (1970).

PROFILOMETRIC AND METALLOGRAPHIC INVESTIGATIONS OF THE DEVELOPMENT OF HELIUM POROSITY IN COPPER

V. F. Reutov, K. G. Farkhutdinov, and Kh. G. Kadyrov

UDC 620.179.18:621.039.553

Helium porosity in metals is usually investigated by means of electron and optical microscopy, which require complex technological procedures and operations during the preparation and conduct of experiments as well as during the processing of the results. In order to determine the level of radiation swelling of metals and alloys which have been bombarded with heavy ions a new method was proposed [1] on the basis of profilometric measurement of the height of a bulge that appears on the surface of a specimen as a result of the formation of vacancy pores in a limited surface region. For the purpose of using this profilometric method to study the helium porosity that develops in a region at a substantial distance from the surface of the specimen we determined the comparative changes in the profile of the surface of copper irradiated with α particles, under various conditions of postradiation annealing.

Our investigations were carried out on plates of polycrystalline copper (99.99% pure) which had been preannealed at 900°C for an hour in a vacuum ($\sim 5 \cdot 10^{-3}$ Pa); the thickness of the plates substantially exceeded the range of 50-MeV α particles, $R_0 = 0.37$ mm.

When the plates were irradiated (at 60°C) with α particles through a special mask, helium-doped regions with a thickness of about 20 μm and a diameter of 2 mm are formed in them. After mechanical thinning of the specimens the distance from the layer with helium to the planar surface studied was 0.15, and 0.35 mm. After profilometric measurements on an M-201 contact profilograph–profilometer, we cut the specimens along planes perpendicular

Translated from Atomnaya Énergiya, Vol. 55, No. 3, pp. 170-172, September, 1983. Original article submitted June 2, 1982.

0038-531X/83/5503-0605$07.50

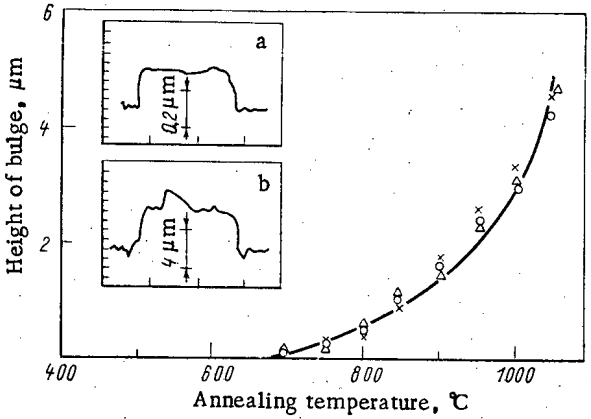

Fig. 1. Height of bulge as a function of the temperature of isochronous annealing when the helium layer in the copper specimens is at a depth of 50 μm (Δ), 150 μm (○), and 350 μm (×). Profilograms of the irradiated surface after annealing at 700°C (a) and 1025°C (b).

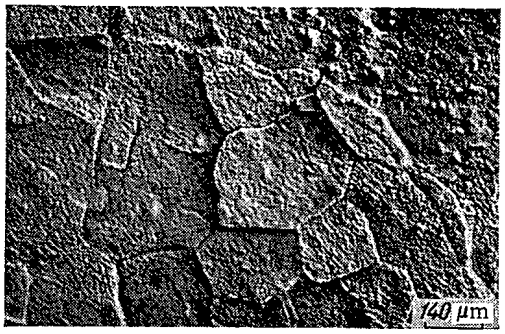

Fig. 2. Scanning-electron-microscope photograph of the surface of a specimen after annealing at 1025°C for 1 h.

to the doped layer and after chemically etching [2] the sections so obtained we determined the parameters of the helium porosity with an REM-200 scanning electron microscope.

The specimens were annealed in a vacuum ($\sim 5 \cdot 10^{-1}$ Pa) for 1 h with the temperature being raised by steps of 50°C from 400 to 1025°C. The concentration of helium atoms, determined by mass spectrometry from the gas liberation from the molten specimen, was 0.07 at.% when calculated for the doped volume. The average size and concentration of the pores were determined by the method of reciprocal diameters from electron-microscope photographs [3].

The influence of the annealing temperature on the results of profilometric measurement of the suface of specimens with the helium layer at different layers is illustrated by Fig. 1, from which we can conclude that a bulge (profilogram *a*) appears simultaneously in all of the specimens after annealing at 700°C, with the height of the bulge growing monotonically as the annealing temperature is raised to 1025°C. Upon examining the surface of the specimen under a scanning electron microscope we found that the oscillation of the profilogram of the irradiated surface, which intensifies with the annealing temperature, is caused by the uneven "protrusion" of some grains with respect to others (Fig. 2). We must point out that the shape and size of the bulge almost completely reproduces the shape and size of the openings in the mask through which the irradiation had been carried out.

Form the data of structural analysis in the scanning electron microscope we see the first signs of helium pores at 500°C, when a characteristic dark band about 23 μm wide is formed (Fig. 3a). At 750°C pores with a diameter of 0.1 μm appear in the middle of this band and on the boundaries of grains which intersect the helium-doped region. The doped region becomes filled with pores at 900°C (Fig. 3b). With a further rise in the annealing

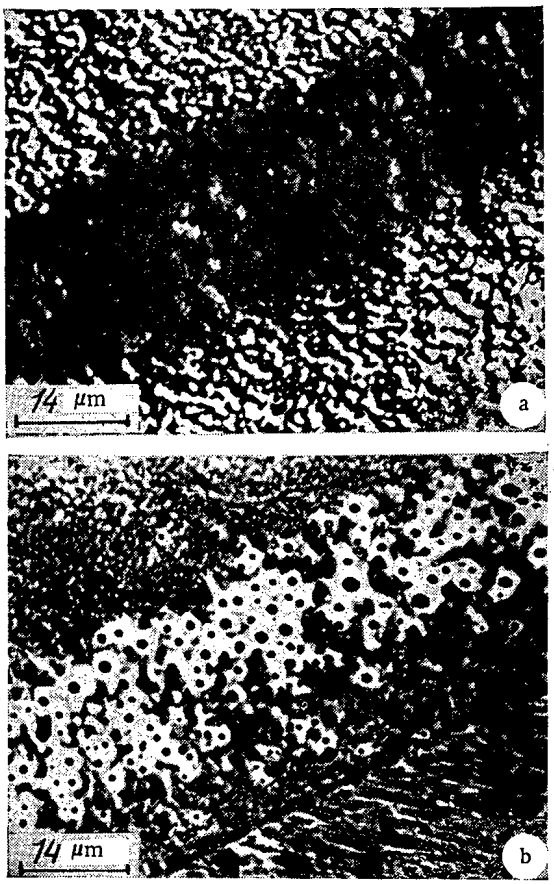

Fig. 3. Helium doping of a region after annealing at 700°C (a) and 900°C (b).

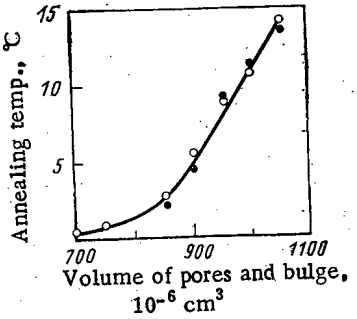

Fig. 4. Total volume of pores (○) and volume of bulge (●) as a function of the temperature in successive isochronous annealing of 1 h each.

temperature the total volume of the visible pores in the layer increases appreciably. The results of measurements of the volume of the bulge on the surface of the specimen and the total volume of pores in the doped region after annealing at different temperatures (Fig. 4) indicate a complete correlation between these parameters, regardless of the depth at which the doped region occurs. These data enable us to make the conclusion that profilometry can and should be used to study the laws governing the development of helium porosity.

LITERATURE CITED

1. W. Johnston et al., J. Nucl. Mater., 47, 155 (1973).
2. Sh. Sh. Ibragimov, V. F. Reutov, and K. G. Farkhutdinov, in: Radiation Defects in Metallic Crystals [in Russian], Nauka, Alma-Ata (1978), p. 217.
3. S. A. Saltykov, Stereometric Metallography [in Russian], Metallurgiya, Moscow (1970).

EFFECT OF COLLIMATION OF A MONOENERGETIC SOURCE ON THE ACCUMULATION FACTOR

F. M. Zav'yalkin
and S. P. Osipov

UDC 621.039.58

It is necessary when solving radiation protection problems and designing process monitoring devices to know the contribution of scattered radiation to the total intensity at the detection point behind an infinite barrier which is irradiated by a bounded (collimated) beam of radiation.

The publications [1, 2], in which the accumulation factors for a limited barrier are evaluated, are well known. However, these results cannot be used to evaluate the accumulation factor B_a for an infinite barrier irradiated by a bounded beam of radiation. This difference is caused by the fact that quanta emitted as a result of scattering through the side surface of a bounded medium now do not return to it. At the same time quanta scattered in the region not irradiated by the primary flux return to the detector upon the irradiation of an infinite barrier by a collimated beam.

A calculation of the energy accumulation factor behind a barrier with thickness l (Fig. 1) at a detection point separated by a distance R from the shield and positioned perpendicularly to the protective barrier is made in this paper by the Monte Carlo method in the double-scattering approximation with account taken of coherently scattered quanta. A point isotropic monoenergetic source of γ radiation with an irradiation field restricted by a collimator with an exit aperture of circular or square shape is mounted on the opposite side of the barrier on the same perpendicular at a distance A from the barrier. The formulas for cross sections differential in angle of noncoherent and coherent scattering were taken from [3]; the total cross sections of the interaction of γ radiation with matter were taken from [4].

Since only double scattering was employed in the calculations, the energy accumulation factors of the radiation of an uncollimated source in the barrier geometry for $l = 1$-3 m.f.p. (mean free paths) were calculated to check the permissibility of this restriction. Understated results are calculated in comparison with the data of [5], in which multiple scatter-

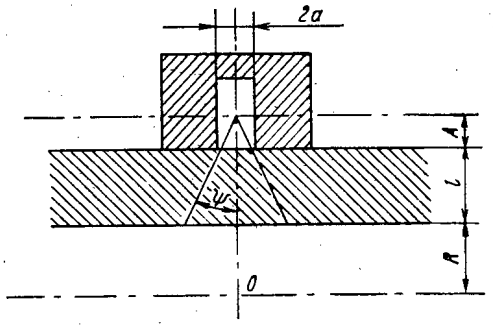

Fig. 1. Geometry of the irradiation.

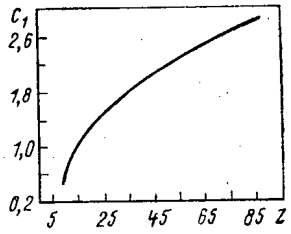

Fig. 2. Dependence of the coefficient C_1 on the atomic number Z of the barrier material.

Translated from Atomnaya Énergiya, Vol. 55, No. 3, pp. 172-173, September, 1983. Original article submitted July 6, 1982.

 0038-531X/83/5503-0608$07.50

ing was taken into account. For barriers 1 and 3 m.f.p. in thickness the error amounts to 3-5 and 10-15%, respectively. Such an error, which is permissible for practical problems, is reduced upon collimation of the source.

It has been clarified as a result of the analysis that the dependence of the accumulation factor of a collimated γ radiation source from one-half the collimation angle Ψ can be expressed by the formula

$$(B_a-1)/(B_b-1)=1-\exp(-C\operatorname{tg}\Psi), \tag{1}$$

where $B_b = B_b(E, Z, A, R, l)$ is the energy accumulation factor of the radiation for a source located at a distance A from the barrier at a detection point separated by a distance R from the barrier, $B_a = B_a(E, Z, A, R, l, a)$ is the energy accumulation factor for collimated radiation, and $C = C(E, Z, A, R, l, a)$ is a coefficient which depends on the energy of the primary γ-quanta, the shield material, and the mutual arrangement of the source, detector, and protective barrier.

Investigation of the dependence of the coefficient C(E, Z, A, R, l, a) on these factors has shown that the expression

$$C(E, Z, A, R, l, a)=\frac{(l+A)(1+\mu l/2)C_1(Z)}{(l+R)(1-a/l)^{1/3}\mu} \tag{2}$$

is applicable with an error of 5-7%, where μ is the radiation attenuation coefficient of the material under investigation and $C_1(Z)$ is a coefficient which depends on the atomic number of the material of the protective barrier (Fig. 2). We note that formula (2) is defined for $a < l$, since the energy accumulation factor for an irradiation field radius $a \approx l$ agrees with the accumulation factor in the barrier geometry (a discrepancy of no more than 3).

A comparison of the results of a calculation by the Monte Carlo method and calculations based on formulas (1) and (2) has shown that when the formulas for calculation of the energy accumulation factor of a collimated source is used the error is no greater than 5%. One can also use formula (1) to estimate the collimator effectiveness.

LITARATURE CITED

1. V. A. Klimanov, V. P. Mashkovich, and Yu. N. Podsevalov, At. Energ., 22, No. 3, 228 (1967).
2. V. P. Mashkovich et al., in Problems of Dosimetry and Protection from Radiations [in Russian], No. 8, Atomizdat, Moscow (1968), p. 62.
3. S. V. Mashkovich, Instrumentation and Methods of Fluorescence X-Ray Radiometric Analysis [in Russian], Atomizdat, Moscow (1976).
4. O. F. Nemets and Yu. V. Gofman, Handbook on Nuclear Physics [in Russian], Naukova Dumka, Kiev (1975).
5. Manual on Radiation Protection for Engineers [in Russian], Vol. 1, Atomizdat, Moscow (1972), p. 162.

AN ESTIMATE OF THE SYSTEMATIC ERRORS IN THE CALCULATION OF CRITICALITY BY THE MONTE CARLO MEHTOD

V. G. Zolotukhin
and L. V. Maiorov

UDC 539.125.52:621.039.51.12

It is well known that it is necessary to accept a systematic error (a shift in the estimates of the functionals) in all programs for the solution of the problem of reactor criticality by the Monte Carlo method [1-3]. It arises as a result of the use of different versions of approximations of the solution (the methods of "supplements" and of "a constant number of division points") when the number of neutrons in each generation is reduced to an a priori specified value — N with the help of some rules which are often theoretically unjustified, and the distribution of the additional neutrons in the reactor is selected on the basis of qualitative notions.

A theory has been worked out in [3] for the supplement methods on the basis of a finite-dimensional reactor model which permits the construction in particular of an algorithm for estimating the shift in the course of the modeling. Formulas for a priori estimates of the shift in the values of functionals are also obtained there which are suitable in the approximation in which the ratio of the first two eigennumbers of the criticality problem $\lambda_1/\lambda_0 \ll 1$.

At present the calculation of large systems for which $\lambda_1 \approx \lambda_0$ is of special interest. Therefore, the authors have continued their investigations with the goal of obtaining working formulas for evaluating the systematic errors in the calculation of the criticality coefficient by the Monte Carlo method which are suitable for large systems. Some of the results obtained are given in this paper.

Let us consider a reactor surrounded by a black absorber. We shall write the integral equation for determination of the criticality coefficient in the form

$$\lambda\rho(x)=\int_{V_R} K(x, y)\,\rho(y)\,dy. \tag{1}$$

The function $\rho(x)$ describes the density of absorbers (version A) or the density of the generation of secondary fission neutrons (version F) at the point $x = (r, \Omega, E)$ of the region V_R of the phase space of the reactor.

For version A: $K(x, y) = \int T(x, x')C(x', y)dx'$; (2)

for version F: $K(x, y) = \int C(x, x')T(x', y)dx'$. (3)

Here $T(x, x')$ is the probability density of the absorption of a fission neutron at the point x upon the condition that it was produced at a point x', and $C(x', y)$ is the average number of fission neutrons which are produced at the point x' upon the condition that the neutron causing the fission was absorbed at the point y. Both functions are assumed to be defined in the entire phase space V_∞, including the black surroundings of the reactor.

We shall denote the integral

$$\eta(y)=\int_{V_\infty} K(x, y)\,dx. \tag{4}$$

For version A $\eta(y)$ is the average number of secondary fission neutrons at the point y, and for version F it is the average number of secondary fission neutrons which are formed after absorption of a fission neutron produced at the point y.

Translated from Atomnaya Énergiya, Vol. 55, No. 3, pp. 173-175, September, 1983. Original article submitted July 12, 1982.

 0038-531X/83/5503-0610$07.50

Both versions of Eq. (1) are used in constructing the schemes which implement modeling of a chain reaction by the Monte Carlo method: for the density of absorptions and for the density of generation of secondary neutrons. Making the physical meaning of the function $\rho(x)$ more specific is not important for what follows, since the formulas are derived identically for both cases. For definiteness' sake we shall assume that $\rho(x)$ is the density of absorptions.

For calculation of the criticality coefficient $k_{eff} = \lambda_0$, where λ_0 is the chief eigenvalue of Eq. (1), investigators usually construct a chain Markov process with transition probabilities $P_n(x,y)$ which models the multiplication of neutrons in the reactor. Then the distribution function $\Psi_n(x)$ of the points at which absorption of the neutrons of the generation with number n occurs is expressed in terms of the neutron distribution function in the preceding $(n-1)$-th generation by the relationship

$$\Psi_n(x) = \int_{V_\infty} P_n(x, y)\, \Psi_{n-1}(y)\, dy. \tag{5}$$

Here $x(x_1, x_2, \ldots, x_{Ln})$ and $y(y_1, y_2, \ldots, y_{Ln-1})$ are random vectors which describe the positions of the neutrons in the generations with numbers n and $n-1$, respectively, and L_n and L_{n-1} are the number of neutrons in a generation, which may be equal.

In a conditionally critical reactor the density of absorptions of successive generations can be adequately described by giving the function $K(x, y)$ if the transition probability function satisfies the relationship

$$\int \sum_{l=1}^{L_n} \delta(x - x_l)\, P_n(x, y)\, dx = \lambda_0^{-1} \sum_{l=1}^{L_{n-1}} K(x, y_l). \tag{6}$$

Actually, the density of absorptions of neutrons of the n-th generation is

$$\rho_n(x) = \int \sum_{l=1}^{E_n} \delta(x - x_l)\, \Psi_n(x)\, dx. \tag{7}$$

It follows from the relations (5) and (6) that

$$\rho_n(x) = \lambda_0^{-1} \int K(x, y)\, \rho_{n-1}(y)\, dy.$$

Since λ_0 is unknown in advance, it is necessary to use approximate expressions for $P_n(x, y)$, which we shall denote as $\tilde{P}_n(x,y)$. In other words one or another approximate models of the actual process are used in the Monte Carlo calculations. They are usually selected so that the total (or at least the average) number of neutrons N in a generation is kept constant and the condition

$$\int \sum_{l} \delta(x - x_l)\, \tilde{P}_n(x, y)\, dx = N \sum_{l} K(x, y_l) \Big/ \sum_{l} \eta(y_l) \tag{8}$$

is satisfied. Investigators assume that for sufficiently large N the mathematical expectation is

$$\left\langle N \Big/ \sum_{l} \eta(y_l) \right\rangle \approx \lambda_0^{-1}. \tag{9}$$

The approximation (8) results in a systematic error in the determination of functionals of the neutron flux which decreases for the correct models as $N \to \infty$. Models for which the error decreases according to a 1/N law have been investigated in [2, 3]. The cause of the decrease in the shift of the estimates as $N \to \infty$ is that models describable by the functions $P(x, y)$ of a special class are selected as a rule for the approximate modeling. It is characterized by the fact that one can use the central limit theorem of probability theory [4] to estimate averages over the distributions $\tilde{P}(x, y)$ at large N.

Then for the average neutron density $\rho_n(x)$ in generation n, which due to formulas (5), (7), and (8) is expressed by the relationship

$$\rho_n(x) = N \int \left[\sum K(x, y_l) \Big/ \sum \eta(y_l) \right] \Psi_{n-1}(y)\, dy, \tag{10}$$

one can write the asymptotic formula

$$\rho_n(x) = \frac{N \langle \hat{K} \rangle_{n-1}}{\langle \hat{\eta} \rangle_{n-1}} \left[1 + \frac{\langle (\hat{\eta} - \langle \hat{\eta} \rangle_{n-1})^2 \rangle_{n-1}}{\langle \hat{\eta} \rangle_{n-1}^2} - \frac{\langle (\hat{K} - \langle \hat{K} \rangle_{n-1})(\hat{\eta} - \langle \hat{\eta} \rangle_{n-1}) \rangle_{n-1}}{\langle \hat{K} \rangle_{n-1} \langle \hat{\eta} \rangle_{n-1}} \right], \tag{11}$$

where $\hat{K} = \sum_{\zeta} K(x, y_\zeta)$; and $\hat{\eta} = \sum_{\zeta} \eta(y_\zeta)$. The symbol $\langle \ldots \rangle_{n-1}$ denotes the mathematical expectation over the distribution $\Psi_{n-1}(y)$.

Assuming that a steady distribution is established for sufficiently large n, one can omit the subscript "n − 1" in the formula (11), assuming the angular brackets to be the symbol for averaging over this distribution. One can show by using the well-known formula for the dispersions of a random quantity $D\xi = M.O.\,(D\xi \mid y) + D\,(M.O.\,\xi \mid y)$, that then the expression (11) is converted into an integral equation in the function $\rho(x)$. Its first term for large N is equal, as follows from the expressions (5) and (6), to $\int K(x, y)\, \rho(y)\, dy$, and one can treat the last two terms as a small pertubation. The corresponding proofs for finite-dimensional models are given in [3].

Applying pertubation theory, let us multiply the expression (11) by the importance function $\rho^+(x)$ [the solution of the equation conjugate to Eq. (1) with $\lambda = \lambda_0$], and after the standard operations we obtain an expression for the difference $\Delta\lambda$ between the eigenvalues of the perturbed (11) and unperturbed equations for the absorption density

$$\Delta\lambda = \left\langle \left(\frac{\hat{\eta}}{\langle \hat{\eta} \rangle} - 1 \right) \left(\frac{\hat{\eta}}{\langle \hat{\eta} \rangle} - \frac{\hat{\rho}^+}{\langle \hat{\rho}^+ \rangle} \right) \right\rangle, \tag{12}$$

where $\hat{\eta} = \Sigma\eta(y_\zeta)$; and $\hat{\rho}^+ = \Sigma\rho^+(y_\zeta)$.

One can use formula (12) to evaluate the shift of the criticality coefficient in calculations by the Monte Carlo method, in particular specifying a priori approximate expressions for the function $\rho^+(x)$. Direct evaluation of it in the course of the calculations is possible in principle.

For theoretical estimates of the shift one can, again using a formula of the type $D\xi = M.O.\,(D\xi \mid y) + D\,(M.O.\,\xi \mid y)$, write the expression (12) in the form of a series

$$\Delta\lambda = \sum_{m=0}^{\infty} \int D_m(y)\, \rho(y)\, dy, \tag{13}$$

where

$$D_m(y) = \int \left[\sum_{i=1}^{J} \alpha_m(x_i) - \bar{\alpha}_m(y) \right] \left[\sum_{i=1}^{J} \beta_m(x_i) - \bar{\beta}_m(y) \right] p(X, y)\, dX;$$

$$\alpha_m = (\lambda_0^{-1} K_+)^m \alpha_0; \quad \beta_m = (\lambda_0^{-1} K_+)^m \beta_0;$$
$$\alpha_0 = \langle \eta \rangle^{-1} \eta(x) - N^{-1}; \quad \beta_0 = \langle \eta \rangle^{-1} \eta(x) - \langle \rho^+ \rangle^{-1} \rho^+(x);$$
$$P(\mathbf{x}, \mathbf{y}) = \prod_{l=1}^{L_{n-1}} p(X_l, y_l). \tag{14}$$

Here K_+ is the symbol for the integral operator conjugate to the integral operator of Eq. (1), $X_\zeta = X_{\zeta+1}, \ldots, x_{\zeta+J})$, J is the maximum number of neutrons produced in the system upon the fission of a single nucleus, and $p(X_\zeta, y_\zeta)$ is the probability density of absorption of the descendants in the next generation from a progenitor absorbed at the point y_ζ.

One should recall that nowhere in the derivation of the formulas was the fact that the coordinates of their absorption points (version A) and not their creation points (version F) were assigned to each new generation of neutrons used. The formulas given are valid for both cases: It is necessary to substitute the appropriate expressions for K(x, y) and $\eta(y)$ into them.

The error in calculating the criticality coefficient for large systems can be evaluated as a function of the size of the system with the help of expression (13), using expansions in its eigenfunctions. It turns out to be weakly dependent on the ratio λ_1/λ_0. The specific modeling method affects the nature of the dependence. Formula (12) demonstrates the decrease of the shift $\Delta\lambda$ according to the 1/N law, which was first justified theoretically in [3]. The asymptote obtained does not contradict the upper limit to the shift found by Khairullin [5]: $|\Delta\lambda| < C(N^{-1} + \gamma^N)$, where C and γ are some constants, an algorithm for which has not been indicated in [5] ($\gamma < 1$).

In conclusion we give an expression for the shift of the chief eigenvalue λ_0 for the Liberoth method for supplementing the number of particles in a generation in the case $\eta < 1$. The method is specified by the transition probability function [2]

$$\tilde{\mathcal{P}}(x, y) = \prod_{l=1}^{N} \left[\sum_{l'=1}^{N} K(x_l, y_{l'}) \Big/ \sum_{l'=1}^{N} \eta(y_{l'}) \right]. \tag{15}$$

Making simple calculations according to formulas (13) and (14), we obtain

$$N \frac{\Delta\lambda}{\lambda_0} = \sum_{m=0}^{\infty} Q_m(x) V_m(x) \rho(x)\, dx, \tag{16}$$

where

$$Q_m = \left(\frac{K_+}{\lambda_0}\right)^m \left(\frac{\eta}{\lambda_0} - 1\right);$$

$$V_m = \left(\frac{K_+}{\lambda_0}\right)^{m+1} \left(1 - \frac{\rho^+}{\int \rho^+ \rho\, dx}\right),$$

and $\rho(x)$ is the eigenfunction of Eq. (1) corresponding to the eigenvalue λ_0 and normalized to unity.

Expanding unity into a series in the eigenfuctions ρ_s^+ of the conjugate equation and making use of the property of biorthogonality of ρ_s^+ and ρ, we reduce the expression (16) to the form

$$N \frac{\Delta\lambda}{\lambda_0} = \sum_{r=1}^{\infty} \sum_{s=1} \frac{\lambda_r}{\lambda_0} \left(\frac{\lambda_s}{\lambda_0} - 1\right) \left(1 - \frac{\lambda_r}{\lambda_0} \frac{\lambda_s}{\lambda_0}\right)^{-1} C_r C_s \int \rho(x) \rho_r^+(x) \rho_s^+(x)\, dx, \tag{17}$$

where $1 = \sum_{s=0}^{\infty} C_s \rho_s^+(x)$; $\rho_0^+ = \rho^+$. An approximate summation of the series (17) now gives the formula

$$N \frac{\Delta\lambda}{\lambda_0} \approx -\frac{\lambda_1}{\lambda_0} \left(1 + \frac{\lambda_1}{\lambda_0}\right)^{-1} \times \left\{1 - \int \rho^{+2}(x) \rho(x)\, dx \Big/ \left[\int \rho(x) \rho^+(x)\, dx\right]^2\right\}, \tag{18}$$

which is suitable for practical estimates of the shift.

LITERATURE CITED

1. G. A. Mikhailov, Zh. Vychisl. Mat. Mat. Fiz., No. 1, 71 (1966).
2. E. Liberoth, Nukleonik, 11, No. 5, 213 (1968).
3. V. G. Zolotukhin, in: Transactions fo the Physics–Energy Institute [in Russian], Atomizdat, Moscow (1973), p. 185.
4. G. A. Korn and T. M. Korn, Manual of Mathematics; McGraw-Hill (1967).
5. R. Kh. Khairullin, Izv. Vyssh. Uchebn. Zaved., Mat., No. 8, 77 (1980).

DETERMINATION OF THE NUCLIDE COMPOSITION AND BURNUP OF VVÉR-440 FUEL SAMPLES

V. Ya. Gabeskiriya, Yu. V. Efremov,
V. V. Kalygin, M. P. Maslennikova,
V. B. Mishenev, Yu. S. Popov, P. A. Privalova,
V. M. Prokop'ev, and A. P. Chetverikov

UDC 621.039.54:539.166.3

An experimental investigation of the dependence of the content of heavy nuclides on the burnup in spent VVÉR fuel is essential for optimization of the fuel cycle, for the purpose of increasing the operating efficiency of a nuclear power station, for forecasting the production of secondary nuclear fuel, correction of physical methods of calculating the buildup of nuclides in reactors, and for solving problems of the utilization of the transuranic elements accumulated in nuclear power reactors. However, the experimental paper devoted to the measurement of the nuclide content of spent fuel from power reactors are very few [1-4].

We investigated two samples of spent VVÉR-440 nuclear fuel, cut off at distances of 1375 and 1625 mm from the lower boundary of the active part of a fuel-element assembly. The fuel-element assembly had operated in the fouth unit of the Novovoronezh nuclear power station for 1222 days. The initial ^{235}U enrichment amounted to 3.6%.

After total dissolution of the samples, the relative contents of isotopes of the actinide elements (^{235}U, ^{236}U, ^{238}U, ^{239}Pu, ^{240}Pu, ^{241}Pu, ^{242}Pu, ^{241}Am, ^{243}Am, ^{244}Cm) and fission products (^{133}Cs, ^{134}Cs, ^{135}Cs, ^{137}Cs, ^{140}Ce, ^{142}Ce, ^{144}Ce, ^{142}Nd, ^{143}Nd, ^{144}Nd, ^{145}Nd, ^{146}Nd, ^{148}Nd, ^{150}Nd) were measured by the mass-spectroscopic method of isotopic dilution using a complex tracer [6]. In order to reduce the error for each sample, six parallel determinations with three different complex tracers were carried out; the latter were prepared such that the ratios of the isotopes of the elements being determined in the mixture of tracer and the original solution were optimal. The content of ^{238}Pu and ^{242}Cm were calculated by using the α-emission spectrum of the plutonium and curium separated from the original solutions of the fuel samples being investigated. The burnup was determined by two methods: the method of heavy atoms (MHA) and by the content of fission products (MFP). In order to increase the reliability of the results, eight monitors were used: $^{133}Cs + ^{134}Cs$, ^{137}Cs, ^{140}Ce, ^{142}Ce, $^{144}Ce + ^{143}Nd + ^{144}Nd$, $^{145}Nd + ^{146}Nd$, and ^{150}Nd [6]. The results obtained are presented in

TABLE 1. Content of Actinide Isotopes in Samples of Spent VVÉR-440 Fuel at the Time of Unloading the Fuel-Element Assemblies from the Reactor, kg/ton U

Isotope	First sample	Second sample
^{235}U	8,28±0,06	10,01±0,07
^{236}U	5,10±0,05	4,553±0,048
^{238}U	938,8±0,6	941,8±0,5
^{238}Pu	0,198±0,007	0,181±0,018
^{239}Pu	5,65±0,07	5,77±0,07
^{240}Pu	2,332±0,028	2,172±0,027
^{241}Pu	1,431±0,018	1,328±0,017
^{242}Pu	0,588±0,008	0,468±0,006
ΣPu	10,20±0,12	9,91±0,11
^{241}Am	$(4,02\pm0,17)\cdot10^{-2}$	$(3,91\pm0,16)\cdot10^{-2}$
^{243}Am	$(11,4\pm0,5)\cdot10^{-2}$	$(7,6\pm0,3)\cdot10^{-2}$
^{242}Cm	$(1,91\pm0,26)\cdot10^{-2}$	$(2,6\pm0,4)\cdot10^{-2}$
^{244}Cm	$(4,0\pm0,4)\cdot10^{-2}$	$(2,64\pm0,26)\cdot10^{-2}$

Translated from Atomnaya Énergiya, Vol. 55, No. 3, pp. 175-176, September, 1983. Original article submitted September 13, 1982.

 0038-531X/83/5503-0614$07.50

TABLE 2. Burnup of Fuel Samples, Determined by the Heavy Atom Method, kg/ton U

Isotope	First sample	Second sample
^{235}U	22,01±0,21	20,90±0,22
^{238}U	2,4±0,6	2,2±0,6
^{239}Pu	10,7±0,6	9,2±1,2
^{241}Pu	1,76±0,10	1,35±0,13
Total	36,9±1,5	33,7±1,4

Tables 1 and 2. The error were calculated for a confidence coefficient of 0.95. The burnup according to the fission product method amounted to 38.1 ± 0.6 for the first sample, and 33.5 ± 0.6 for the second sample.

The investigations carried out showed that about 10 kg of plutonium and tens of grams of americium and curium are built up per ton of initial uranium. The principal α-radiation activity of the plutonium build-up (about 80%) is due to the decay of ^{238}Pu. The contribution of fissions of plutonium isotopes to the total burnup, calculated by the heavy nuclides built up [4], amounts to 31-33%.

LITERATURE CITED

1. V. Ya. Gabeskiriya et al, Preprint of the Scientific-Research Institute of Nuclear Reactors (NIIAR) P-24 (290), Dimitrovgrad (1976).
2. V. Ya. Gabeskiriya et al, At. Energ., 44, No. 5, 446 (1978).
3. A. V. Stepanov et al, At. Energ., 49, No. 4, 225 (1980).
4. A. G. Zelenkov et al, At. Energ., 51, No. 1, 53 (1981).
5. G. Timofeev et al, J. Radioanal. Chem., 51, No. 2, 377 (1979).
6. Yu. B. Novikov et al, At. Energ., 43, No. 4, 240 (1977).

DOSE FACTORS OF THE BUILD-UP OF COLLIMATED γ RADIATION IN A SHIELDING GEOMETRY FOR CYLINDRICAL MEDIA CONSISTING OF WATER, ALUMINUM, AND IRON

M. B. Vasil'ev and N. F. Chubashev

UDC 539.1.09

Scattered γ radiation substantially influences the development of the radiation field in a scattering medium and behind a shield. The contribution of scattered γ radiation to the total radiation of a source is usually taken into account by the build-up factor. It is in many cases very important to know the value of this factor. This refers equally to radiometry, dosimetry, and radiation techniques of nondestructive testing. In practice, collimated radiations of isotropic sources are most frequently employed. For example, in radiative defectoscopy, only collimated radiation is employed; the same applies to the practice of radiology and dosimetry. But the build-up factor of collimated radiation from isotropic sources has not been determined in many cases, neither by calculations nor by experiments. A single paper [1] has been dedicated to the energy factors of the build-up of collimated radiation in water, the values having been obtained by calculation. The build-up factors for other media and other geometries have not been studied to the present time.

The present work relates to an experimental determination of the dose factors of the build-up resulting from pointlike isotropic sources in a shielding geometry. The shield was formed by cylindrical media consisting of water, aluminum, and iron.

Cylinders for the water were made of thick, 80-cm-high cellophane; when expressed in free path lengths μr of γ quanta with the energy $E_0 = 0.661$ MeV, the cylinder diameter was

Translated from Atomnaya Énergiya, Vol. 55, No. 3, pp. 176-177, September, 1983. Original article submitted September 27, 1982.

0038-531X/83/5503-0615$07.50

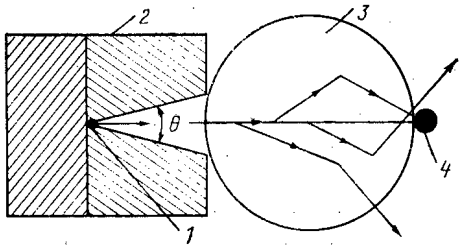

Fig. 1. Geometry of the experiment: 1) source; 2) collimator; 3) cylindrical medium; 4) detector.

TABLE 1. Dose Factors of the Build-Up of Collimated γ Radiation behind a Shield Consisting of Various Cylindrical Media

Angle of the collimation	Water			Aluminum			Iron		
	μr	^{137}Cs	^{60}Co	μr	^{137}Cs	^{60}Co	μr	^{137}Cs	^{60}Co
0°	1,0	1,12	1,07	1,0	1,08	1,05	2,0	1,14	1,08
	1,4	1,20	1,11	1,5	1,12	1,08	2,5	1,21	1,11
	2,0	1,27	1,18	2,0	1,15	1,10	3,0	1,28	1,14
	3,0	1,63	1,46	2,5	1,20	1,15	4,0	1,32	1,18
	4,0	2,32	1,94	3,0	1,34	1,18	7,0	1,70	1,20
				4,0	1,38	1,20			
16°	1,0	1,36	1,24	1,0	1,26	1,18	2,0	1,60	1,51
	1,4	1,56	1,30	1,5	1,53	1,39	2,5	1,78	1,65
	2,0	1,79	1,88	2,0	1,70	1,60	3,0	1,95	1,80
	3,0	2,39	2,07	2,5	1,92	1,78	4,0	2,09	2,26
	4,0	3,71	3,20	3,0	2,10	1,94	7,0	3,34	3,15
				4,0	2,59	2,43			
32°	1,0	1,68	1,51	1,0	1,50	1,45	2,0	2,04	1,73
	1,4	1,93	1,84	1,5	1,76	1,64	2,5	2,32	2,10
	2,0	2,25	1,96	2,0	2,07	1,85	3,0	2,68	2,36
	3,0	3,36	3,14	2,5	2,30	2,12	4,0	3,20	2,87
	4,0	5,47	5,08	3,0	2,83	2,43	7,0	5,45	4,60
				4,0	3,30	3,0			
45°	1,0	1,82	1,65	1,0	1,70	1,57	2,0	2,21	2,05
	1,4	1,99	1,85	1,5	2,04	1,76	2,5	2,37	2,18
	2,0	2,56	2,40	2,0	2,41	2,17	3,0	2,85	2,50
	3,0	4,58	4,02	2,5	2,72	2,40	4,0	3,26	3,00
	4,0	6,93	6,60	3,0	3,06	2,80	7,0	7,15	6,32
				4,0	3,75	3,35			
90°	1,0	1,93	1,71	1,0	1,75	1,70	2,0	2,60	2,35
	1,4	2,40	2,20	1,5	2,15	2,07	2,5	2,81	2,58
	2,0	3,11	2,90	2,0	2,52	2,46	3,0	3,12	2,76
	3,0	5,10	4,73	2,5	2,95	2,80	4,0	4,0	3,80
	4,0	7,24	6,76	3,0	3,30	2,92	7,0	7,70	7,17
				4,0	4,25	4,03			

1, 2, 3, and 4 range lengths. The aluminum cylinders had a height of 20 cm and diameters of 1.3, 2, 2.4, and 3 free path lengths. The diameters of the 20-cm-high iron cylinders were 4.3, 5.74, 7.2, and 8.62 free path lengths.

The collimated radiation of pointlike isotropic sources was directed toward the center of the cylinder and was propagating in a direction perpendicular to the cylinder axis. The collimation angles were 0, 16, 32, 45, and 90°. The lead collimators had a diameter of 9 cm and a channel length of 14.8 cm and were inserted in a lead shield of the bases of a BDBSZ-1eM detector. A small SBM-10 halogen counter with filters [2, 3] for obtaining equal counting sensitivities to the quanta of various energies was used a detector of γ quanta. The geometry of the experiment is shown in Fig. 1.

The dose factors of the build-up were obtained for ^{137}Cs and ^{60}Co isotope sources. The numerical values of the build-up factors were converted to full free path lengths of those sources (see Table 1); the error of the determination did not exceed 8%.

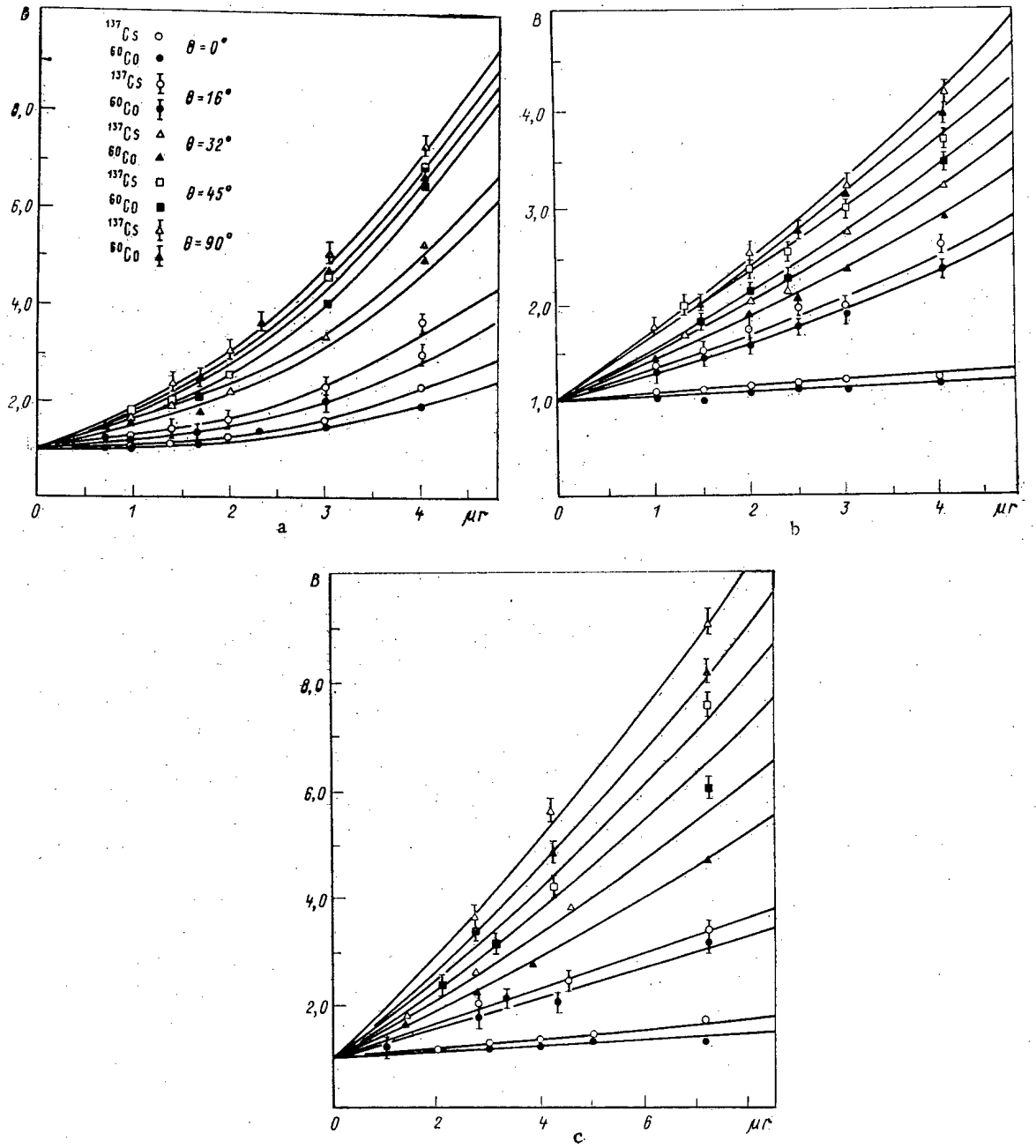

Fig. 2. Dependence of the build-up factors of collimated sources behind a shield consisting of a) water, b) aluminum, and c) iron upon the angle θ of the collimation and the path length μr.

The dependence of the build-up factors B upon the angle of collimation and the path length μr is shown in Fig. 2. A difference in the dependence of the build-up factors upon the distance between the source and the detector is noted for a collimated source in a shielding geometry and for an isotropic source in an infinite medium. Owing to the anisotropy of emission, the build-up factors of a collimated source are smaller near the source than build-up factors of an isotropic source in an infinite medium. In the latter case, the development of the radiation field and the build-up factor depend also upon quanta emitted by the source into the backward half-space. Therefore, except for the dependence of the collimation angle, the build-up factors are small near the collimator; they increased first slowly and then more rapidly with increasing distance between the source and the detector. This seems to be related to the fact that a certain spherical region, which can be distinguished between the source and the detector and which increases in proportion to the increase in the radius of the cylindrical media, is in all cases very important for the development of the radiation field and the build-up factor.

The build-up factors which we have indicated for collimated radiation of isotropic sources are of particular interest in dosimetric applications, in defectoscopy, and in medical radiology when the field of collimated radiation behind shields made from cylindrical media is to be assessed.

LITERATURE CITED

1. V. G. Zolotukhin et al., The Radiation Field of a Unidirectional Point Source of γ Radiation [in Russian], Atomizdat, Moscow (1974).
2. A. M. Panchenko, At. Energ., 14, No. 4, 408 (1963).
3. V. P. Mashkovich and V. A. Klimanov, At. Energ., 20, No. 2, 127 (1966).

STABLITY OF THE CALIBRATION CHARACTERISTICS OF DIFFERENTIAL-TRANSFORMER STRAIN TRANSDUCERS IN A NUCLEAR REACTOR

A. V. Kondrashov, P. P. Oleinikov, A. N. Sokolov, T. B. Ashrapov, and Kh. R. Yunusov

UDC 621.039.564

Differential-transformer transducers are used extensively for in-reactor monitoring of strain [1]. Practically no information, however, is available about the behavior of their calibration characteristics during operation. The present paper is devoted to the investigation of the effect that reactor radiation has no the stability of the output characteristics of one design of differential-transformer transducers for monitoring the radiation creep of structural materials.

The differential-transformer transducer is a coil, inside which is a plunger. The coil has three windings: one primary and two secondaries. The windings are made of PNÉT-IMID wire with a diameter of 0.1 mm, with 4160 turns in the secondaries. The coil form is made of 12Kh18N10T stainless steel and has a diameter of 11 mm and a height of 79 mm. The coil form is coated on the outside with insulating varnish 20-30 μm thick. The plunger, made of É10 steel, has a diameter of 3.8 mm and a length of 60 mm.

The in-reactor investigation was carried out by comparing the output signals of transducers with periodic identical displacements of the plungers inside the differential-transformer coils. The displacement of the plungers from a fixed lower position to a fixed upper position was carried out with an electromagnet built into the upper part of each transducer.

The measurements were carried out with a KSD-2-007 recorder with a linear characteristic and a scale with 100 divisions. As a result of laboratory tests of three differential-transformer coils we established that their calibration characteristics are linear, with measuring ranges of 0-600, 0-610, and 0-640 μm. The principal error of the equipment is ± 2%. The temperature error is 0.12 div/deg K. All of the transducers were adjusted so that the recorder showed 25 divisions when the plungers were in the fixed lower position and 75 divisions in the upper fixed position, i.e., the reading changed by 50 divisions during the displacement of the plungers. The spread of the readings in this case did not exceed ± 1 unit.

Our investigations were carried out on the VVR-SM reactor of the Nuclear Physics Institute, Academy of Sciences of the Uzbek SSR. Transducers 1, 2, and 3 were placed in a helium medium at distances of 140 (the distance to the lower part of the differential-transformer coil), 460, and 660 mm, respectively, from the reactor core. During the investigations, voltage was applied to the transducer only for a short time (10-15 sec) as the reading was taken in order not to subject the transducer to additional heating.

Each transducer was provided with a Chromel–Alumel thermocouple. The thermocouple was fastened by a yoke to the outside of the transducer casing in the middle part of the differential-transformer coil. The transducers were in the reactor for a total of 8400 h and of this time 4739 h were under power, the breakdown of this time being 38% at 5 MW, 16% at 6 MW, 21% at 8 MW, and 7% at 10 MW, while for the remaining 18% of the time the reactor was

Translated from Atomnaya Énergiya, Vol. 55, No. 3, p. 178, September, 1983. Original article submitted October 28, 1982.

 0038-531X/83/5503-0618$07.50

operating at intermediate power. During the investigations the fluence of thermal and fast (> 1.15 MeV) neutrons and the absorbed doses of γ-rays were, respectively, $1.6 \cdot 10^{20}$, $1.2 \cdot 10^{20}$, and $4.6 \cdot 10^{19}$ thermal neutrons/cm^2, $8.5 \cdot 10^{19}$, $6.75 \cdot 10^{18}$, and $8.2 \cdot 10^{17}$ fast neutrons/cm^2, and $2.4 \cdot 10^{11}$, $2.5 \cdot 10^{10}$, and $2 \cdot 10^{9}$ rd (1 rd = 0.01 Gy). The error of these values was ± 50%.

The highest temperature of the casings of transducers 1, 2, and 3 during the investigations was 182, 60, and 40°C, respectively. The temperature of the differential-transformer windings, housed inside the casings, in this case exceeds the value given above as a consequence of radiation-induced energy release in the (steel) casing and plunger, and the copper wire of the winding, and as a result of Joule heating. The last component was small (10°K) since voltage is applied to the coils only for a short time. The extent to which the windings are heated as a result of the energy release can be determined from data on measurement of the ohmic resistance of the deenergized windings in the reactor and in the storage vault. We found that during the time in the reactor the ohmic resistance of all the windings of transducer 1 increased by 8-10% while the temperature of the windings of transducers 1, 2, and 3 at a power level of 10 MW was, respectively, 310, 87, and 70°C in the differential-transformer coils and 220, 83, and 70°C in the electromagnets. The error in the measurement of the temperature was ±5%. Comparing the values of the temperature, we can conclude that the component due to the energy release is significant for transducer 1 (140 mm from the reactor core) and is negligible for transducers 2 and 3 (460 and 600 mm from the reactor core). Thus, the maximum operating temperature of the windings was 310 ± 15°C for transducer 1. All of the differential-transformer tranducers remained serviceable during the investigation.

The agreement of the readings of the transducers (within the limits of the experimental error of ±5-10 μm) with the reactor operating at different power levels indicates that neutron flux densities of up to $1 \cdot 10^{13}$ thermal neutrons/cm^2•sec and up to $7.6 \cdot 10^{11}$ fast neutrons/cm^2•sec as well as a fluence of $1.6 \cdot 10^{20}$ thermal neutrons/cm^2 and 8.5×10^{19} fast neutrons/cm^2 do not affect the output characteristic of the differential-transformer transducers. The fact that the spread of the readings about the average value is up to ±2 divisions (±12 μm) is explained by the oscillations of the winding temperature, by the fact that the fixed positions are not completely reproducible, by the instrumental error, etc. In the case of all of the transducers the readings I_l corresponding to the lower position of the plunger remain stable (with an error of ±2 divisions) throughout the entire period of the investigations while the readings I_u corresponding to the upper position of the plunger, and hence $I_u - I_l$ as well, grow with the temperature. When the temperature correction is taken into account, however, the instability of the readings does not exceed 2%.

Thus, during our testing of differential-transformer transducers in the nuclear reactor we established that under the conditions described above their calibration characteristics remain stable (to within ±2%). Since these transducers preserved their initial calibration characteristics to the end of the tests, we can assume that their total service lifetime exceeds the real time of the tests, i.e., 4379 h. It cannot be ruled out that in an inert medium their operating temperature can be increased and they can be used in radiation fields with a higher intensity.

LITERATURE CITED

1. J. Boland, Monitoring Instruments for Nuclear Reactors [Russian translation], Atomizdat Moscow (1973), p. 77.
2. G. I. Sochilin, Abstracts of an All-Union School on In-Reactor Methods of Investigation [in Russian], NIIAR, Dimitrovgrad (1977), p. 28.
3. French Patent No. 2064761, Class G 01 b7/00 (1969).

AUTOMATED MONITORING SYSTEM FOR THE TECHNOLOGICAL PROCESS OF SEPARATION OF TRANSPLUTONIUM ELEMENTS

V. A. Bikineev, N. S. Glushak, V. V. Pevtsov,
A. N. Filippov, I. V. Tselishchev,
and V. I. Shipilov

UDC 621.039.59:66.012

In order to determine the content of α-emitting elements in solutions extensive use is made of radiometric methods based on immersible silicon semiconducting detectors (SD) [1-5]. Detection blocks based on such SD are compact, simple to use, and are employed successfully for rapid analysis of the activity of solutions during the processing of spent fuel [3] and the separation of transplutonium elements (TPE) from irradiated materials [4]. The continuous nature of the radiochemical processes of separation and purification of TPE necessitates the creation of multichannel local systems for data acquisition and processing.

In this paper we describe a simple automated system for monitoring the technological process of TPE separation; the system is based on a 15VSM-5 computer (Fig. 1) and contains 32 counting and 8 spectrometric immersible α-ray semiconductor detectors (Table 1). The connection between the computer and the electronic units are made through an interface [6]. It forms words of the necessary length from a series of byte transfers from the computer and ensures exchange of information between the digital units and the computer. The latter is used with a 4-kbyte VZU 1530-17 external memory unit and a "Consul 260" printer.

The system operates in two modes: in a counting mode (two pulse counters for 32 channels) and in a spectrometric mode (one 512-channel pulse analyzer for 8 channels). The period and cycle of the measurements are prescribed in a program by means of the computer, the BKI-01 timer, and the BKU-32 and BKU-8 controlled commutator units (see Fig. 1). When information is accumulated from the counting SD, the signals travel through the PU-01 preamplifiers, the BID-32 block of integral descriminators, and the BKU-32 unit to arrive at the input of two 24-bit BSchTs2-90 counters. The input pulses from the selected spectrometric SD are trans-

TABLE 1. Parameters of Immersible Detectors*

Parameters	Surface-barrier, counting	Surface-barrier, spectrometric	Silicon–lithium drift, spectrometric
Material	n-type Si	p-type	type Si(Li)
Sensitive area, mm^2	1—25	5—25	10,15
Operating voltage, V	1,5	25—50	25—100
Capacitance, pF	50—500	10—30	5—10
Resistance of body, Ω	100—250	100—250	1000
Range of activity measured, Bq/liter	$2\cdot10^8$—$4\cdot10^{10}$	$4\cdot10^7$—$5\cdot10^{11}$	$2\cdot10^7$—$4\cdot10^{11}$
Energy resolution, %	—	0,5—1	1,5—2
Radiation measured	α	α	α, β
Temp. range, °C	20—80	20—60	20—25

*The SD casing — glass; working medium — solutions of nitric acid with concentration of 0.1-0.8 mole/liter.

Translated from Atomnaya Énergiya, Vol. 55, No. 3, pp. 179-180, September, 1983. Original article submitted December 8, 1982.

 0038-531X/83/5503-0620$07.50

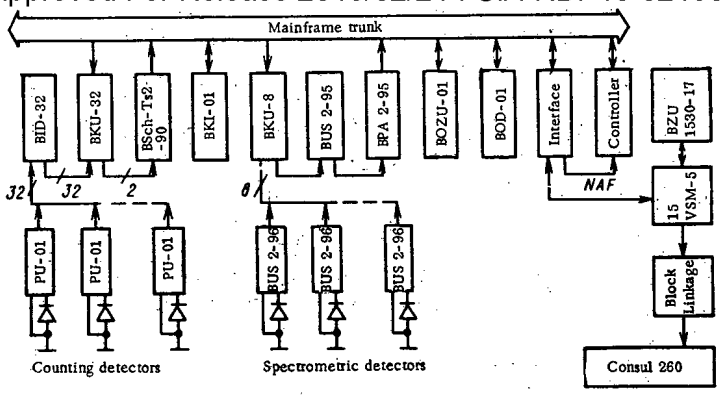

Fig. 1. Block diagram of the system: PU-01) amplifier; BKU-32) and BKU-8) controlled commutator units; BKI-01) timer unit; BOZU-01) immediate-access memory unit; BOD-01) data-display unit; BZU 1530-17) external memory unit; BPA 2-95) analog-to-digital converter; BSchTs2-90) block of counters; BUS 2-95 and BUS 2-96) spectrometric amplifiers; BID-32 block of integral discriminators.

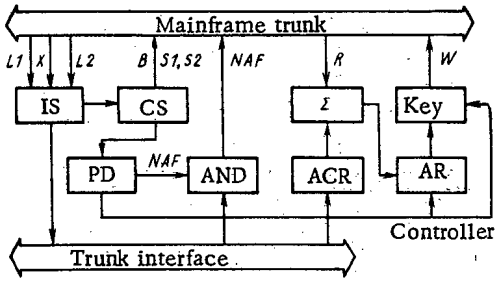

Fig. 2. Block diagram of controller: IS) interrupt shaper; CS) CAMAC cycle shaper; PD) pulse distributor; ACR) auxiliary-code register, and AR) address register.

mitted through the BUS 2-96 preamplifier, the BKU-8 commutator built with hercons, and the BUS 2-95 amplifier, after which they are converted into digital code by the BPA 2-95 analog-to-digital converter and are stored in the BOZU-01 immediate-access memory which has a capacity of 512 16-bit words.

The continuous spectral distribution, consisting of characteristic steps in the region of maximum amplitudes which correspond to the energy of the α-emitter, is observed with the aid of a BOD-01 data display unit based on an Élektronika VL-100 commerical TV receiver [7]. The display shows graphical and digital information on its screen. The vertical scale is 512, 1024, .., 65,536 pulses per channel while the horizontal scale is 32 or 256 channels. The address of the first channel, the current address of the marker, and the relative scale of reproduction of the graphical information are displayed in digital form. The marker is controlled by keys which move the marker by one address when depressed for a short time and at an increasing rate when in the locked-in state.

In order to organize the analyzer mode with allowance for the limited speed of the 15VSM-5 computer we designed a simple mainframe controller (Fig. 2), which permits operation with the digital units of the system according to the program with the computer as well as in an autonomous mode according to a firm routine for processing high-priority inquiries from the BPA 2-95 and BOD-01 units. When an inquiry L1 or L_{ADC} appears from the analog-to-digital converter signals from the output of the interrupt shaper (IS) trigger the CAMAC cycle shaper (CS) and the pulse distributor (PD), which generate a certain sequence of CAMAC commands (NAF, B signal, and strobes S1 and S2). In response to these commands the address is read from the ADC along the buses W and the address-register (RA) and is then transmitted to the immediate-access memory along the buses W with +1 added to the address. In response to a command from the controller the unit should display a COMMAND RECEIVED signal X. The BOD-0

TABLE 2. Results of Spectrometric Measurements

Solution	Elements	Rel. content, %	
		remote measurement	laboratory analysis
1	^{243}Am	7,93±0,4	$8,3^{+1,6}_{-0,2}$
	^{241}Am	3,97±0,35	$4,2^{+2,3}_{-0,2}$
	^{244}Cm	88,1±0,6	87,5±0,3
2	^{243}Am	1,89±0,4	$2,0^{+0,4}_{-0,1}$
	^{241}Am	1,09±0,65	$1,2^{+0,6}_{-0,1}$
	^{244}Cm	97,22±0,3	96,8±0,8

TABLE 3. Results of Counting Measurements

Solution	Specific activity, Bq/liter	
	remote measurement	laboratory analysis
1	$(1,36\pm0,13)\cdot10^{6}$	$(1,43\pm0,07)\cdot10^{6}$
2	$(3,08\pm0,03)\cdot10^{10}$	$(3,10\pm0,02)\cdot10^{10}$
3	$(0,68\pm0,07)\cdot10^{7}$	$(0,67\pm0,04)\cdot10^{7}$
4	$(4,62\pm0,46)\cdot10^{10}$	$(4,61\pm0,02)\cdot10^{10}$

unit displays an L2 or L_{BOD} inquiry and the current address of the displayed information, according to which data are transmitted from the immediate-access memory for display. Since the servicing time of each inquiry is 3 μsec, the increase in the dead time of the analyzer as a result of the execution of the observation functions is insignificant. Sicne the BOD-01 unit makes it possible to observe 32 or 256 channels, in order to examine the entire spectral distribution the current address of the displayed information is augmented with a constant code which is prerecorded in the auxiliary-code register (ACR) of the computer.

The data are displayed as follows. From the counts of the channels, the calibration coefficients are predetermined using a solution of the specimens and are recorded in the computer. The specific activity of the measured solution is determined from the product of the measured α-particle counting rate and the corresponding coefficient.

The spectrometric information is processed by using the method of digital windows which are established at every step in the amplitude distribution of pulses from the immersed SD. The relative specific activity of each component is determined from the drop between steps. The program makes it possible for the digital data about the specific activity of the solution to be provided sequentially for the channels of the analyzer, thus permitting visual observation of the variations in the technological process.

As an example Tables 2 and 3 present some results of remote measurement of the parameters of technological parameters by means of this system when monitoring one process of separation of transplutonium elements and laboratory analysis of specimens. When the data obtained by these methods are compared, it is seen that they agree within the limits of the indicated error of measurements.

The results presented here suggest that this system possesses fairly broad capabilities for rapid monitoring of the processes of separation of transplutonium elements by the extraction technology since it can provide information about the course of continuous technological processes without taking samples and thus to adjust the necessary parameters at the proper time.

LITERATURE CITED

1. V. V. Pevtsov and V. V. Krayukhina, Prib. Tekh. Eksp., 4, 80 (1976).
2. M. I. Krapivin et al., Proceedings of Fourth COMECON Symposium "Research on the Processing of Spent Fuel," Atomic Energy Commission, Czechoslovakia, Prague (1977), Vol. 3, p. 188.

3. M. I. Krapivin et al., Radiokhimiya, 21, 321 (1979).
4. V. V. Pevtsov and G. A. Timofeev, Radiokhimiya, 19, 450 (1977).
5. V. V. Pevtsov et al., At. Energ., 44, No. 4, 369 (1978).
6. N. S. Glushchak et al., Preprint NIAAR-26 (434), Dimitrovgrad (1980).
7. V. S. Baklanov and V. D. Loginov, Preprint NIAAR-19 (472), Dimitrovgrad (1981).

NEUTRON GENERATION IN A HIGH-VOLTAGE GLOW DISCHARGE

L. N. Pustynskii

UDC 621.039.531

A high-voltage glow discharge (HGD) in deuterium in the region of a working potential of ~0.2 MV allows intense neutron fluxes to be obtained [1]. In the present work, the neutron yield is calculated in the excitation of the reactions $T(d, n)^4He$ and $D(d, n)^3He$ in thick titanium targets with occluded tritium or deuterium bombarded by fast automatic and molecular ions accelerated in the region of the cathodic drop in HGD potential.

If a target with a nuclear concentration n of one of the heavy hydrogen isotopes is bombarded by particles of type i with energies in the range from T to T + dT and a flux density $d\Gamma_i(T)$, then the number of neutrons emitted from unit surface of the target in unit time is

$$dN_i = d\Gamma_i(T) \int_0^T \frac{n\sigma_i(W)}{|dW/dx|} dW. \quad (1)$$

Here $\sigma_i(w)$ is the energy dependence of the total reaction cross section for particles i; $|dW/dx|_i$ is the specific energy loss by particles i in the target. By definition

$$d\Gamma_i(T) = \Phi_i(T)\, dT, \quad (2)$$

where $\Phi_i(T)$ is the spectral density of the flux of particles i at the target surface. The method of calculating $\Phi_i(T)$ for the HGD in deuterium was considered in detail in [2]. Substituting Eq. (2) into Eq. (1), and integrating over all possible values of the energy T for i particles, it is found that

$$N_i = \int_0^{T_{max}} \Phi_i(T) \int_0^T \frac{n\sigma_i(W)}{|dW/dx|_i} dW\, dT. \quad (3)$$

Summing Eq. (3) over all forms of neutronlike particles (D_3^+, D_2^+, D^+, and D), it is found that

$$N_\Sigma = \sum_{i=1}^{5} N_i. \quad (4)$$

It is assumed that, on entering the target, molecular particles dissociate into atomic components with the velocity of the molecular particles. The specific energy losses in the solid do not depend on the charge state of the incident particles, since, on passing through

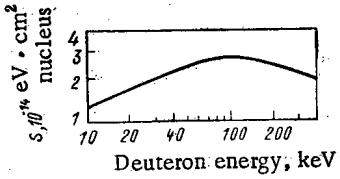

Fig. 1. Deuteron retardation cross section in titanium targets with occluded deuterium or tritium.

Translated from Atomnaya Énergiya, Vol. 55, No. 3, pp. 180-182, September, 1983. Original article submitted December 9, 1982.

0038-531X/83/5503-0623$07.50

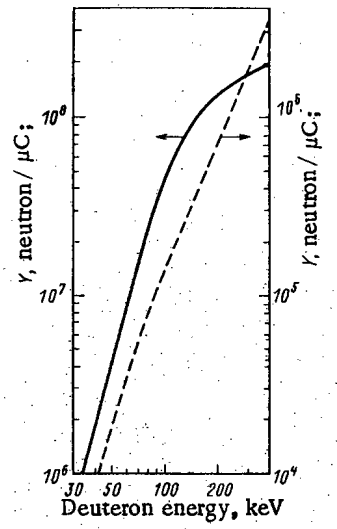

Fig. 2. Excitation functions of the reactions T(d, n)^{4}He (continuous (curve) and D(d, n)^{3}He (dashed curve) in titanium targets.

a few atomic layers of material, a charge equilibrium determined solely by the particle velocity is established in the particle flux [3]. Therefore, instead of individual types of particles i, the total spectral flux of the deuteron flux $\Phi_\Sigma(T)$ with the corresponding energy dependence may be considered. Then Eq. (4) is written in the form

$$N_\Sigma = \int_0^{T_{max}} \Phi_\Sigma(T) \int_0^T \frac{n\sigma(W)}{|dW/dx|_i} dW\, dT. \tag{5}$$

The excitation functions of the reactions D(d, n)^{3}He and T(d, n)^{4}He are calculated using the well-known experimental dependences of the cross sections of these reactions on the energy of the incident deuterons [4].

If the energy loss of the deuterons on passing through a target layer of thickness dx is the sum of the energy losses at titanium atoms and the corresponding hydrogen isotope (Bragg rule), then

$$\frac{1}{n}\left|\frac{dW}{dx}\right| = \varepsilon + \frac{n_{Ti}}{n}\varepsilon_{Ti}. \tag{6}$$

The retardation cross sections at titanium atoms ε_{Ti} and atoms of the heavy hydrogen isotope ε (taken to be that for protium) are calculated from the empirical formula [5]

$$\frac{dW}{dx} = \frac{av + bv^2}{0{,}01v^{2{,}25} + c}, \tag{7}$$

where v is the proton velocity, 10^8 cm/sec; a, b, c are constants characterizing the target material. The accuracy of Eq. (7) was estimated in [4] as 10-15% for protons of energy between 5 keV and 50 MeV. The energy dependence of the deuteron retardation cross section $S = (1/n)\left|(dW/dx)\right|$ in titanium targets with an atomic ratio $^j_1$H/Ti = 1.65 (j = 2.3) is shown in Fig. 1 and the excitation function

$$Y(T) = \int_0^T \left[\sigma(W)\Big/\frac{1}{n}\left|\frac{dW}{dx}\right|\right] dW$$

of the reactions D(d, n)^{3}He and T(d, n)^{4}He in such targets in Fig. 2.

Calculations show that, in the working-potential range 80-300 kV, 70-80% of the neutrons are produced by atomic ions, while the neutron field from T—Ti targets is 270-300 times higher than from D—Ti targets, other conditions being equal. For verification that the model is adequate and comparison with experiment [1], the neutron yield is calculated for the reaction $D(d, n)^3He$ from the experimental dependence of the working potential on the time. The total yield is found to be three times less than the measured value. Taking into account the unavoidable errors in the cross sections of the elementary processes in the model of [2] and the one-dimensionality of the model, such agreement is somewhat unexpected, since the yield of the reaction $D(d, n)^3He$ is extremely sensitive to the deuteron energy (see Fig. 2).

With constant pressure in the discharge chamber the dependence of the neutron yield on the working potential U may be represented approximately as $N \sim U^{5.2}$, i.e., increases significantly more rapidly than the excitation function of the reaction (Fig. 2). This is due to two factors: The discharge current density increases with increase in U: $I \sim U^{2.3}$ [1, 2]; the mean deuteron energy over the spectrum $\bar{T}$ increases more rapidly than U, on account of the fall in recharging cross section with increase in deuteron energy.

A power-law dependence of the neutron yield on the pressure is also observed: $p = (0.9\text{-}2.15)\ 10^2$ mm Hg*; U is a constant, which may be expressed in the form $N_\Sigma \sim p^{3.6}$. With increase in pressure, there is not only an increase in discharge current ($I \sim p^{2.3}$ [1, 2]), but also the deuteron energy spectrum at the cathode becomes harder as a result of decrease in the reduced length pd of the region of cathodic drop in HGD potential and the reduction in mean number of rechargings. Therefore, further experimental investigations are necessary in order to resolve the question as to whether increase in pressure or increase in potential is preferable as a means of increasing the neutron yield, since a maximum of the neutron yield has been found experimentally [1] as a function of the working potential and pressure. The presence of such a maximum is due to the finite electrical strength of the cathode element, which is the weakest component of the discharge tube.

Calculations confirm the conclusion of [1] that a neutron flux of $> 10^{15}$ neutron/sec may be obtained using a HGD in deuterium at 200 kV, if the reaction $T(d, n)^4He$ is excited. This flux may be increased by an order of magnitude by increasing the working potential to 300 kV, without change in pressure in the tube, if the necessary electrical strength of the insulator surface in the cathode region is maintained, since the electric field at the cathode is no more than 100 kV/cm.

It remains to thank A. F. Surin for assistance in developing the algorithm for numerical solution of the HGD model.

LITERATURE CITED

1. L. N. Pustynskii, S. R. Kholev, and G. V. Yakushin, At. Energ., 52, No. 4, 262 (1982).
2. L. N. Pustynskii, Teplofiz. Vys. Temp., 21, No. 3, 441 (1983).
3. Yu. V. Gott and Yu. N. Yavlinskii, Interaction of Particles with Matter and Plasma Diagnostics [in Russian], Atomizdat, Moscow (1973).
4. Dzh. Brolli and Dzh. Fauler, in: Physics of Fast Neutrons, Vol. 1, Experimental Procedures [Russian translation], Gosatomizdat, Moscow (1963), p. 20.
5. Yu. V. Gott, At. Energ., 27, No. 4, 543 (1969).
6. L. N. Pustynskii, S. R. Kholev, and G. V. Yakushin, Teplofiz. Vys. Temp., 20, No. 2, 207 (1982).

*Note that 1 mm Hg = 133.322 Pa.

TWO-PARAMETER REPRESENTATION IN THE BINARY-COLLISION APPROXIMATION OF THE CROSS SECTION OF ATOMIC K IONIZATION BY A HEAVY CHARGED PARTICLE

V. F. Volkov, S. A. Gerasimov, and A. N. Eritenko

UDC 539.186.2

The ionization cross sections of K-shell electrons have been calculated in a number of works in the binary-collision (BEA) model, on the basis of hydrogenlike [1, 2], Slater [3], and self-consistent [4-6] one-electron wave functions describing the 1s state of an electron in an atom. In [3], the influence of the type of electron distribution with respect to the momentum on the energy dependence of the ionization cross section was investigated, and it was concluded that the use of the correct wave functions improves the agreement of the experimental and theoretical results. The calculations of the ionization cross section using self-consistent wave functions were performed in most works for a limited number of target elements and a relatively narrow range of incoming-particle energies, and represented, in general, in graphical form. All this complicates the use of the calculation results already obtained in analyzing experimental data.

The aim of the present work is to obtain a universal scale dependence (analogous to that in [2]) determining the ionization cross section of the atom when using parametrized self-consistent wave functions. In the present work, this problem is solved for the ionization of K-shell electrons, described by the wave functions of [7-10]. The results given below are valid for any radial single-electron wave functions that may be represented in the form

$$\Psi_{1s} = A \exp\left(-\gamma \frac{r}{a_0}\right). \quad (1)$$

TABLE 1. Values of the Universal Scalar Dependence $S_K(T, \beta)$

T	β							
	0,5	0,6	0,7	0,8	0,9	1,0	1,1	1,2
1,00—3	3,73—5	8,95—6	2,66—6	9,23—7	3,69—7	1,57—7	7,36—8	3,68—8
1,59—3	1,78—4	4,40—5	1,30—5	4,56—6	1,80—6	7,80—7	3,73—7	1,86—7
2,51—3	8,23—4	2,06—4	6,40—5	2,23—5	8,85—6	3,86—6	1,82—6	9,12—7
3,98—3	3,67—3	9,56—4	2,99—4	1,07—4	4,38—5	1,89—5	8,98—6	4,53—6
6,31—3	1,56—2	4,25—3	1,38—3	5,06—4	2,07—4	9,20—5	4,47—5	2,26—5
1,00—2	5,97—2	1,81—2	6,06—3	2,31—3	9,68—4	4,38—4	2,12—4	1,09—4
1,59—2	2,09—1	6,87—2	2,56—2	1,02—2	4,37—3	2,03—3	1,00—3	5,22—4
2,51—2	6,49—1	2,39—1	9,53—2	4,08—2	1,90—2	9,17—3	4,59—3	2,44—3
3,98—2	1,75	7,32—1	3,24—1	1,51—1	7,37—2	3,76—2	2,04—2	1,12—2
6,31—2	4,27	1,94	9,60—1	4,93—1	2,61—1	1,43—1	8,03—2	4,64—2
1,00—1	8,31	4,41	2,44	1,43	8,05—1	4,77—1	2,88—1	1,77—1
1,59—1	1,46+1	8,55	5,21	3,26	2,08	1,35	8,85—1	6,06—1
2,51—1	2,20+1	1,40+1	9,31	6,35	4,41	3,10	2,21	1,59
3,98—1	2,86+1	1,83+1	1,38+1	1,00+1	7,48	5,65	4,32	3,33
6,31—1	3,18+1	2,26+1	1,68+1	1,29+1	1,01+1	8,04	6,49	5,00
1,00	3,05+1	2,23+1	1,71+1	1,36+1	1,10+1	9,06	7,59	6,42
1,59	2,56+1	1,90+1	1,49+1	1,20+1	9,91	8,36	7,15	6,20
2,51	1,93+1	1,45+1	1,14+1	9,29	7,76	6,62	5,73	5,03
3,98	1,35+1	1,02+1	8,04	6,58	5,53	4,74	4,13	3,64
6,31	9,02	6,80	5,38	4,42	3,72	3,20	2,79	2,47
1,00+1	5,87	4,43	3,51	2,88	2,43	2,09	1,83	1,62

Note. The values of T and $S_K(T, \beta)$ are given in floating-point form: for example, $3.73-5 = 3.73 \cdot 10^{-5}$; $1.46+1 = 1.46 \cdot 10^{1}$, etc.

Translated from Atomnaya Énergiya, Vol. 55, No. 3, pp. 182-183, September, 1983. Original article submitted December 28, 1982.

 0038-531X/83/5503-0626$07.50

TABLE 2. Coefficients A_{lm}

l	m			
	1	2	3	4
1	−1,6401	−19,5481	4,3163	1,0022
2	2,5526	2,1828	−1,1294	0,2555
3	$-6{,}7861\cdot10^{-3}$	−0,2007	0,3542	−0,4899
4	$-4{,}4739\cdot10^{-2}$	$6{,}2682\cdot10^{-2}$	$1{,}3289\cdot10^{-3}$	0,1133
5	$2{,}4598\cdot10^{-3}$	$-1{,}2106\cdot10^{-2}$	$-1{,}7717\cdot10^{-3}$	$-1{,}2684\cdot10^{-2}$
6	$-9{,}2936\cdot10^{-6}$	$7{,}7271\cdot10^{-4}$	$-1{,}8168\cdot10^{-4}$	$6{,}2660\cdot10^{-4}$

Here a_0 is the first Bohr radius; A is a constant which may be found from the normalization condition; values of the constant γ for various atoms and for the Clementi—Raimodi and Gombas-Szondy functions may be found in [8-10].

For Slater orbitals, the screening constant s is determined from the Slater rule and the nuclear charge of the target Z_2: $\gamma = Z_2 - s$. For hydrogenlike atoms in the classical [11] BEA approximation, the parameter γ, equal to the effective nuclear charge of the target, is determined for the given subshell from the relation

$$U = \frac{\gamma^2}{n^2}\,\mathrm{Ry}, \tag{2}$$

where n is the principal quantum number of the subshell; Ry is the Rydberg energy constant; U is the binding energy of the given electron. In the BEA approximation, the ionization is described using the expressions of [12, 13], which are valid for atomic ionization by a heavy charged particle and are expedient for analytical and numerical calculations. Scaled results of calculating the ionization cross sections may be performed taking account of the dependence on the quantities

$$T = E_1/\lambda U \tag{3}$$

and

$$\beta = 2U/m_2\gamma^2\alpha^2c^2, \tag{4}$$

where E_1 is the kinetic energy of the incoming particle; $\lambda = M_1/m_2$ is the mass ratio of the incoming particle and the electron; α is the fine-structure constant; c is the velocity of light.

For all target atoms with $Z_2 < 87$, β varies in the range $0.5 < \beta < 1.2$. The dependence of the ionization cross section σ on T and β and the charge of the incoming particle Z_1 may be written in terms of the universal function $S_K(T, \beta)$

$$\sigma = \frac{Z_1^2\beta^2}{U^2}\,S_K(T, \beta). \tag{5}$$

Values of $S_K(T, \beta)$ as a function of T and β obtained in the binary-collision model are shown in Table 1 in units of 10^{-20} cm^2•keV^2. The particular case when $\beta = 1$, as follows from Eqs. (2) and (4), corresponds to calculation in the classical BEA approximation using a hydrogenlike wave function of the 1s state of the electron in the atom.

The tabulated values of $S_K(T, \beta)$ are not always expedient in practice. Therefore, with an error of less than 10%, the following appropriate expression may be used in the range $3\cdot10^{-3} \leqslant T \leqslant 10$:

$$S_K(T, \beta) = \exp\sum_{l=1}^{6}\sum_{m=1}^{4} A_{lm}\beta^{m-1}\ln^{l-1}(1{,}01\cdot10^3T), \tag{6}$$

which is obtained by approximating the tabular values of $S_K(T, \beta)$. The coefficients A_{lm} are given in Table 2. The results obtained may be useful in solving a series of problems associated with describing the K-electron ionization of an atom by heavy charged particles.

LITERATURE CITED

1. J. Garcia, Phys, Rev., A1, 280 (1970).
2. J. Garcia, R. Fortner, and T. Kavanagh, Rev. Mod. Phys., 45, No. 2, 111 (1973).
3. F. F. Komarov and A. P. Novikov, Zh. Tekh. Fiz., 48, No. 7, 1449 (1978).
4. T. Bonsen and L. Vriens, Physica, 47, 307 (1970).
5. F. F. Komarov and A. P. Novikov, Zh. Tekh. Fiz., 49, No. 2, 264 (1979).
6. F. Komarov and A. Novikov, Phys. Lett., 66A, No. 4, 287 (1978).
7. J. Slater, Quantum Theory of Atomic Structure, Vol. 1, London—New York—Toronto (1960).
8. E. Clementi and D. Raimodi, J. Chem. Phys., 38, 2686 (1963).
9. E. Clementi, D. Raimodi, and W. Reinhardt, J. Chem. Phys., 47, 1300 (1967).
10. P. Gombas and T. Szondy, Solution of Simplified Self-Consistent Field for All Atoms of Periodic System of Elements from Z = 2 to Z = 92, Adam Hilger, London (1970).
11. J. Hansen, Phys. Rev., A8, No. 2, 822 (1973).
12. E. Gerjuoy, Phys. Rev., 148, No. 1, 54 (1966).
13. M. Rudd, D. Gregoire, and J. Crooks Phys. Rev., 3A, No. 5, 1635 (1971).

FEATURES OF A RADIOACTIVE FLOW IN A PIPELINE

G. Yu. Kolomeitsev, I. E. Nakhutin, and P. P. Poluéktov

UDC 539.16.04

When a radioactive gas moves along a pipeline, electric fields are produced near the wall because of the differences in diffusion speed between the different types of ions during recombination at the surface. This may have a substantial effect on the distribution of aerosol particles over the cross section and on the deposition on the wall.*

We consider the electric fields arising in a gas flowing between two planes separated by a distance l. Pairs of ions of two kinds are formed uniformly over the volume by radioactive decay: type i with charge e and type e with charge $-e$. If the specific activity of the gas is A, while one decay generates Z pairs, then $a = ZA$ ions of each sign arise in unit time in unit volume. We assume that the ions recombine at the surfaces, not in the volume (an inequality governing this is given below). The current due to ions of either type is the sum of the diffusion and drift currents, but the drift current can be neglected over a wide range in specific activity.†

With these assumptions, the spatial distribution of the ions is found by solving the diffusion equations with sources for the densities n_i and n_e of the two types of particles supplemented by boundary conditions at the surfaces $-\mathbf{jk}|_{x=0,\ l} = \varkappa n_i n_l|_{x=0,\ l}$, where the x axis is perpendicular to the surfaces, k is unit vector normal to the surface and directed into the volume, $\mathbf{j} = \mathbf{j}_{e\ (i)} = -D_{e(i)} \nabla n_{e(i)}$ is the diffusion current, and $\varkappa$ is the surface recombination coefficient.† The electric field is found by integrating Poisson's equation. The solution takes the form

$$D_e n_e = D_i n_i = -\frac{a}{2}\left(x-\frac{l}{2}\right)^2 + b; \quad E = 4\pi e\left(\frac{1}{D_i}-\frac{1}{D_e}\right)\left(x-\frac{l}{2}\right)\left[-\frac{a}{6}\left(x-\frac{l}{2}\right)^2 + b\right],$$

where $b = \sqrt{\frac{D_e D_i l a}{2\varkappa}} + \frac{a l^2}{8}$. The maximum ion concentrations $n_{e(i)\ \max} = D_{e(i)}^{-1} b$ occur at points half

*Although these topics are obviously important, they appear not to have been considered previously (see [1] for example).

†The case where the drift current is important has been considered in [2].

†Boundary conditions of this kind are obvious for insulating surfaces. They can be used for a metal if the time of charge tunneling through the oxide layer at the surface is greater than the recombination time for a pair. Other boundary conditions do not greatly complicate solution of this linear problem.

Translated from Atomnaya Énergiya, Vol. 55, No. 3, pp. 183-184, September, 1983. Original article submitted January 24, 1983.

 0038-531X/83/5503-0628$07.50

way between the planes, while the maximum field

$$E_{\max}=4\pi e\,|\,D_i^{-1}-D_e^{-1}\,|\,\frac{l}{2}\left(b-\frac{a}{6}\frac{l^2}{4}\right)$$

occurs near the surfaces. It is characteristic that no field occurs if $D_i = D_e$, but usually D_i and D_e differ substantially: For example, if the carriers of negative charge are electrons then $D_e \gg D_i$.

We assume that for gases under normal conditions $D_i \approx 0.3$ cm^2/sec $D_i^{-1} - D_e^{-1} \approx D_i^{-1}$; $l = 10$ cm. To estimate $\varkappa$ we use the fact that the number of ions moving towards the surfaces is equal to the number of ions that recombine there: $\varkappa n_e n_i = \beta n_{en} n_{in}$, where the subscript n denotes the surface ion density, with a number equal to the number of ions adsorbed in unit time from the flux of incident particles; $\sim 1/6 n_{e(i)} v_{e(i)}$, where $n_{e(i)}$, $v_{e(i)}$ are the values of the density and average velocity of the ions near the surface, and $n_{e(i)n} = \delta_{e(i)} n_{e(i)} = \frac{1}{6}\frac{\alpha_{e(i)}}{\gamma_{e(i)}} v_{e(i)}$, with

$\alpha_{e(i)}$ the probability of attachment of an ion to the surface and $\gamma_{e(i)}$ the rate of ion desorption from the surface. Then $\varkappa = \beta\delta_e\delta_i$ and estimates give $\alpha_e \approx 1$, $\gamma_e \approx 10^{-8}$—10^{-10} [3] (it is assumed that $\gamma = 10^{-8}$ sec) and $v_{e(i)} \approx 3\cdot 10^4$ cm/sec, $Z = 100$. Then $\delta_{e(i)} \approx 10^{-4}$ см, $\varkappa \approx 10^{-10}$ cm$^4\cdot$sec^{-1}. The terms in b are of the same order for A 10^{-3} Ci/liter (1 Ci = 3700×10^{10} Bq), and in that case $E_{\max} \approx 5\cdot 10^3$ V/cm. For decreasing activity, the field decreases as $\sqrt{A}$. For example, for $A \approx 10^{-7}$ Ci/liter we get $E_{\max} \approx 50$ V/cm.

The above argument applies if we neglect ion recombination in the volume and assume that the drift current is small by comparison with the diffusion one. It is then necessary to obey the following inequalities:

$$\alpha n_{i\max} n_{e\max} \ll a;$$

$$D_{e(i)}\left|\frac{\partial n_{e(i)}}{\partial x}\right|_{x=0} \gg E n_e(i)\,|_{x=0}.$$

The treatment can be extended to cases where one incorporates bulk recombination and ion drift in the electric field, as well as secondary ion and electron emission from the surface, while one can refine the boundary conditions and include diffusion of the neutral atoms (an inhomogeneity in these arises from recombination at the surfaces).

Aerosol particles acquire charges in a radioactive atmosphere, which are determined by their properties and the characteristics of the medium. The situation is best defined for hot radioactive particles, whose charges have been examined by Petryanov and his school [1]: Hot particles, no matter what the nature of the emitter, are positively charged, and the charge increases with the particle size; the charge can be very considerable. For example, a particle of radius 1 μm bears a charge of 100e, if its activity is about 10^{-9} Ci. A macroscopic particle having a charge coincident in sign with the uncompensated charge in the gas flow is acted on by forces directed towards the wall and vice versa. Particles of the first type will be deposited rapidly on the wall, while those of the second will be focused at the axis, where they coalesce and are deposited. This means that the electric field near the wall in a pipeline produces dust deposition. For example, in a pipe of diameter 10 cm particles of radius 1 μm are deposited on the wall by diffusion in about 10^5 sec in the absence of electric fields. The above field estimates indicate that with an activity of about 10^{-3} Ci/liter the drift velocity for a particle of radius 1 μm is of the order of the diffusion velocity (about 0.1 cm/sec) and the deposition time is smaller by three orders of magnitude.

Therefore, strong electric fields (sometimes up to breakdown level) arise in pipelines at high specific activity levels, and these cause rapid deposition of aerosol particles on the wall and may improve the performance in nuclear power station cleaning systems such as filters under emergency conditions.

LITERATURE CITED

1. V. V. Gromov, Electrical Charges in Irradiated Materials [in Russian], Energoizdat, Moscow (1982).
2. M. S. Benilov, V. I. Kovbasyuk, and G. A. Lyubimov, Dokl. Akad. Nauk SSSR, 266, No. 4, 812 (1982).
3. J. De Boer, The Dynamical Character of Adsorption [Russian translation], IL, Moscow (196

METHODS OF MEASURING ^{10}B BURNUP IN REACTOR ABSORBING COMPONENTS

V. P. Koroleva
and P. S. Otstavnov

UDC 621.039.519:621.039.562

The large thermal-neutron abosrption cross section of ^{10}B means that it is used as one of the basic materials for reactor control rods. During the use of the absorbing rods, the ^{10}B is burned out unevenly. The rod performance then alters. However, a fairly high content of the isotope still persists in some parts, and so the rods can be further used.

This makes methods of measuring ^{10}B burnup important.

Here we examine the determination of ^{10}B by methods based on the nuclear-physics properties of the boron isotopes or of the products from the reaction of ^{10}B with neutrons as used in measuring burnup in reactor absorbing rods. We have considered about 70 papers, and references are given to some of them.

The following methods were examined:

1) neutron transmission by the medium or neutron backscattering from it followed by recording [1];

2) measurement of the $^{10}B/^{11}B$ concentration ratio by mass spectrometer before and after neutron irradiation [2, 3];

3) recording the products from $^{10}B(n, \alpha)^{7}Li$, i.e., the α particles and the lithium nuclei during neutron irradiation [4];

4) determination of ^{10}B burnup from the amount of helium formed in the medium [5];

5) determination of ^{10}B burnup from the amount of lithium formed during neutron irradiation [6, 7];

6) activation analysis [8];

7) 8) prompt γ-ray recording α-particle bombardment with neutron or γ-ray recording [9]; and from the ^{7}Li formed by the interaction of neutrons with ^{10}B [10, 11].

The following points may be made from the papers and the analysis of these methods.

Virtually all the methods that have been used to determine boron in media with small enrichments in ^{10}B ($\leqslant 1\%$) can be used to measure ^{10}B contents in absorbing rods. The effects of possible interfering impurities must be borne in mind.

When the $^{10}B/^{11}B$ ratio is measured with a mass spectrometer before and after irradiation in order to determine ^{10}B burnup in absorbing rods, it is necessary to allow for the change in the ^{11}B, since the concentration of this does not remain constant during the operation of an absorbing rod.

It is impossible to determine ^{10}B burnup from the amount of lithium formed since the existing methods of collecting the lithium do not provide complete collection at the points of formation because of features of the behavior.

It is difficult to determine ^{10}B burnup from the amount of helium formed because of the high mobility and fluidity of helium, and also because there are neutron reactions on ^{10}B that do not involve the formation of α particles, while there are ones on impurities that do produce α particles. Therefore, the method cannot produce reliable results.

The best methods are activation analysis and recording the prompt γ rays produced by neutrons reacting with ^{10}B as regards the minimum effects from interfering impurities in determining ^{10}B contents in absorbing rods.

Translated from Atomnaya Énergiya, Vol. 55, No. 3, pp. 184-185, September, 1983. Original article submitted January 24, 1983.

 0038-531X/83/5503-0630$07.50

Of all the possible methods, nondestructive analysis is possible only by recording the prompt γ rays from the excitation of ^{7}Li in the reaction ^{10}B (n, α)^{7}Li.

LITERATURE CITED

1. V. P. Bovin, V. L. Chulkin, and S. V. Shagov, At. Energ., 38, No. 5, 283 (1975).
2. M. Zerner, "The analysis of elemental bron," USAEC, Div. Tech. Inform. Extension, Oak Ridge (1970), p. 37.
3. G. Palmer, Advances in Mass Spectrometry [Russian translation], IL, Moscow (1963).
4. Ya. Chudars et al., Izv. Akad. Nauk Latv. SSR, 57 (1960).
5. V. D. Klimov et al., Preprint FEI-1026, Obninsk (1980).
6. P. D. Kervalishvili, At. Energ., 51, No. 2, 123 (1981).
7. D. Secrist, J. Am. Ceram. Soc., 50, No. 10, 520 (1967).
8. Proceedings of the First All-Union Coordination Conference on Activation Analysis [in Russian], Nauka, Tashkent (1964).
9. G. N. Mikhailov and L. P. Starchik, in: Nuclear-Physics Analysis Methods [in Russian], Atomizdat, Moscow (1971), p. 188.
10. B. Garbrah and J. Whitley, Anal. Chem., 39, 345 (1967).
11. Ya. Boganch et al., in: Proceedings of the Third Conference on the Use of New Nuclear-Physics Methods for Handling Scientific and Economic Tasks [in Russian], JINR, Dubna (1979), p. 131.

AN EXAMPLE OF THE LARGE EFFECT OF ENTRAINMENT OF NEUTRONS BY MOVING COOLANT ON THE CRITICAL STATE OF A REACTOR

A. A. Kostritsa

UDC 621.039.5

Entrainment of neutrons by a moving medium is significant in the region where the moderator flows into the active zone or, vice versa, in the part of the active zone where the moderator leaves it. In a symmetrical reactor, flow of neutrons at the inlet of the coolant into the active zone can be suppressed by increasing the flow at the outlet of the coolant. When the coolant flows straight through a cosinusoidally distributed neutron flux, the influence of entrainment of neutrons on the reactivity is not large, as was shown in [1], and, apparently, it is rarely accounted for. For very high coolant velocities the effects described in [2] should occur, but such velocities are not yet used in practice. If the properties of the upper and lower reflectors differ [3] and the fuel is distributed unsymmetrically in the active zone or an asymmetry of the neutron flux arises in the course of xenon oscillations [4], then the effect of entrainment of neutrons on the reactivity can be significant. An ideal reactor could consist only of fuel and moving moderator and be regulated by neutron entrainment, if asymmetry did not conflict with the concept of an ideal reactor. We shall examine a model of the usual reactor with a uniform distribution of fuel and symmetrical end-face reflectors.

We shall show that in a high-flow stationary reactor with a large concentration of xenon, entrainment of neutrons by the coolant within the limits of coolant velocities encountered in practice has a considerable stabilizing action.

We shall examine the stationary state of a thermal reactor in the two-group approximation. We shall denote the density of thermal neutrons by N, and the density of moderated neutrons by n. In the model presented, the moderator is identified with the moving coolant; the reflector contains only coolant; the active zone contains, in addition to coolant, stationary fuel, distributed homogeneously over the active zone together with the absorber; the reactor is flat; the reflectors are infinite; and, the age of the thermal neutrons τ is the same in the active zone and in the reflector. We shall denote by Ψ the ratio of the neutron absorption cross section in the fuel Σ_{af} to the absorption cross section in the moderator Σ_{am}; Ψ is constant in the active zone and in the reflectors $\Psi = 0$, η is the number of secondary neutrons per neutron captured in the fuel. The system of equations for n and N has the form

$$d^2n/dz^2 - n/\tau + \eta(\Psi/\tau)N = 0; \tag{1}$$

$$d^2N/dz^2 - \zeta\, dN/L\, dz - (1 + \Psi + \Sigma_{af}/\Sigma_{am})N/L^2 + n/L^2 = 0. \tag{2}$$

Here z, $\sqrt{\tau}$, and the diffusion length of the moderator L refer to the half-width of the active zone; in the active zone, $1 \leqslant z \leqslant 1$; ζ is the ratio of the displacement of neutrons by the flow uT_0 to the diffusion length in the moderator $Z_0 = \sqrt{DT_0}$, where $T_0 = 1/v\Sigma_{am}$; D is the coefficient of diffusion of thermal neutrons; u is the effective velocity, somewhat less than the velocity of the coolant (see [1, 2] or [4]). Usually, ζ is small. For light water $\zeta \sim 0.1$ if $u \approx 13$ m/sec. To simplify, we shall assume that ζ is the same in the active zone and in the reflector. The absorption cross section includes the cross section for capture by xenon and the cross section Σ_{pn} of the regulating (or some additional) absorber. The stationary xenon concentration equals

$$Xe = \frac{0.064\Sigma_f\Phi}{\lambda_{Xe} + \sigma_{Xe}\Phi} = 0.064\,\frac{\Sigma_f}{\sigma_{Xe}}\,\frac{1}{1 + \lambda_{Xe}/\sigma_{Xe}\Phi}, \tag{3}$$

Translated from Atomnaya Énergiya, Vol. 55, No. 3, pp. 185-186, September, 1983. Original article submitted January 24, 1983.

 0038-531X/83/5503-0632$07.50

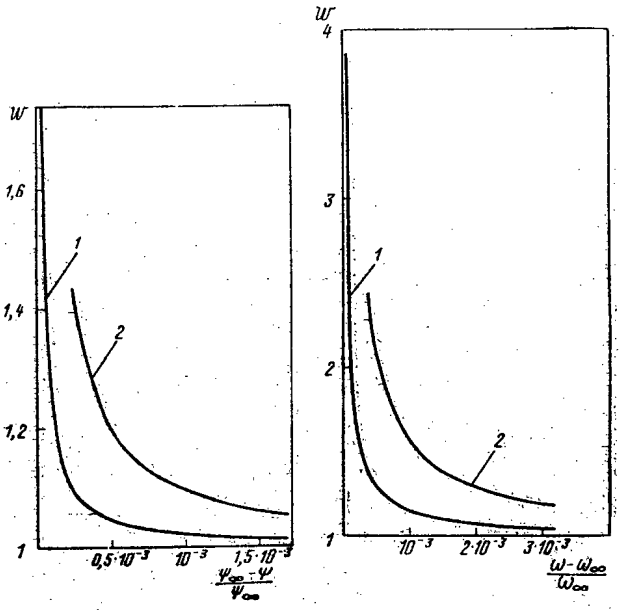

Fig. 1. Stabilizing influence of entrainment of neutrons by the moderator on the reactor power in the vicinity of the fuel concentration Ψ_∞ ensuring criticality with $x_e(\Phi = \infty)$: 1) $\zeta = 0.1$; 2) $\zeta = 0.2$.

Fig. 2. Combined effect of the regulator and entrainment of neutrons by the moderator on the reactor power with $\zeta = 0.1$ (1), 0.2 (2).

where Σ_f is the fission cross section; λ_{Xe} is the decay constant of xenon nuclei. For large neutron fluxes Φ, we shall write approximately

$$\Sigma_{Xe} = Xe\sigma_{Xe} \approx 0.064\Sigma_f[1-(\lambda_{Xe}/\sigma_{Xe}\Phi)]. \tag{4}$$

Then

$$\Sigma_{an}/\Sigma_{am} = 0.0256\eta\Psi(1-\gamma/N) + \Sigma_{pn}/\Sigma_{am} \tag{5}$$

where $\gamma \equiv \frac{\lambda_{Xe}}{\sigma_{Xe}\,\upsilon N^*}$; N^* is the scale of the density of thermal neutrons to which N in Eqs. (1) and (2) is referred. We shall set $\Phi^* \approx 10^{14}$ neutrons/(cm^2·sec). Then $\gamma \approx 0.063$. In order for assumption (4) to be valid, we shall examine only solutions in which N in the active zone is several units and more, so that $\gamma/N \leqslant 10^{-2}$. Further, in the numerical calculations, we set $L/\sqrt{\tau} = 0.5$, $\eta = 1.4$, $L = 0.15$.

We shall denote the value of Ψ, which makes the reactor critical with $\gamma = 0$ and Σ_{pno}, by Ψ_∞. We shall denote the coordinate-independent component of the absorber in Eq. (5) by ω and, in addition, $\omega_\infty = 0.0256\eta\Psi$. In Figs. 1 and 2 the ratio of the reactor power w calculated with $\zeta = 0$ to the power with $\zeta \neq 0$ is marked along the ordinate axis.

Figure 1 shows the dependence of w on Ψ for $\Psi < \Psi_\infty$. In this case, $\omega = \omega_\infty$. The stabilizing effect of neutron entrainment on the reactor state as $\Psi \to \Psi_\infty$ is clearly evident. For $\Psi \geq \Psi_\infty$ and $\zeta = 0$, the state would be supercritical, while for $\zeta \neq 0$, the reactor could be in a stationary state (for very small excesses of Ψ above Ψ_∞. The latter circumstance could be of interest in examining reactor stability.

Figure 2 shows the dependence of w on the excess of the absorber cross section above the value of ω_∞ at $\Psi = \Psi_\infty$. In this case, the regulating effect of the absorber and the entrainment of neutrons by the moderator appear together in the narrow range of weakly controllable (small) variations in the absorber near the dangerous value ω_∞. In the case of

a heavy-water moderator, w depends on ζ more strongly than for light water.

Thus, within the framework of the model used, the deviations of the absorption of xenon from the limiting value at $\Phi = \infty$ have a considerable effect on reactor power, but neutron entrainment under these conditions appears as a considerable stabilizing factor. We have been talking about the stationary state. A change in the velocity could give rise to a transient process according to the following scheme: increase in $\zeta \rightarrow$ decrease in $\Phi \rightarrow$ growth of Xe $\rightarrow$ further decrease in Φ.

LITERATURE CITED

1. B. Wolfe, Nucl. Sci. Eng., 13, No. 2, 80 (1962).
2. Ya. V. Shevelev, Third Geneva Conference (1964), Dokl. SSSR, No. 374.
3. E. A. Garusov, A. A. Kostritsa, and Yu. V. Petrov, At. Energ., 21, No. 2, 128 (1966).
4. A. A. Kostritsa, Theory of Neutron Transport in a Moving Medium [in Russian], Énergoizdat, Moscow (1981).

HEALING OF TRACKS ON THE SURFACE OF ALKALI GLASS

V. F. Zelenskii, Yu. A. Gribanov, V. V. Mozgin, and V. F. Rybalko

UDC 539.1.074

It is well known that tracks of nuclear fission fragments in mica and glass are very stable relative to the action of high temperatures. In this connection, it was predicted that the tracks would have high temporal stability at $T \approx 300$ °K and $p \approx 1$ MPa. According to estimates in [1], the healing time of tracks in these materials under normal conditions must be $\sim 10^6$-10^7 years.

However, it was soon discovered that for alkali glasses, appreciable healing of tracks is observed already after one year of holding them under normal conditions [2]. The healing was observed by the decrease in the diameter of grooves produced by etching when the holding time between the time at which the glasses were irradiated and the time at which they were etched increased. Thus, in glasses etched after holding for 10 months, the diameter of the etching grooves was 20% smaller than for control specimens irradiated immediately prior to etching. In studying tracks after annealing at temperatures of 500-800°K, it was established [3] that the rate of healing depends appreciably on the pressure of the medium above the surface of the glass. When the pressure varied from atmospheric to 10^{-2} Pa, this rate decreased severalfold and, in addition, the largest change in the rate occurred in the pressure range ~ 10-10^3 Pa. In [3], accelerated healing of tracks was related with the mechanical effect of atmospheric pressure on near-surface layers of glass and, in addition, attempts were made to generalize this conclusion to all materials.

It has been proposed [4] that all observed characteristics of track healing [2, 3] are related with the chemical action of the gaseous medium on the glass surface, since it is known [5] that alkali glasses interact actively with the components of the medium. To check this assumption, the change in the rate of healing was studied as a function of the depth (distance from the glass surface), duration of holding of the glasses between irradiation and etching, and composition and pressure of the gaseous medium.

We irradiated specimens of alkali glass with dimensions $10 \times 10 \times 1$ mm by fission fragments using the isotopic source ^{252}Cf, emitting $\sim 2 \cdot 10^5$ fragments/sec into a solid angle 2π. We conducted the irradiation at room temperature and atmospheric pressure. The duration of irradiation of each specimen was 20 min. To reveal the tracks, we etched the glasses in a 2.5% solution of hydrofluoric acid. We observed healing of tracks by comparing the diameter of the etching grooves in the specimens studied, subjected to holding after irradiation under the given conditions, and in control specimens irradiated immediately prior to etching. To guarantee identical conditions, we etched, washed, and dried the specimens studied and the control specimens simultaneously in a special holder.

Translated from Atomnaya Énergiya, Vol. 55, No. 3, pp. 186-188, September, 1983. Original article submitted April 8, 1983.

 0038-531X/83/5503-0634$07.50

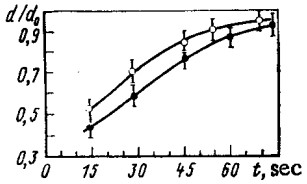

Fig. 1

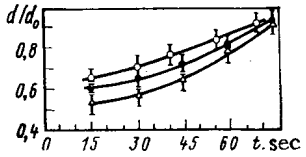

Fig. 2

Fig. 1. Dependence of d/d_0 on the etching time for specimens held after irradiation under standard atmospheric pressure for 300 h (○) and 1000 h (●).

Fig. 2. Dependence of d/d_0 on the etching time for specimens held in an atmosphere with 100% humidity for 150 (○), 386 (●), and 1000 h (Δ).

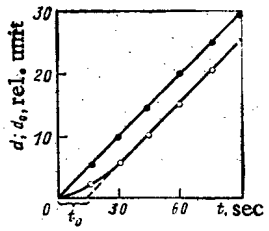

Fig. 3

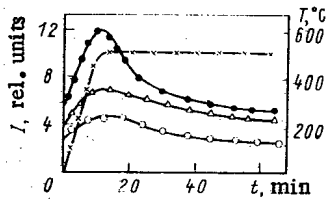

Fig. 4

Fig. 3. Dependence of the track diameters on the etching time for the control specimen (●) and a specimen held 300 h in the atmosphere (○).

Fig. 4. Change in the line intensities in the mass-spectrum of thermodesorption from the surface of glass with annealing: ×) change in the glass temperature in the annealing process; ●, Δ, and ○) line intensities of O^+, OH^+, and H_2O^+, respectively.

To obtain data on the rate of healing of tracks at different depths, we used the method of layer-by-layer etching. The etching time required to remove one layer was 10-15 sec. We studied the surface after each etching with the help of replicas, observed under an ÉMV-100L microscope. The total etching time did not exceed 2 min.

We constructed the dependences $d/d_0 = f(t)$ and $d(t)$, where d and d_0 are the average values of the diameters of the etching grooves on the specimens studied and on the control specimens, respectively, from the microphotographs of surfaces, obtained from the specimens studied and from the control specimens; t is the etching time. These dependences were obtained for three series of irradiated glasses (nine specimens each), differing by the holding conditions after irradiation.

We held the specimens in the first series in air at 300°K under standard conditions. We likewise held the specimens in the second series at room temperature, but in a medium with 100% humidity. We held the third series of specimens after irradiation in liquid nitrogen under atmospheric pressure. We stored all control specimens prior to irradiation at room temperature under standard conditions. After holding for 150, 300, and 1000 h, we subjected three specimens from each series to layer-by-layer etching.

The dependences $d/d_0 = f(t)$ for specimens in the first series are shown in Fig. 1 and for specimens in the second series in Fig. 2. The following general characteristics are evident for both series of specimens:

After the first etching, the dimensions of the grooves on all specimens are 1.5-2 times smaller than on the control specimen;

with further etching, the diameters of the etching grooves on the specimen studied and on the control specimens gradually become equal.

The first circumstance is convincing proof of the presence of the track healing process, occurring in the near-surface layer of glass; in addition, an estimate shows that in our case, the rate of healing is 30–40 times higher than in [2].

It is evident from Figs. 1 and 2 that for holding times exceeding 150 h, the diameters of the etching grooves remain practically unchanged with increasing holding time up to 1000 h. This means that the healing process proceeds mainly over a time less than 150 h. In addition, the high rate of healing is characteristic only for a thin near-surface layer of glass and drops rapidly with increasing distance from the surface. The presence of the layer which inherently has a high rate of healing of tracks is illustrated well in Fig. 3. It is evident that on the control specimen, the diameter of the tracks increases practically linearly with increasing etching time. The rate of etching of tracks on the surface of the specimens studied during the initial etching period is approximately two times smaller than for the control specimen. After 30 sec of etching, the rates begin to equalize and, then the curves $d(t)$ and $d_0(t)$ are practically parallel. The displacement of the curve $d(t)$ relative to $d_0(t)$ indicates the presence of a layer with finite thickness, in which healing occurs. Having determined t_0 (see Fig. 3) and having measured experimentally the rate of etching of glass, it is possible to find the thickness of this layer, which turned out to equal 350–400 Å (1 A = 10^{-10} m). It is independent of the medium in which the specimens were held as well as time. The high rate of healing in this layer is apparently related with the relatively high mobility of particles in it. This is confirmed by the fact that in specimens placed in liquid nitrogen for 100 h there were no signs of healing.

It is well known that a film of silicic acid with a thickness approximately up to 10^3 Å forms on the surface of alkali glasses as a result of interaction with water vapor and oxygen in air [6]. Its characteristic property is the considerably higher mobility of molecules, owing to the presence of broken bonds in the silicon oxide network. In addition, an indicator of the number of broken bonds and the corresponding degree of mobility of particles in the film is the concentration of the radical OH in it [7]. Dehydration of the films must decrease the mobility of particles, which will be reflected in the rate of healing.

It may be assumed that the surface layer on the glass, in which accelerated healing of tracks occurs, either represents a film of chemical origin or its healing properties differ appreciably from the deeper layers.

To solve the problem, we performed additional experiments, comparing the rate of healing in ordinary glasses and in glasses from which the surface film was removed either by etching in a standard etcher for 1 min followed by careful washing or by annealing the specimens in a vacuum ($2.6 \cdot 10^{-4}$ Pa) at T = 800°K for 1 h.

We irradiated glasses worked in this manner together with glasses not subjected to working and held them in a vacuum $2.6 \cdot 10^{-4}$ Pa at 300°K for 300 h. After this, we etched the specimens together with the control specimens (unworked glasses, irradiated immediately prior to etching). We compared the rates of healing of tracks after etching for 15 sec, when the healing effect must be strongest. We observed healing of tracks in glasses with a starting film after holding in a vacuum for 300 h, although the rate of healing was approximately 1.5 times slower than in air with the same holding time. No signs of healing were observed in glasses from which the surface film was removed first (independent of the method used). After control measurements, it was established that immediately after irradiation, the rate of etching of tracks on the glasses with different surface preparation is the same.

Analogous experiments with holding of irradiated specimens with and without a surface film for 300 h in a medium of pure helium at 300°K and p = 1 MPa showed that healing proceeded in specimens with a film in helium with the same rate as for holding in air, while in specimens without the film, no signs of healing were observed. The results of these experiments indicate that accelerated healing of tracks is due to the presence of the surface film. To obtain data on the nature of this film, we performed a mass-spectrometric analysis of the composition of the products, desorbing from the surface of the glass during annealing in a vacuum at 800°K. It is evident from Fig. 4 that with heating up to 800°K and subsequent holding, the intensity of O^+, OH^+, H_2O^+ lines increases and, in addition, the behavior of the curves $I(t)$ is characteristic for the rate of desorption of water. Since the intensity of H_2O^+ lines practically does not exceed the background level after annealing for 1 h, this means that the surface film was dehydrated, which, as already mentioned, must lead to a decrease in the mobility and, correspondingly, to a sharp decrease in the rate of healing of tracks.

Thus, the reason for accelerated healing of tracks on the surface of alkali glasses is the presence of a surface film on them, whose formation and properties are due to the chemica interaction of the glass with the components of the surrounding medium.

LITERATURE CITED

1. R. Fleisher, P. Price, and R. Walker, Ann. Rev. Nucl. Sci., 15, 1 (1965).
2. V. K. Gorshkov, At. Energ., 28, No. 6, 504 (1970).
3. V. K. Gorshkov, Preprint ITÉF No. 24, Moscow (1976).
4. Yu. A. Gribanov et al., Problems in Atomic Science and Technology. Series on the Physics of Radiation Damage and Radiation Material Processing [in Russian], (1977), No. 1(4), p. 46.
5. K. Gurney in: Mechanical Properties of New Materials [Russian translation], Mir, Moscow (1966), p. 255.
6. S. A. Imanov and S. A. Smirnov, Handbook on Insulating Materials for the Nuclear Industry [in Russian], Gosénergoizdat, Moscow (1947), p. 97.
7. V. A. Bershtein, L. D. Volovets, and V. A. Stepanov, Fiz. Tverd. Tela, 13, No. 3, 734 (1971).

MEASUREMENT TECHNIQUES
Izmeritel'naya Tekhnika
Vol. 27, 1984 (12 issues) $520

MECHANICS OF COMPOSITE MATERIALS
Mekhanika Kompozitnykh Materialov
Vol. 20, 1984 (6 issues) $430

METAL SCIENCE AND HEAT TREATMENT
Metallovedenie i Termicheskaya Obrabotka Metallov
Vol. 26, 1984 (12 issues) $540

METALLURGIST
Metallurg
Vol. 28, 1984 (12 issues) $555

PROBLEMS OF INFORMATION TRANSMISSION
Problemy Peredachi Informatsii
Vol. 20, 1984 (4 issues) $420

PROGRAMMING AND COMPUTER SOFTWARE
Programmirovanie
Vol. 10, 1984 (6 issues) $175

PROTECTION OF METALS
Zashchita Metallov
Vol. 20, 1984 (6 issues) $480

RADIOPHYSICS AND QUANTUM ELECTRONICS
Izvestiya Vysshikh Uchebnykh Zavedenii, Radiofizika
Vol. 27, 1984 (12 issues) $520

REFRACTORIES
Ogneupory
Vol. 25, 1984 (12 issues) $480

SIBERIAN MATHEMATICAL JOURNAL
Sibirskii Matematicheskii Zhurnal
Vol. 25, 1984 (6 issues) $625

SOIL MECHANICS AND FOUNDATION ENGINEERING
Osnovaniya, Fundamenty i Mekhanika Gruntov
Vol. 21, 1984 (6 issues) $500

SOLAR SYSTEM RESEARCH
Astronomicheskii Vestnik
Vol. 18, 1984 (6 issues) $365

SOVIET APPLIED MECHANICS
Prikladnaya Mekhanika
Vol. 20, 1984 (12 issues) $520

SOVIET ATOMIC ENERGY
Atomnaya Énergiya
Vols. 56-57, 1984 (12 issues) $560

SOVIET JOURNAL OF GLASS PHYSICS AND CHEMISTRY
Fizika i Khimiya Stekla
Vol. 10, 1984 (6 issues) $235

SOVIET JOURNAL OF NONDESTRUCTIVE TESTING
Defektoskopiya
Vol. 20, 1984 (12 issues) $615

SOVIET MATERIALS SCIENCE
Fiziko-khimicheskaya Mekhanika Materialov
Vol. 20, 1984 (6 issues) $445

SOVIET MICROELECTRONICS
Mikroélektronika
Vol. 13, 1984 (6 issues) $255

SOVIET MINING SCIENCE
Fiziko-tekhnicheskie Problemy Razrabotki Poleznykh Iskopaemykh
Vol. 20, 1984 (6 issues) $540

SOVIET PHYSICS JOURNAL
Izvestiya Vysshikh Uchebnykh Zavedenii, Fizika
Vol. 27, 1984 (12 issues) $520

SOVIET POWDER METALLURGY AND METAL CERAMICS
Poroshkovaya Metallurgiya
Vol. 23, 1984 (12 issues) $555

STRENGTH OF MATERIALS
Problemy Prochnosti
Vol. 16, 1984 (12 issues) $625

THEORETICAL AND MATHEMATICAL PHYSICS
Teoreticheskaya i Matematicheskaya Fizika
Vol. 58-61, 1984 (12 issues) $500

UKRAINIAN MATHEMATICAL JOURNAL
Ukrainskii Matematicheskii Zhurnal
Vol. 36, 1984 (6 issues) $500

Send for Your Free Examination Copy

Plenum Publishing Corporation, 233 Spring St., New York, N.Y. 10013
In United Kingdom: 88/90 Middlesex St., London E1 7EZ, England
Prices slightly higher outside the U.S. Prices subject to change without notice.

RUSSIAN JOURNALS IN THE PHYSICAL AND MATHEMATICAL SCIENCES

AVAILABLE IN ENGLISH TRANSLATION

ALGEBRA AND LOGIC
Algebra i Logika
Vol. 23, 1984 (6 issues) $360

ASTROPHYSICS
Astrofizika
Vol. 20, 1984 (4 issues) $420

AUTOMATION AND REMOTE CONTROL
Avtomatika i Telemekhanika
Vol. 45, 1984 (24 issues) $625

COMBUSTION, EXPLOSION, AND SHOCK WAVES
Fizika Goreniya i Vzryva
Vol. 20, 1984 (6 issues) $445

COSMIC RESEARCH
Kosmicheskie Issledovaniya
Vol. 22, 1984 (6 issues) $545

CYBERNETICS
Kibernetika
Vol. 20, 1984 (6 issues) $445

DIFFERENTIAL EQUATIONS
Differentsial'nye Uravneniya
Vol. 20, 1984 (12 issues) $505

DOKLADY BIOPHYSICS
Doklady Akademii Nauk SSSR
Vols. 274-279, 1984 (2 issues) $145

FLUID DYNAMICS
Izvestiya Akademii Nauk SSSR, Mekhanika Zhidkosti i Gaza
Vol. 19, 1984 (6 issues) $500

FUNCTIONAL ANALYSIS AND ITS APPLICATIONS
Funktsional'nyi Analiz i Ego Prilozheniya
Vol. 18, 1984 (4 issues) $410

GLASS AND CERAMICS
Steklo i Keramika
Vol. 41, 1984 (6 issues) $590

HIGH TEMPERATURE
Teplofizika Vysokikh Temperatur
Vol. 22, 1984 (6 issues) $520

HYDROTECHNICAL CONSTRUCTION
Gidrotekhnicheskoe Stroitel'stvo
Vol. 18, 1984 (12 issues) $385

INDUSTRIAL LABORATORY
Zavodskaya Laboratoriya
Vol. 50, 1984 (12 issues) $520

INSTRUMENTS AND EXPERIMENTAL TECHNIQUES
Pribory i Tekhnika Eksperimenta
Vol. 27, 1984 (12 issues) $590

JOURNAL OF APPLIED MECHANICS AND TECHNICAL PHYSICS
Zhurnal Prikladnoi Mekhaniki i Tekhnicheskoi Fiziki
Vol. 25, 1984 (6 issues) $540

JOURNAL OF APPLIED SPECTROSCOPY
Zhurnal Prikladnoi Spektroskopii
Vols. 40-41, 1984 (12 issues) $540

JOURNAL OF ENGINEERING PHYSICS
Inzhenerno-fizicheskii Zhurnal
Vols. 46-47, 1984 (12 issues) $540

JOURNAL OF SOVIET LASER RESEARCH
A translation of articles based on the best Soviet research in the field of lasers
Vol. 5, 1984 (6 issues) $180

JOURNAL OF SOVIET MATHEMATICS
A translation of Itogi Nauki i Tekhniki and *Zapiski Nauchnykh Seminarov Leningradskogo Otdeleniya Matematicheskogo Instituta im. V. A. Steklova AN SSSR*
Vols. 24-27, 1984 (24 issues) $1035

LITHOLOGY AND MINERAL RESOURCES
Litologiya i Poleznye Iskopaemye
Vol. 19, 1984 (6 issues) $540

LITHUANIAN MATHEMATICAL JOURNAL
Litovskii Matematicheskii Sbornik
Vol. 24, 1984 (4 issues) $255

MAGNETOHYDRODYNAMICS
Magnitnaya Gidrodinamika
Vol. 20, 1984 (4 issues) $415

MATHEMATICAL NOTES
Matematicheskie Zametki
Vols. 35-36, 1984 (12 issues) $520

continued on inside back cover